UNIVERSITÀ DEGLI STUDI DI PALERMO

Dottorato in Ingegneria Chimica, Gestionale, Informatica, Meccanica
Indirizzo: Ingegneria Chimica e dei Materiali
Dipartimento di Ingegneria Chimica, Gestionale,
Informatica, Meccanica
SSD: ING-IND/22

PREPARATION OF MULTIFUNCTIONAL NANO-STRUCTURED POLYMER NANOHYBRIDS CONTAINING CARBON COMPOUNDS

PhD STUDENT
Reza Khatibi

HEAD OF THE PhD BOARD
Prof. Salvatore Gaglio

SUPERVISOR
Prof. Roberto Scaffaro

CYCLE XXV
TITLE AWARDED IN 2015

Index

Chapter 1

1. introduction

1.1. Nanotechnology

Nanotechnology is science, engineering, and technology conducted at the nanoscale, which is about 1 to 100 nanometers. Nanoscience and nanotechnology are the study and application of extremely small things and can be used across all the other science fields, such as chemistry, biology, physics, materials science, and engineering. The associated research and applications are equally diverse, ranging from extensions of conventional device physics to completely new approaches based upon molecular self-assembly, from developing new materials with dimensions on the nanoscale to direct control of matter on the atomic scale.

Nanotechnology may be able to create many new materials and devices with a vast range of applications, such as in medicine, electronics, biomaterials energy production, and consumer products. On the other hand, nanotechnology raises many of the same issues as any new technology, including concerns about the toxicity and environmental impact of nanomaterials that it requires more research and study to overcome.

1.2. Nanoparticles:

In terms of nanotechnology a small particle must behave as whole unit respect to its intrinsic features. Then particles are categorized based on their own diameters. Large particles are classified in 2,500 and 10,000 nanometers, Fine particles are known in a range of 100 and 2,500 nanometers and at the end ultrafine particles (nanoparticles) are specified in a range of 1 and 100 nanometers. Nanoparticles will or will not express properties which are related to their diameter and size that is totally different from the observed properties in fine particles or bulky materials. However the size of a major part of molecules could be in accordance with above mentioned definition, but individual molecules are not almost considered as nanoparticles. Based on the regular definitions, nanoparticle

must posses at least one dimension between 1 and 10 nanometers that it also has to have a restricted and uniform size distribution. Researchers recently categorize nanoparticles based on their dimension including: 1dimensional (carbon nanotube), 2dimensional (graphite, silicate and spherical or cubic-shaped (fullerene, nano-carbonate calcium) [1, 2]. A bulk material should have constant physical properties regardless of its size, but at the nano-scale size-dependent properties are often observed. Thus, the properties of materials change as their size approaches the nanoscale and as the percentage of atoms at the surface of a material becomes significant.

Nanoparticles often possess unexpected optical properties as they are small enough to confine their electrons and produce quantum. Other size-dependent property changes include quantum confinement in semiconductor particles, surface plasmon resonance in some metal particles and superparamagnetism in magnetic materials.

In the beginning it is tried to introduce briefly some of the most important nano-particles which are widely used and in continue it will be illustrated more by giving detailed information about the main group of nanomaterials which was used in this research.

1.2.1. Silica

Silicon dioxide, that is known as silica (from the Latin *silex*) as well, is a chemical composition that is performed of a dioxide of silicon with the chemical formula SiO_2. Silica has been known since long time ago and ancient. Silica is mainly accessible in nature as quartz, and also in various living creatures, Silica is one of the most multiplex and most accessible group of materials, which is obtainable both as minerals and being produced synthetically. The main common application of silica is glass and cement industry but the main part of optical fibers for are also produced from silica and there are a large number of other applications which are not so related

to this topic. Layered silica because of its molecular structure and special geometry is known as a 2 dimensional material [3].

1.2.2. Calcium carbonate

Calcium carbonate is a chemical compound with the formula $CaCO_3$. Calcium carbonate is a common material in stones and rocks in the whole of world, and it is also the main part of shells ofsnails, marine organisms, snails, pearls, eggshells and coal balls. Carbonate is widely used as an extender in paints industry, for instance about 30% by weight of a special matte paint is marble or chalk. It should be mentioned that carbonate calcium is popular filler in plastics. In spite of layered structure of silica in calcium carbonate, some new generations of cubic/spherical structures recently were produced which have attracted attentions as filler in industry [4].

1.2.3. Magnetic nanoparticles

Magnetic nanoparticles are a group of nanomaterials which are tunable using electromagnetic field. These kinds of nanomaterials are usually produced of electromagnetic elements including: iron, nickel and cobalt and their chemical compounds. The electromagnetic nanomaterials have been attracted a lot of attentions in much research recently because of their special properties which is a huge potential use in catalysis such as nanomaterial-based catalysts, biomedicine, magnetic resonance imaging, magnetic particle imaging, data storage, environmental remediation, nanofluids, optical filters, defect sensor and cation sensors [5-9].

Up to this point it was tried to introduce the basics of nanoparticles by mentioning to some kind of those well known in research and industrial field. Now we are going to go more in deep by focusing on a family of materials which have all a common aspect in organic and carbonic base.

1.2.4. Carbon-based materials

Carbon, as the sixth element in the Periodic Table of Elements, is really considerable for its special catenation capability to combine with itself and other chemical elements with different methods and therewith make the basis for organic chemistry and life. Abundantly available natural graphite, coal and less available Diamond are just some examples of this family material. Diamond and graphite, (allotropes) of carbon have now been joined by fullerenes (C60, C70) [10,11], fullerene-related materials (like carbon onions) [12], carbon nanofibers [13,14] and also carbon nanotubes [15–17]— all belong to carbon-based nanomaterials (figure 1.1). The discovery of fullerenes in 1985 [18] and carbon nanotubes in 1991 [19] provoked the study of carbon nanostructure materials. This is closely related to the fact that fullerenes act as prototypes for zero-dimensional quantum dots but in the same time, nanotubes behave as prototypes for one-dimensional (1D) quantum wires [16].

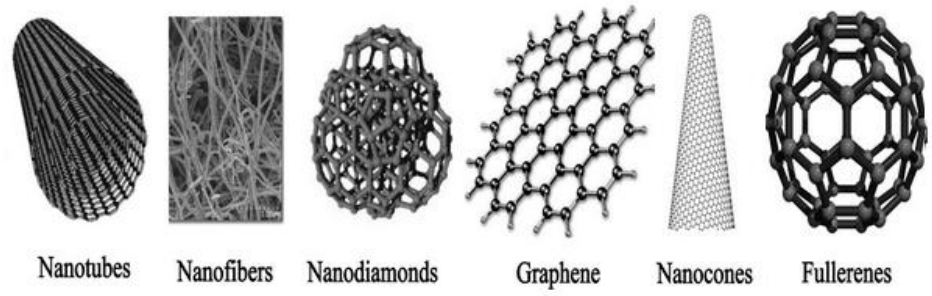

Figure 1.1) Carbon based nanomaterials

A lot of other forms of carbon (engineered carbons) has been invented that some of these are introduced here: synthetic diamonds and synthetic graphite, adsorbent carbon, carbon black, cokes, carbon and graphitic fibers, glassy carbons, diamond-like carbon, etc., for application in various end uses like electrodes and electrical contacts, lubricants, shoe polish, gemstones, cutting wheels, gas adsorption, catalytic support, helium gas barrier, tire and elastomer reinforcement, toner for photocopying machines

and printing inks, high performance tennis rackets, aircraft and spacecraft composites, heat sinks for ultrafast semiconductors, etc.[20–22].

All these different carbon forms can be attributed to the unique properties of hybridization of carbon. The ground state orbital configuration of carbon is $1s^2\ 2s^2\ 2p^2$. Because of the confine energy gap existed between the 2s and 2p orbitals it is rather easy to promote one 2s electron to a vacant higher energy 2p orbital. This electron operation permits carbon to hybridize into other configurations sp, sp^2 and sp^3 and leads to fascinating and diverse molecular structures. The sp bonding forms the chain structures, sp^2 bonding forms the planar structures and at the end, sp^3bonding forms the tetrahedral structures. The hybridization states of some well known carbon-based nanomaterials are exhibited in (figure 1.2).

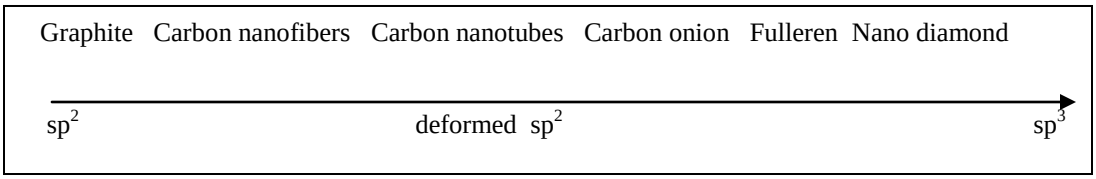

Figure 1.2) Hybridization states of some typical carbon nanomaterials.

However, due to some challenging steps such as processing and dispersion the use of CNTs in nanocomposites has been limited yet, but the biggest taken step for wide use is the exorbitant price of materials. Multiwall carbon nanotubes (MWNTs) are priced at~$8/g, single wall carbon nanotubes (SWNTs) cost ~$170/g and graphite nanoplatelets are priced at ~$2/kg[23].

In fact, from a geometric point of view, carbon nanostructures like CNTs and VGCNFs can be obtained by scrolling the covalent graphene building units around an axis in order to result in a three dimensional structure of material (figure 1.3) [24].

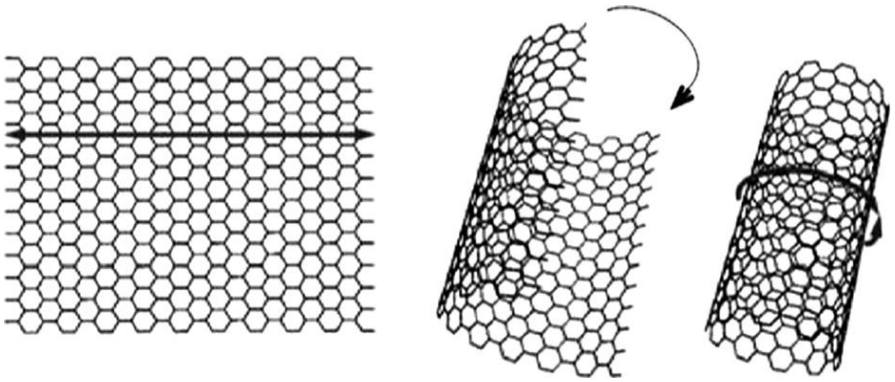

Figure 1.3) Rolling up of graphene sheet to form CNT

It should be noted that elemental carbon has the lowest energy state at room temperature and pressure in graphite [17,25]. The graphite lattice made of a lot of stocked parallel two dimensional (2D) graphene sheets (a single carbon layer in the graphite lattice is known as a graphene sheet) with sp2 hybridized carbon atoms which is confined in hexagonal rings with other adjacent rings. When 2pz orbitals of the carbon atoms are completely flat, they can overlap with the highest efficiency especially when they are parallel (out-of-plane-bond) and the graphene sheet has lowest energy. Therefore, graphite is an anisotropic material because of the existed difference between in-plane and out-of-plane bonding of the confined carbon atoms in the hexagonal rings. Yong's modulus in in-plane direction is much higher than perpendicular direction of graphene sheets and it makes graphite stronger in-plane than diamond. The π orbital is dispersed along graphene sheet and endows that electrically and thermally conductivity. The layered structure of graphite is shown in (figure 1.4).

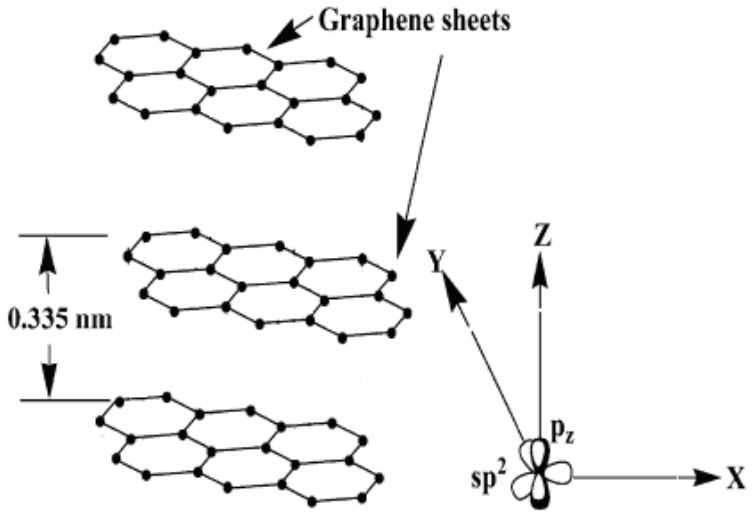

Figure 1.4) Layered structure of graphite showing the sp^2 hybridized carbon atoms tightly bonded in hexagonal rings

There is a 0.335 nm space between each two adjacent graphene sheet, which is half the crystallographic spacing of hexagonal graphite. Weak van der Waals forces keep the adjacent graphene sheets together, so the graphene sheets can rather easily slip on each other that it makes graphite soft and lubricating. Sliding the graphene sheets on each other is what helps to make graphene sheets from graphite.

1.3. Modification and functionalization methods

Since due to Van der Waals forces graphene sheets have strong tendency to become agglomerated, dispersing them within the polymer matrixes is extremely difficult. Therefore, a big challenge in developing polymer/graphite composites with high efficiency is achieving to the individual graphene sheets within a polymer matrix in order to have a better dispersion and strong interfacial interactions, in order to decrease percolation threshold in graphene sheets loading and enhancing the graphene-polymer matrix interface. The functionalization of carbon-based materials is an effective way to prevent carbon sheets from agglomeration and helps to have better dispersion and stabilize the graphene sheets within

a polymer matrix by enhancing their interfacial bonds. There are a lot of methods for functionalization of carbon-based including defect functionalization, covalent functionalization and non-covalent functionalization [26]. These functionalization methods are summarized in the next sections.

1.3.1. Defect functionalization

The main aim of this approach is purification of carbon-based materials by oxidative methods to eliminate metal particles or amorphous carbon from the raw materials [27,28]. In this approach, defects are rather detectable on the edges of carbon lattice. The functionalized final product includes oxidized carbon atoms in the form of –COOH group (figure 1.5) [29,30]. By studying the volume of CO2(g) and CO(g) released after heating to 1273°K in defect sites of SWCNTs defect functionalized, it was understood that about 5% of the carbon atoms in the SWNTs are located exactly in defected points. Acid base titration approach [31] was utilized to distinguish the percentage of defected sites of functionalized SWNTs was between 1 and 3%. Although, the located defective sites at the CNT surfaces by this method are very narrow, and is not capable to result in a good dispersion within the polymer/carbon-based nanoparticle composites. However, they can be exerted for covalent attachment of organic groups by converting them into acid chlorides and in continue reacting with amine groups to give amides [32,33]. The functionalized carbon materials have stronger solubility in organic solvents respect to the raw material.

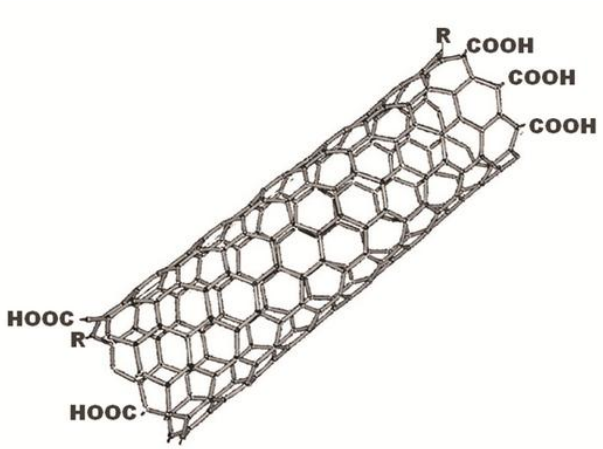

Figure 1.5) Defect functionalized carbon naotube with joint carboxyl groups on the edges.

1.3.2. Non-covalent functionalization

Non-covalent functionalization because of preserving physical properties and improving solubility and processability of carbon-based materials is extremely attractive in researches. This type of functionalization usually makes use of surfactants, biomacromolecules or scrolling around the polymers. In this kind search in order to have non-destructive purification, carbon-based material can be directly added to the aqueous phase containing surfactants [34,35]. In this case, hydrophobic side of the micelles is joined to the surface of carbon-based materials. In case of having aromatic groups in in hydrophobic side of the amphiphilic surfactant we can expect stronger interaction. Using anionic, cationic, and non-ionic surfactants can improve extremely solubility of hexagonal rings of carbon-base materials within water [36–39]. Sodium dodecylsulfate (SDS) [40–42] and sodium dodecylbenzene sulfonate (NaDDBS) [43,44] that are classified as anionic surfactants are usually utilized to decrease carbon material aggregation probability in water phase (figure 1.6). Some parameters such as alkyl chain length, head group size, and charge can strongly affect the intensity of interaction between carbon-base materials and surfactants.

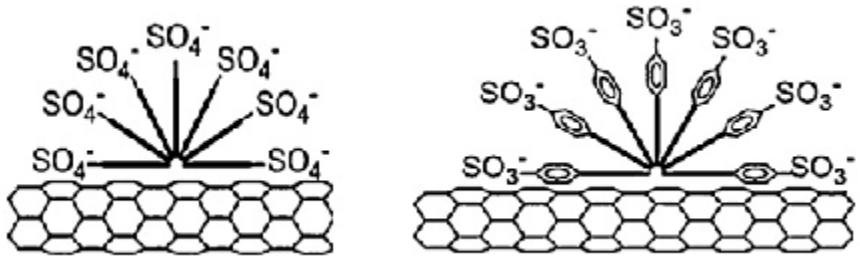

Figure 1.6) Sodium dodecylsulfate (SDS) (left) and sodium dodecylbenzene sulfonate (NaDDBS) (right) surfactants on carbon nanotubes.

1.3.3. Covalent functionalization

In covalent functionalization in order to endow or change in electronic or other properties to the material, it is tried to disrupt the symmetry of carbon-based material from sp^2 carbon atom to sp^3 carbon atom [92]. It must be mentioned that, this approach can results in improving the solubility in polymers and solvents. There are two main ways to perform covalent functionalization including, modification of surface-bound carboxylic acid groups on the carbon-based material or directly introduce of the agents on the carbon surface. Generally, by having an intensive oxidation step by oxygen, concentrated sulfuric acid, nitric acid, aqueous hydrogen peroxide, and acid mixture we can install functional groups such as –COOH or –OH on the carbon material [45,46]. It seems to be normal having some defects on the carbon-carbon bonds in carbon sheets right after acid treatment that is also associate with carboxylic groups, while the raw material shows uniform surfaces and a because of their untouched lattice structure of carbon–carbon bonds [47–49]. There is a proportion between acid treatment temperature and time with the number of carboxylic groups on the surface of carbon, this increase by increasing the processing temperature [48]. The extent of the carboxyl and hydroxyl functionality also is related to the oxidation procedures and oxidizing agents [50].

1.3.4. Functionalization using click chemistry

Click chemistry is a really useful approach in order to synthesize small molecules and make use of azide and alkyne groups introducing into organic and polymer molecules and it is necessary to mention that stability of these groups in a wide range of reactions and high compatibility/tolerability in presence of other types of functional groups are just small part of those positive aspect in this approach. Toleration of other functional groups that was mentioned, a short reaction time, high performance and high purity as well as its suitability for use under aqueous conditions are other benefits of this approach that makes fascinating for the researchers [51].

It requires to be mentioned that functionalization and modification is a really broad issue and there is a lot of other less known and practical methods which were not mentioned here. It has been just tried to give some basics about the most current methods and ignoring the others. As it has been mentioned carbon material is broad family consist of a lot of different materials in configuration point of view and the same from the component standing point of view, and as far as it has been clarified graphite is one the cheapest and primary components. Thus all above mentioned methods are more or less applicable to use with all carbon material family members. Therefore we have turned our attention to graphite and modification of that to highlight its considerable natural features such as mechanical properties and dispersal ability in mixture with polymer, solubility in aqueous phase and etc. So in continue we make our efforts to deal with graphite and graphite modification.

1.4. Modification of graphite

Generally, graphite exists in the nature as a layered material. In order to have an efficient utilization of graphite as filler in a polymer composite, this

layered structure must be disrupted by separation and dispersing throughout the polymeric matrix. Graphite nanoplatelet (GNP), (the basic unit of bulky graphite) is obtainable by exfoliation of the natural graphite flakes with having a range of platelet thickness from less than 0.34 to 100 nm, is an attractive alternative to metal- and carbon nanotubes which possess low cost and lightweight benefits and can be used as electrically conducting filler for conducting polymer nanocomposites [52-61]. Unlike silica which bear net charge, graphite does not possess this ability. In the natural form, there are no reactive ion groups on the graphene sheets and it gives an opportunity to insert monomers between graphene stocked sheets by ion exchange operation as is possible for the layered silicates. However, graphite flakes is easily intercalated and can be modified by various atoms, molecules, metal particles and salts between the space of caused by expansion operation of graphene sheets in order to form graphite intercalation compounds (GICs). Till now the main way to obtain graphene oxide (GO) from graphite flakes is sulfuric acid treatment. Because of the methods which are used to treat graphite and prepare graphite modified there are three termination to name the resulted product including; graphene oxide (graphite oxide), graphite intercalated compounds (GICs) and expanded graphite (EG).

1.4.1. Graphene oxide (GO)

Graphene oxide also known as graphite oxide, graphitic oxide or graphitic acid is usually processed by the modification of graphite flakes with strong oxidizing agents to introduce the polar groups on the surface and the interlayer space of graphene sheets to endow some features and also widen the this interlayer space [62]. The first time that graphene oxide was prepared it was in 1859 by Brodie that made use of potassium chlorate, fuming nitric acid and graphite flakes [63]. Hummers and Offeman suggested a better and safer way to prepare GO by reacting anhydrous sulfuric acid, sodium nitrate and potassium permanganate, that is followed even today (figure 1.7) [64]. The structure of GO contains epoxide and

hydroxyl groups within the graphene sheets and carboxyl and carbonyl groups at the sheet edges. GO plays an important role as an intermediate to prepare GNPs as it will be discussed in continue. It must be considered in continue by intercalation, expantion and reduction of graphene oxide we can obtain graphene sheets which are desirable for electronic industry and other research areas. Each step of this way has its own technique that we are not going to neither go in deep nor discuss about. The main goal of this research is finding an optimum approach to achieve to a uniform distribution of graphene oxide within polymer. Thus we conclude the graphite modification at this step and start the next section in dealing with nanocomposite preparation methods.

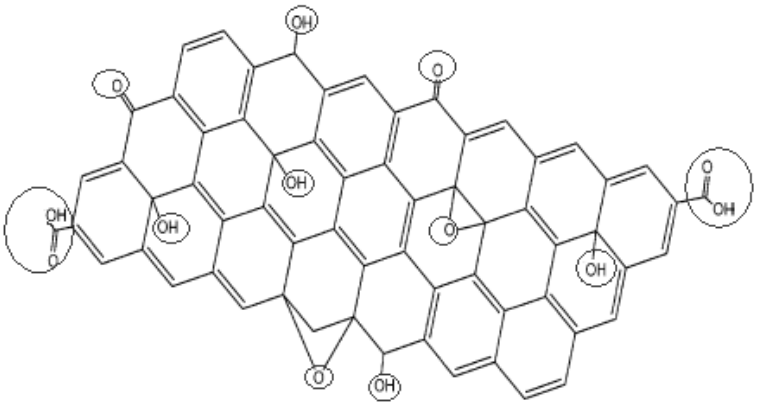

Figure 1.7) schematic of an oxidized graphene sheet containing oxygen functional groups.

1.5. Polymer nanocomposites

Polymer nanocomposites (PNC) contain a polymer or copolymer reinforced with nanoparticles or nanofillers which are homogenously dispersed within the polymer matrix. The fillers could be in different geometrical shapes (e.g., platelets, fibers, spheroids), but at least one dimension must be in the range of 1–50 nm. These PNC's belong to the category of multi-phase systems (MPS, viz. blends, composites, and foams) that include nearly 95% of plastics production. Polymer nanocomposite preparing system consists of

controlled mixing/compounding, stabilization of the achieved dispersion, orientation of the dispersed phase, and the compounding strategies for all MPS, including PNC.

Polymer nanoscience is the study and application of nanoscience to polymer-nanoparticle matrices, where nanoparticles are those with at least one dimension of less than 100 nm.

Nowadays graphitic carbon dispersing within polymers is a critical issue in the preparation of nanocomposites. There will be better results if graphitic carbon do not agglomerate during processing and gives better dispersion through the polymer. Currently there are several methods used to improve the dispersion of carbon material in polymer matrices such as solution mixing, melt blending, and in-situ polymerization method.

1.6. Polymer Nanocomposites pereparation methods

1.6.1. Solution mixing (solvent mixing)

In this method, graphitic carbon is dispersed in a solution of solvent and polymer and makes the mixture. After making the mixture, the composite of polymer and graphitic carbon is obtained by precipitation or evaporation of the solvent. The most known problem in this way is difficulty of dispersing graphitic carbon (insoluble materials) in solvent by simple stirring. A high power ultrasonication process is more helpful in making a dispersion of carbon material within the solvent. It must be mentioned that ultrasonic irradiation has been widely utilized in dispersion, emulsifying, crushing, and activating the particles before this approach. Ultrasonication method benefits from extraordinary power of ultrasonic irradiations in breaking aggregations of graphitic carbon. For example, Li et al. [65] used a simple solution–precipitation technique to enhance the dispersion of CNTs in a polycarbonate solution by ultrasonication at a frequency of 20 kHz for 10 min. the results showed that the CNTs were homogenously dispersed in polycarbonate matrix. In this way, ultrasonication as well as mechanically

stirring played important roles in the forming nanocomposites with a homogenous particle size.

1.6.2. Melt mixing

In solution casting, polymer need to be soluble in at least one solvent and this is a serious problem for polymers. Melt mixing is a common and simple method, particularly useful for thermoplastic polymers. In melt compounding carbon-based material is mechanically dispersed through the polymeric matrix with means a high temperature and high shear force mixer or compounder [66]. Easiness and compatibility of this method to industrial particles is the main positive point. The shear forces accelerate also breaking aggregations down and prevent their formation again. Zhang et al. [67] prepared nylon-6/MWNTs composites containing 1 wt% MWNTs by a melt blending method using a Brabender twin-screw mixer. SEM image indicate a homogeneous dispersion of MWNTs achieved in the polymeric matrix, with a significant enhancement in mechanical properties.

1.6.3. In-situ polymerization

In this method, the carbon-based material is dispersed through monomers is terminated by polymerization. In in-situ approach there is the possibility using higher percentage of the filler, and reach to a strong interaction with the polymer matrixes. This method is useful especially to prepare nanocomposites with polymers which are not soluble in solvents or melt blending, e.g., and sensible against high temperature.

1.7. The research area

In this study it was tried to produce a multifunctional material based on a thermoplastic polar polymer (polyamide-6) as matrix and a modified graphitic carbon (graphene oxide) as the filler. In order to improve the dispersion of filler within the polar polymer, graphite was oxidized based on Marcano's method. In continue graphene oxide was mixed through polyamide-6 by thee methods including:

1. melt mixing
2. solvent mixing
3. solvent/melt mixing (hybrid method)

It must be mentioned; the third method consists of two steps which starts up with solution mixing (pretreatment) to prepare a masterbatch which then is applied in melt mixing method.

The variable elements in this research are preparation methods, processing time, filler percentage and filler types. Based on the above mentioned methods graphene oxide was mixed within polyamide to endow its special features such as mechanical and thermal to the polymer. Mechanical test (by tensile test), thermomechanical test (by DMTA), crystinality test (by DSC, XRD, Raman) and rheological test (by rheometer) were done on the prepared specimens. Interpretation of the results is based on two main aims: process optimization and measuring the mechanical, thermal, rheological and morphological properties of the produced materials.

1.8. References

1. Hirscher, M/ Handbook of Hydrogen Storage: New Materials for Future Energy Storage/Wiley-VCH/2010/DOI: 10.1002/9783527629800.
2. ASTM E 2456 – 06/ Standard Terminology Relating to Nanotechnology/ 2012.
3. Iler, R.K/ The chemistry of silica/ 1979.
4. calcium carbonate powder/ http://www.reade.com/ Reade Advanced Materials/ 2006.
5. A.-H. Lu, W. Schmidt, N. Matoussevitch, H. Bönnemann, B. Spliethoff, B. Tesche, E. Bill, W. Kiefer, F. Schüth/ Nanoengineering of a Magnetically Separable Hydrogenation Catalyst/ Angewandte Chemie International Edition 43 (33): 4303–4306/doi:10.1002/anie.200454222/ 2004.
6. A. K. Gupta, M. Gupta/ Synthesis and surface engineering of iron oxide nanoparticles for biomedical applications/Biomaterials 26 (18): 3995–4021. doi:10.1016/j.biomaterials.2004.10.012/ 2005.
7. S. Mornet, S. Vasseur, F. Grasset, P. Verveka, G. Goglio, A. Demourgues, J. Portier, E. Pollert, E. Duguet/ Prog. Solid State Chem. 34: 237/ 2006.
8. B. Gleich, J. Weizenecker/ Tomographic imaging using the nonlinear response of magnetic particles/ Nature 435 (7046): 1214–1217/ doi:10.1038/nature03808/ 2005.
9. J. Philip, Shima.P.D. B. Raj/ Nanofluid with tunable thermal properties/ *Applied Physics Letters* 92: 043108/ doi:10.1063/1.2838304/ 2008.
10. Kroto HW. The stability of the fullerenes C-24, C-28, C-32, C-36, C-50, C-60 and C-70. Nature 1987;329:529–31.
11. Dresselhaus MS, Dresselhaus G, Eklund PC. Science of fullerenes and carbon nanotubes. San Diego: Academic Press; 1996. p. 15–59.

12. Ugarte D. Curling and closure of graphitic networks under electronbeam irradiation. Nature 1992;359:707–9.
13. Rodriguez NM. A review of catalytically grown carbon nanofibers. J Mater Res 1993;8:3233–50.
14. Tibbetts GG, Lake ML, Strong KL, Rice BP. A review of the fabrication and properties of vapor-grown carbon nanofiber/polymer composites. Compos Sci Technol 2007;67:1709–18.
15. Ajayan PM. Nanotubes from carbon. Chem Rev 1999;99:1787–99.
16. Dresselhaus MS, Avouris P. Introduction to carbon materials research. In: Dresselhaus MS, Dresselhaus G, Avouris P, editors. Carbon nanotubes: synthesis, structure, properties and application. Berlin: Springer; 2001. p. 1–9.
17. Han J, Structures. Properties of carbon nanotubes. In: Meyyappan M, editor. Carbon nanotubes: science and applications. Boca Raton: CRC Press; 2005. p. 1–24.
18. Kroto HW, Heath JR, O'Brien SC, Curl RE, Smalley RE. C60: Buckminsterfullerene. Nature 1985;318:162–3.
19. Iijima S. Helical microtubules of graphitic carbon. Nature1991;354:56–8.
20. Pierson HO. Handbook of carbon, graphite, diamond and fullerenes—properties, processing and applications. Park Ridge: Noyes Publications; 1993. p. 1–10.
21. McEnaney B. Structure and bonding in carbon materials. In: Burchell TD, editor. Carbon materials for advanced technologies. Oxford: Elsevier Science Ltd; 1999. p. 1–33.
22. Yasuda E, Inagaki M. Introduction. In: Yasuda E, Inagaki M, Kaneko K, Endo M, Oya A, Tanabe Y, editors. Carbon alloys—novel concepts to develop carbon science and technology. Oxford: Elsevier Science Ltd.; 2003. p. 3–11.

23. Li J, Sham ML, Kim J-K, Marom G. Morphology and properties of UV/ozone treated graphite nanoplatelet/epoxy nanocomposites. Compos Sci Technol 2007;67:296–305.
24. Ganguly A, George JJ, Kar S, Bandyopadhyay A, Bhowmick AK. Rubber nanocomposites based on miscellaneous nanofillers. In: Bhowmick AK, editor. Current topics in elastomers research. Boca Raton: CRC Press; 2008. p. 89–99.
25. Kelly BT. Physics of graphite. London: Applied Science Publishers; 1981. p. 1–33.
26. Hirsch A. Functionalization of single-walled carbon nanotubes. Angew Chem Int Ed 2002;41:1853–9.
27. Nalwa HS, editor. Handbook of nanostructured materials and nanotechnology,vol. 5. New York: Academic Press; 2000.
28. Ebbesen TW, Ajayan PM, Hiura H, Tanigaki K. Purification of nanotubes. Nature 1994;367:519–1519.
29. Hiura H, Ebbesen TW, Tanigaki K. Opening and purification of carbon nanotubes in high yields. Adv Mater 1995;7:275–6.
30. Kuznetsova A, Mawhinney DB, Naumenko V, Yates JT, Liu J, Smalley RE. Enhancement of adsorption inside of single-walled nanotubes: opening the entry ports. Chem Phys Lett 2000;321:292–6.
31. Hu H, Bhowmik P, Zhao B, Hamon MA, Itkis ME, Haddon RC. Determination of the acidic sites of purified single-walled carbon nanotubes by acid-base titration. Chem Phys Lett 2001;345:25–8.
32. HemonMA, Chen J,HuH, Chen Y, Itkis ME, Rao AM, et al. Dissolution of single-walled carbon nanotubes. Adv Mater 1999;11:834–40.
33. Chen J, Hamon MA, Hu H, Chen Y, Rao AM, Eklund PC, et al. Solution properties of single-walled carbon nanotubes. Science 1998;282:95–8.

34. Bandow S, Rao AM, Williams KA, Thess A, Smalley RE, Eklund PC. Purification of single-wall carbon nanotubes by microfiltration. JPhys Chem B 1997;101:8839–42.
35. Duesberg GS, Burghard M, Muster J, Philipp G. Separation of carbon nanotubes by size exclusion chromatography. Chem Commun 1998:435–6.
36. Paredes JI, Burghard M. Dispersions of individual single-walled carbon nanotubes of high length. Langmuir 2004;20:5149–52.
37. Duesberg GS, Muster J, Krstic V, Burghard M, Roth S. Chromatographic size separation of single-wall carbon nanotubes. Appl Phys A 1998;67:117–9.
38. Moore VC, Strano MS, Haroz EH, Hauge RH, Smalley RE, Schmidt J, et al. Individually suspended single-walled carbon nanotubes in various surfactants. Nano Lett 2003;3:1379–82.
39. Islam MF, Rojas E, Bergey DM, Johnson AT, Yodh AG. High weight fraction surfactant solubilization of single-wall carbon nanotubes in water. Nano Lett 2003;3:269–73.
40. Yurekli K, Mitchell CA, Krishnamootri R. Small angle neutron scattering from surfactant assisted aqueous dispersion of carbon nanotubes. J Am Chem Soc 2004;126:9902–3.
41. Jiang L, Gao L, Sun J. Production of aqueous colloidal dispersions of carbon nanotubes. J Coll Interf Sci 2003;260:89–94.
42. Poulin P, Vigolo B, Launois P. Films and fibers of oriented single wall nanotubes. Carbon 2002;40:1741–9.
43. Safar GAM, Ribeiro HB, Malard LM, Plentz FO, Fantini C, Santos AP, et al. Optical study of porphyrin-doped carbon nanotubes. Chem Phys Lett 2008;462:109–11.
44. Tan Y, Resasco DE. Dispersion of single-walled carbon nanotubes of narrow diameter distribution. J Phys Chem B 2005;109:14454–60.

45. Liu J, Rinzler AG, Dai H, Hafner JH, Bradley RK, Boul PJ, et al. Fullerene pipes. Science 1998;280:1253–6.
46. Zhang X, Sreekumar TV, Liu T, Kumar S. Properties and structure of nitric acid oxidized single wall carbon nanotube films. J Phys Chem B 2004;108:16435–40.
47. Cho JW, Kim JW, Jung YC, Goo NS. Electroactive shape-memory polyurethane composites incorporating carbon nanotubes. Macromol Rapid Commun 2005;26:412–6.
48. Georgakilas V, Kordatos K, Prato M, Guldi DM, Holzingger M, Hirsch A. Organic functionalization of carbon nanotubes. J Am Chem Soc 2002;124:760–1.
49. Zhang Y, Shi Z, Gu Z, Iijima S. Structure modification of single-wall carbon nanotubes. Carbon 2000;38:2055–9.
50. Datsyuk V, Kalyva M, Papagelis K, Parthenios J, Tasis D, Siokou A, et al. Chemical oxidation of multiwalled carbon nanotubes. Carbon 2008;46:833 40.
51. Kumar I, Rode CV. Efficient synthesis of fused 1,2,3-triazolo-deltalactams using huisgen [3+2] dipolar cycloaddition click-chemistry in water. Chem Lett 2007;36:592–3.
52. Jang BZ, Zhamu A. Processing of nanographene platelets (NGPs) and NGP nanocomposites: a review. J Mater Sci 2008;43:5092–101.
53. George JJ, Bhadra S, Bhowmick AK. Influence of carbon-based nanofillers on the electrical and dielectric properties of ethylene vinyl acetate nanocomposites. Polym Compos 2010;31:218–25.
54. Zheng G, Wu J, Wang W, Pan C. Characterizations of expanded graphite/polymer composites prepared by in situ polymerization. Carbon 2004;42:2839–47.
55. Li J, Vaisman L, Marom G, Kim J-K. Br treated graphite nanoplatelets for improved electrical conductivity of polymer composites. Carbon 2007;45:744–50.

56. Debelak B, Lafdi K. Use of exfoliated graphite filler to enhance polymer physical properties. Carbon 2007;45:1727–34.
57. George JJ, Bandyopadhyay A, Bhowmick AK. New generation layered nanocomposites derived from ethylene-co-vinyl acetate and naturally occurring graphite. J Appl Polym Sci 2008;108:1603–16.
58. Wakabayashi K, Pierre C, Dikin DA, Ruoff RS, Ramanathan T, Brinson LC, Torkelson JM. Polymer–graphite nanocomposites: effective dispersion and major property enhancement via solid-state shear pulverization. Macromolecules 2008;41:1905–8.
59. Du X, Yu Z-Z, Dasari A, Ma J, Mo M, Meng Y, Mai Y-W. New method to prepare graphite nanocomposites. Chem Mater 2008;20: 2066–8.
60. Kim H, Macosko CW. Morphology and properties of polyester/exfoliated graphite nanocomposites. Macromolecules 2008;41:3317–27.
61. Steurer P, Wissert R, Thomann R, Mulhaupt R. Functionalized graphenes and thermoplastic nanocomposites based upon expanded graphite oxide. Macromol Rapid Commun 2009;30:316–27.
62. George JJ, Bandyopadhyay A, Bhowmick AK. New generation layered nanocomposites derived from ethylene-co-vinyl acetate and naturally occurring graphite. J Appl Polym Sci 2008;108:1603–16.
63. Brodie BC. On the atomic weight of graphite. Phil Trans R Soc Lond Ser A 1859;149:249–59.
64. Hummers WS, Offeman RE. Preparation of graphitic oxide. J Am Chem Soc 1958;80:1339–1339.
65. Li C, Pang XJ, Qu MZ, Zhang QT, Wang B, Zhang BL, et al. Fabrication and characterization of polycarbonate/carbon nanotubes composites. Compos Part A 2005;37:1485–9.
66. Andrews R, Jacques D, Minot M, Rantell T. Fabrication of carbon multiwall nanotube/polymer composites by shear mixing. Micromol Mater Eng 2002;287:395–403.

67. Zhang WD, Shen L, Phang IY, Liu T. Carbon nanotubes reinforced nylon-6 composite prepared by simple melt-compounding. Macromolecules 2004;37:256–9.

Chapter 2

2. Literature review

2.1. Modification functionalization

2.1.1. Defect functionalization

Kuznetsova et al [1] instead of using H_2SO_4/HNO_3 mixture started utilizing H_2SO_4/H_2O_2, which was associated with ultrasonication, and suspending in methanol or dimethyl formamide. Samples were prepared by the drop/dry method for future study. It was interesting that, defects were rather observable at the open ends of nanotubes. The modified SWCNTs contain oxygen contain functional groups in the form of carboxyl group.

Mawhinney et al [2] in order to determine the fraction of oxidized carbon sites present oxidized SWCNTs by acidic oxidation. The SWNTs sample used in the study was produced by laser ablation method purified by the HNO_3/H_2SO_4 method to assure more than 90% purity. By monitoring the evolution of CO_2 (g) and CO (g) by heating in 1273 K revealed that about 5% of the carbon atoms in the SWNTs are located at sites which were defected before.

H.Hu et al [3] in order to remove impurities and amorphous carbon from the surface of SWCNTs, subjected them to nitric acid treatment. The samples were washed later with deionized water and then heated at 100°C for 30 minutes and at last the titration procedure was carried out. In fact this method was used to determine the percentage of acidic sites of purified SWNTs that was about 1–3%. However the other performed similar researches by Mark A.Hamon et al [4] and Jian Chen et al [5] confirmed, the defective sites created at the CNT surfaces by this method are extremely sporadic, and can not enhance dispersion in the nanocomposites.

2.1.2. Non-covalent functionalization

Non-covalent functionalization does not disrupt physical properties of carbon sheets and just improves the solubility and processability that makes them fascinating for the researchers. This type of functionalization usually makes use of surfactants, macromolecular (biomoleculars) or scrolling with polymers. In the researches that preserving the intrinsic structure of the carbon sheets is essential, carbon–based material can be transferred into the aqueous phase. In this case, the carbon sheets are covered by the hydrophobic site of the surfactant. Whenever the hydrophobic part of the surfactant contains an aromatic group we can expect a strong interaction.

Shunji Bandow et al [6] by using filtration and sonication in an aqueous solution of surfactants (0.1% surfactant) and carbonaceous samples and microfiltration at the end of procedure were achieved to purified SWCNTs.
J.I.Peredes et al [7] dispersed SWCNTs through the suspension of water and the surfactant sodium dodecylbenzene sulfonate (SDBS) which permitted the dispersion of tubes as individual tubes in the aqueous solution. The combination of mild tip and ultrasonication played an efficient role in this procedure to achieve to the final individual tubes.
G.S.Duesberg et al [8] tried to disperse SWCNTs by immersing SWCNTs in aqueous mixture 1wt% sodium dodecylsulfate (SDS) solution associated with 2 min ultrasonication. The results confirmed size exclusion chromatography as an efficient and non-destructive method for purification and separating carbon SWNTs. G.A.M.
Safar et al [9] were succeed in dispersing Porphyrin-doped carbon nanotubes in sodium dodecylbenzenesulfonate (NaDDBS) aqueous solution which had been obtained from NaDDBS/carbon nanotube aqueous dispersions. The results revealed low aggregation of the tubes within the matrix.

Yongqiang Tan et al [10] in order to prepare nanotube suspension added SWCNTs to surfactant solution of dodecylbenesulfonic acid sodium salt (NaDDBS) and in continue by ultrasonication for a period of time they prepared a stable solution with well dispersed individual nanotubes.

2.1.3. Covalent functionalization

In the case of covalent functionalization, the translational symmetry of graphitic carbon is changed by changing sp^2 carbon atoms to sp^3 carbon atoms, and some properties of carbon material, such as electronic and transport are affected. But this technique of functionalization can enhance the solubility and dispersion in solvents and polymer solutions. Covalent functionalization can be associated by surface modification of carboxylic acid groups or by direct using reagents to the carbon surface. usually, functional groups such as –COOH or –OH are inserted on the carbon sheet via oxidation procedure by oxygen, concentrated sulfuric acid, nitric acid, aqueous hydrogen peroxide, and acid mixture.

Xiefei Zhang [11] after immersing SWCNTs in distilled water and associating that with ultrasonication, nitric acid was added and repeated again the ultrasonication step. At the end by filtration and rinsing with distilled water, a really thin film of SWCNTs was obtained. The results show a decrease in electrical conductivity while tensile strength enhanced by increasing the nitric acid concentration as the function of carbon oxidation.

Y.zhang et al [12] immersed as prepared SWCNTs in 36% hydrochloric acid (HCl) for one day and then centrifuged to assure from removing the metal catalysts. In the second step SWCNTs was washed with deionized water and dispersed in 0.2% benzalkonium chloride and then filtered. In the next step SWCNTs was added to a mixture of concentrated sulfuric acid and nitric acid and again ultrasonicated, filtrated and washed to obtain the modified SWCNTs. TEM results showed the modified SWCNTs is clean of

fullerenes and amorphous carbon material. Raman experiment also confirms the modification and functionalization of SWCNTs on the edges and open ends. V.

Datsyuka et al [13] treated MWCNTs with hydrochloric acid to remove impurities and then rinsed with deionized water and filtered. In the second treatment MWCNTs was treated nitric acid and then washed by distilled water and filtered. In the third treatment MWCNTs was exposed to the mixture of sulfuric acid and hydroxide peroxide and then like the previous step followed by washing in distilled water and filtering. In the forth MWCNTs was treated by ammonium hydroxide and hydrogen peroxide and ended by washing in distilled water, filtering and drying. The results showed oxidation with nitric acid under hard conditions (reflux) increases the volume of defects on the CNTs due to length shortening that was also verified by XPS and Raman spectroscopy. Application of a piranha solution showed much lower oxygen content respect to nitric acid oxidation and the absence of additional defects on the graphitic surface. Use of non-acidic treatments such as the mixture of NH_4OH and H_2O_2, pave a road to remove completely disordered carbon from the MWCNT specimens that is was also confirmed by thermogravimetric analysis

2.1.4. Functionalization using click chemistry

Cho et al [14] concentrated on the covalent functionalization by attaching bioactive molecules into SWCNTs surface. After deriving amino acidx through click chemistry and covalently attaching them onto the SWCNTs, functionalization was terminated. After utilizing p-amino propargyl ether treatment on SWNTs by means of a solvent with free diazotization procedure, the alkyne-functionalized SWNTs were prepared. In order to attach different azides derived from amino acids, in the first step a series of chiral azides from corresponding α-amino acids were prepared. The alkyne functionalized SWCNTs in dimethylformamide (DMF)-pyridine-butanol

solution were treated with azide-functionalized amino acid compound and then followed by Cu(I), ascorbic acid and N,N'- diisopropylethylamine. The 1,2,3-triazole ring has also been utilized to link the chiral molecules and SWNTs, which is a promising strategy to attach bioactive molecules like peptides, polysaccharides and others .

Gao et al [15] reported magnetic nanohybrids from magnetic nanoparticles and polymer coated nanomaterials by using Cu(I)-catalyzed azide alkyne cycloaddition reaction. The nanohybrids were prepared from Fe_3O_4 nanoparticles and polymer coated MWCNTs. they prepared uniformed size Fe_3O_4 nanoparticles then functionalized with azide moieties (Fe_3O_4-N_3) and finally with alkyne moieties (Fe_3O_4-Alk). MWNTs were separately modified with polymer containing azide groups (MWNT-pAz) and polymer containing alkyne groups (MWNTpAlk). (Fe_3O_4-N_3) and (Fe_3O_4-Alk) were compounded with polymer coating nanotubes to give magnetic nanohybrids of MWCNT-pAz@Fe_3O_4 and MWCNT-pAlk@Fe_3O_4, respectively.

Cho et al [16] prepared gold nanoparticles functionalized SWCNTs using the click chemistry approach. Gold nanoparticles containing octanethiol were prepared before by reducing tetrachloroauric acid via sodium borohydride in presence of alkanethiol. The alkyl thiol modified gold nanoparticles were later treated with azidoundecane thiol to yield azide moiety containing gold nanoparticles, which were reacted with alkyne functionalized SWNTs.

Campidelli et al. [17] modified SWCNTs with phthalocyanine by the click coupling approach. They functionalized SWCNTs with 4-(2-trimethylsilyl)ethynylaniline in the presence of isoamyl nitrite, which were then treated with azide moiety containing Zinc-phthalocyanine (ZnPc) in presence of CuSO4 and sodium ascorbate to make the nanotubephthalocyanine hybrid. They also studied the photovoltaic properties of synthesized materials and observed that the photocurrent of SWCNT-ZnPc was higher and more stable and reproducible respect to pristine SWNTs.

2.2. Graphite modification

Duc Anh Nguyen et al [18] prepared graphene oxide from graphite flakes by using Staudenmaier method. Based on this method graphite flakes and concentrated H_2SO_4/fuming HNO_3 mixture were mixed together (2/1 v/v) and then in continue cooled to 0 ºC, agitated and then $KClO_3$ (110 g) was carefully added to the prepared mixture. The reaction mixture was left to reach room temperature and then stirred for 120 h. The mixture was transfered into deionized water and then GO was filtered and rinsed with distilled water to reach to neutral PH. The resulted GO was dried at 80 ºC, pulverized and then screened to obtain very fine particles. The results of characterization showed that the GO has $C_{10}O_{3.68}H_{2.48}$ formula. In order to obtain the FGS, the dried GO was inserted in a quartz tube, and the tube was filled with argon gas for 10 min. The quartz tube was then quickly heated in a furnace with 1100 ºC temperature. The tube was remained in the furnace for 5 min while the evolution of CO2 expands and exfoliates the GO into individual sheets. The characterization results showed that the composition of the FGS was $C_{10}O_{0.50}H_{0.51}$.

Peter Steurer et al [19] produced thermally reduced graphene oxide. But first they used two different oxidation methods including Hummers/Offeman and Brodie Method. This oxidation (Hummers/Offeman) method was carried out using 250 ml of concentrated sulfuric acid for each 10 g of graphite to disperse the particles. 5 g $NaNO_3$ were added into the mixture and after 1 hour of stirring it was cooled to 0-8°C. Then 30 g of $KMnO_4$ were slowly added. When this operation was accomplished, the resulting dispersion was stirred at room temperature for 2 h. The reaction was terminated by adding the dispersion into ice water/ H_2O_2 (5 until the excess $KMnO_4$ was destroyed). The GO was then filtered off and washed with HCl until no precipitation of $BaSO_4$ observed in the presence of $BaCl_2$ solution. The GO was carefully rinsed with distilled

water. The purified brown GO was dried to afford GO with the empirical formula $C_6O_3H_2$. In the second modification method (Brodie Method) 10 g of graphite were blended with 85 g of $NaClO_3$ powder. The mixture was cooled with a mixture of ice/salt under vigorous stirring. Then HNO_3 (100%) was added very carefully over 5 h. After additional stirring at room temperature for 30 min the flask was left at room temperature over night. The green mass was heated for 10 h to 60 ºC after breaking down the agglomerated particles. After cooling, the product was stirred in distilled water. After filtration and freeze drying the oxidation was repeated bight brown material was obtained.

Zhengzong Sun et al [20] functionalized thermally expanded graphite with with 4-bromophenyl groups with *in situ* technique and diazonium salt from 4-bromoaniline. ultrasonication in *N,N′*-dimethylformamide (DMF) helps to exfoliate thin chemically-assisted exfoliated graphene (CEG) sheets from the functionalized graphite flakes. It was observed that CEG is more soluble respect to pristine graphene in DMF. In addition, more than 70% of the CEG flakes consist of less than 5 layers.

Ceyhan Celik et al [21] obtained graphite particles with large dimensions of a few micrometers by ball-mill of expanded graphite flakes for 96 h in presence of ethyl alcohol. The slurry then was screened with sieves, dried under air circulation at 60– 658°C for 12 h and then in a vacuum oven at 150ºC for 12 h. In the last step, the particles were dry-ball-milled for an additional 96 h to reduce the particle size and breaking particle agglomerations. The results of mechanical test showed 70% Young's modulus increase in (phenylene ether)/Atactic Polystyrene Nanocomposite with just 5% wet ball milled expanded graphite while this level of neat graphite did not show any significant difference.

Julia J. Mack et al [22] prepared graphite nanoplatelets from intercalated graphite powder. Their process involved the heating of

graphite powder with potassium (K) under vacuum condition to form the GIC. Then, the GIC exposed to ethanol (EtOH) to react which reacts with potassium to form potassium ethoxide and released hydrogen gas. The evolution of hydrogen gas helps in the partial exfoliation of the graphitic layers to form GNPs. The results of AFM shows The GNPs produced by this technique generally have 40±15 graphene layers.

2.3. Properties and applications of polymer/graphitic material nanocomposites

2.3.1. Mechanical properties

Incorporation of graphitic carbon material can improve extremely mechanical properties in terms of Young's modulus and strength at break.

Kyriaki Kalaitzidou et al [23] prepared nanocomposites made of polypropylene reinforced with graphite nanoplatelets by melt mixing, polymer solution and coating techniques. It must be mentioned that coating involves compounding graphite nanoplatelets and polypropylene in isopropyl alcohol with ultrasonication to disperse enough the platelets within individual polypropylene particles. The results showed the coating method is more efficient than polymer solution in terms of lowering percolation threshold of thermoplastic nanocomposites and preserving the large platelet morphology of graphite nanoplatelets in the final produced composite. Mechanical results showed a big enhancement in flexural modulus and strength in more than 1% graphite platelets in both solution and coating methods.

Jul Bian et al [24] fabricated microwave exfoliated graphite oxide (MEGO) reinforced thermoplastic polyurethane (TPU) nanocomposite via melt

blending followed injection molding. The spectroscopic study confirmed a strong interfacial interaction had faced between MEGO and the TPU matrix. Microscopic observation also showed a homogeneous compound of MEGO and TPU. Mechanical properties of the nanocomposite were enhanced by the inserting MEGO into TPU. It is clear that there is a linear elastic behavior at low stress (strain) region and viscoelastic/plastic deformation at high stress (strain) region. However the elongation at break (EB) decreases at first and then increases with increasing MEGO content, the overall elongations of the nanocomposites remain still substantial.

Hui Quan et al [25] prepared nanocomposite of graphite platelets (GNP) and thermoplastic polyurethane (TPU) by solution casting technique. In continue morphological observation confirmed a homogeneous dispersion of GNP within TPU. The results of mechanical properties were also promising and showed an increase in storage modulus of nanocomposites with increasing GNP content. On the other hand nanocomposites containing only 3.9vol (the maximum loading employed in the research) have long elongation at break of over 600%.

G Carotenuto [26] prepared graphite nanoplatelets/low density polyethylene (GNP/LDPE) by the following way. First they broke down the fragile structure of the GNP aerogel which resulted from the drying of a concentrated colloidal suspension of GNP in acetone. In the second step the colloidal GNP suspensions were prepared by exfoliation of expanded graphite via ultrasonication. In the third step GNP were exposed to the thermal shock (600°C) for 4 min. the resulted expanded GNP were blended with LDPE by an extruder. The results showed filling LDPE by GNPs results in an increase of Young's modulus in LDPE and a reduction of the polymer plasticity. In continue DSC results confirmed, mechanical properties is not caused by a variation in the polymer crystallinity and it must be due to GNPs presence that reduces the mobility of polymer chains.

Xian Jiang et al [27] prepared nanocomposite of exfoliated graphite nanoplatelets (xGnP) and high density polyethylene (HDPE). They utilized two kind of xGnP including xGnP-1 with the thickness of 10 nm and a platelet diameter of 1μm, while xGnP-15 has the same thickness but the diameter is around 15μm. the nanocomposites were produced by melt blending and injection molding. Polymer nanocomposites from xGnP/HDPE are the same in flexural stiffness and strength with the composites of glass fiber/HDPE and carbon black/HDPE but slightly less than that of carbon fiber/HDPE at the same volume of fraction. The Izod impact strength of xGnP/HDPE is significantly above (~250%) than all other nanocomposites at the same volume of fraction exhibited.

2.3.2. Electrical properties

The first commercial application of these kinds of nanocomposites is electrical conductive or semiconductive materials in computers, screens or any other electronic devices in industry. Kyriaki Kalaitzidou et al [23] prepared nanocomposites of polypropylene reinforced with graphite nanoplatelets via melt blending, solution blending and coating techniques. The results of electrical conductivity showed the conductivity and percolation threshold both are influenced by various parameters such as the volume fraction and geometric characteristics of the conductive fillers. The filler orientation and spacing within the polymer matrix as well as the crystallinity of the matrix and in the end the fabrication method play as important role in percolation threshold and conductivity since they affect the orientation, dispersion and interlayer spacing within the polymer matrix. In the end the minimum observed electrical percolation threshold was attributed to the coating method with less than 0.1 vol.% however this level in the composites prepared by melt blending and injection molding was about ~7 vol.% which confirms the ability of the coating method in making more homogeneous nanocomposite.

Jun Bian et al [24] fabricated microwave-exfoliated graphite oxide (MEGO) based thermoplastic polyurethane (TPU) nanocomposites by melt blending and injection molding technique. Electrical conductivity measurement indicated a conductivity of 10^{-4} S cm^{-1} was obtained in the nanocomposite containing only 4.0 wt.% of MEGO.

Huang Wu et al [28] fabricated a nanocomposite of Polyetherimide (PEId) and exfoliated graphite nanoplatelets (GNPs) which were compounded by solution casting method assisted by ultrasonication. It was found that the electrical conductivity of the GNP papers can be as high as 2200 S cm^{-1}. In continue it was proved that even with 30 vol.% polymer, the GNP paper composite can still exhibit ~700 S cm^{-1} electrical conductivity due to the highly continuous GNP network formed in the paper making process.

Hyunwoo Kim [29] fabricated nanocomposite of thermoplastic polyurethane (TPU) reinforced with exfoliated graphite. Carbon sheets were produced from graphene oxide via two different modification methods: chemical modification (isocyanate treated GO, iGO) and thermal exfoliation (thermally reduced GO, TRG) and three different techniques of dispersion: solvent blending, in situ polymerization, and melt compounding. The results showed electrical percolation threshold of thermally reduced graphene oxide was the lowest and about 0.5 wt%.

2.3.3. Thermal properties

Adding graphitic carbon material into the polymers as the filler can enhance glass transition temperature (Tg) and thermal degradation temperature because of the contributing macromolecules forces in solving the problem of distributing the temperature equally through the matrix and resulting in thermal stability in plastic materials.

Jun Bian [24] with different formulations of microwave-exfoliated graphite oxide (MEGO) based thermoplastic polyurethane was succeed in preparing nanocomposites via melt blending followed by injection molding. Thermal analysis indicated that the glass transition temperatures (Tg) of the

nanocomposites shifted into the higher temperature with increasing MEGO content and their thermal stability improved respect to pure TPU matrix. It can be also confirmed by numerical results of thermogravimetric analysis (TGA) which showed: Thermal degradation temperature at 5% ($T_{5\%}$) and at 30% ($T_{30\%}$) of the pure TPU are 299.4 and 338.4°C, whereas in nanocomposite with 8.0 wt.% MEGO, they are shifted to 329.2 and 353.2°C, respectively.

Hui Quan et al [25] prepared a nanocomposite by compounding graphite nanoplatelets (GNP) and thermoplastic polyurethane (TPU) via solution blending technique. Thermogravimetric analysis (TGA) showed that the incorporation of GNPs could improve the thermal stability of the nanocomposites. In addition, cone calorimetry results showed that the GNPs could act as intumescent flame retardant and significantly reduced the heat release rate (HRR), thus improved the flame retardancy of the TPU matrix.

Huang Wu et al [28] prepared a nanocomposite of Polyetherimide (PEId) and exfoliated graphite nanoplatelets (GNPs) which were compounded by solution casting method followed by ultrasonication. Thermal analysis showed polymer/GNP/polymer three layer composite has an improvement in in-plane thermal conductivity about 200% compared respect to neat polymer while this improvement in polymer/GNP two layers composite is about 700%. For surface resistance, the polymer/GNP structure also benefits from the presence of GNP phase and shows lower values (0.3 Ω sq^{-1}).

Yeh Wang et al [30] were achieved to a nanocomposite by Graphite oxide (GO) and amine surfactant intercalated graphite oxide (GOS) filled maleated polypropylene (PPgMA) nanocomposites which was prepared directly by solution blending. Thermal analysis showed cooling temperature (Tc) of all the PPgMA composites increased

about 13°C compared with that of neat PPgMA and it was due to the nucleating effect of graphite on the PPgMA crystallization.

2.3.4. Gas Barrier properties

Gas permeability and impermeability are two important properties for a polymer nanocomposite which can be tuned by different nanofillers and in different volumes. Using in gas tank walls and other sensible electronic equipments are the most apparent applications of these properties.

Huang Wu et al [28] prepared a nanocomposite of Polyetherimide (PEId) and exfoliated graphite nanoplatelets (GNPs) which were compounded by solution casting method followed by ultrasonication. The results of oxygen permeability measurement showed, adding exfoliated graphite nanoplatelets (GNPs) into multilayer laminated composite reduces the O_2 permeability and in the same time improves in-plane electrical and thermal conductivity.

Hyunwoo Kim [29] fabricated nanocomposite of thermoplastic polyurethane (TPU) reinforced with exfoliated graphite. Carbon sheets were produced from graphene oxide via two different processes: chemical modification (isocyanate treated GO, iGO) and thermal exfoliation (thermally reduced GO, TRG) and three different compounding methods: solvent blending, in situ polymerization, and melt compounding. The results of nitrogen permeability measurements showed, N_2 permeation is highly reduced demonstrating that exfoliated carbon sheets can play the role of diffusion barriers in polymeric membranes.

2.4. Polyamide-6/graphitic carbon nanocomposites

Tran Duy Thanh et al [31] fabricated PA6-elastomer/graphite nanoplateles (xGnP) nanocomposite by three different elastomers: ethane propene copolymer (EPR), an ethene-methacrylate copolymer (EMA), and an

aminated polybutadiene (ATB). The final results indicate, the xGnP was placed in the PA6 phase because of the presence of epoxy groups on the surface of the xGnP, which enhance the attraction to the PA6 matrix. In the same time the results of mechanical test showed an improvement in strength, stiffness and toughness of the polymers filled with just 1-5 wt.% graphite nanoplatelets (xGnP). With increasing xGnPs content the glass transition temperature (Tg) slightly increased and this is evidence of the effect of xGnPs on the crystallinity of the matrix.

Peter Steurer et al [19] produced thermally reduced graphene oxide. But first they used two different oxidation methods including Hummers/Offeman and Brodie Method. In continue thermally reduced graphene oxide was melt extruded with polycarbonate (PC), polyamide-6 (PA6), poly styrene-co-acrylonitrile (SAN) and poly propylene (iPP). The results of mechanical test indicated, by increasing the percentage of thermally reduced graphene oxide from 5 to 10% in PA6 matrix, Young's modulus shows an increases from 2180±10 to 2430±10. Electrical resistivity also by increasing TrGO from 7.5 to 12% decreases from $4.5x10^{9}$ to $1.4x10^{4}\Omega$.cm. in the end making a comparison between four different matrixes with the same percentage of TrGO confirmed the minimum specific resistivity in SAN/TrGO and the maximum in PA6/TrGO.

Yan Liu et al [32] prepared nanocomposite of polyamide-6 (PA6)/ graphene oxide by solution casting method and using dimethylacetamide as solvent. First of all, TEM showed graphene oxide sheets were completely exfoliated and dispersed along polyamide-6 matrix. The results of DSC showed, crystallinity in polyamide-6 decreases by adding GO which confirmed by the results of half-time of crystallization (t1/2), crystallization rate exponent Zc and log F(T). this phenomenon can be described by the effect of graphene sheets over the crystal shaping in polyamide-6 when the temperature of melt nanocomposite is decreasing and it means more the content of GO, the slower the crystallization rate.

Liu, W et al [33] studied on the effect of processing techniques on the final nanocomposite. In order to achieve to this aim they used exfoliated graphite oxide as filler and polyamide-6 as matrix. It was found that counter rotation (CNR) twin crew processing xGnP/PA6 nanocomposite had similar mechanical properties with co-rotation (CoR) twin screw processing or with CoR conducted with a screw design modified for nanoparticles (MCoR). It was also found that the CNR processed nanocomposite with the same xGnP content showed the lowest graphite X-ray diffraction peak at 26.5° and it confirmed better xGnP dispersion in the nanocomposite. In addition, it was also found that the electrical conductivity of the CNR processed 12 wt.% xGnP-PA6 nanocomposite is more than ten times higher than the CoR and MCoR processed ones.

Kim, M et al [34] manufactured nanocomposite of polyamide-6 (PA6) and exfoliated graphite nanoplatelets by two coagulation and melt spinning process. Two types of xGnPs and acid-treated xGnPs were utilized in this research. The experimental results showed tensile modulus of the nanocomposite fibers improvement by increasing draw ratio (DR) between the first and second take-up rollers of a fiber spinning system during melt spinning process. The modulus improvement of nanocomposite fibers seemed to have been resulted from both the tensile modulus improvement of PA6 and enhancement of xGnP network in the stretched fibers and about the functionalization, acid-treatment might improve interfacial bonding between xGnP and PA6 matrix.

2.5. References

1. Anya Kuznetsova, Douglas B. Mawhinney, Viktor Naumenko, John T. Yates Jr.,), J. Liu, R.E. Smalley. Enhancement of adsorption inside of single-walled nanotubes: opening the entry ports. *Chemical Physics Letters* Volume 321, Issue 3-4, 28 April 2000, Pages 292-296.

2. Douglas B. Mawhinney, Viktor Naumenko, Anya Kuznetsova, John T. Yates Jr.,), J. Liu, R.E. Smalley. Surface defect site density on single walled carbon nanotubes by titration. Chemical Physics Letters Volume 324, Issue 1-3, 30 June 2000, Pages 213-216.

3. *Hu, H., Bhowmik, P., Zhao, B., Hamon, M.A., Itkis, M.E., Haddon, R.C.* Determination of the acidic sites of purified single-walled carbon nanotubes by acid-base titration. *Chemical Physics Letters* Volume 345, Issue 1-2, 7 September 2001, Pages 25-28

4. *Hamon, M.A., Chen, J., Hu, H., Chen, Y., Itkis, M.E., Rao, A.M., Eklund, P.C., Haddon, R.C.* Dissolution of single-walled carbon nanotubes. *Advanced Materials* Volume 11, Issue 10, 9 July 1999, Pages 834-840.

5. *Chen, J., Hamon, M.A., Hu, H., Chen, Y., Rao, A.M., Eklund, P.C., Haddon, R.C.* Solution properties of single-walled carbon nanotubes. *Science* Volume 282, Issue 5386, 2 October 1998, Pages 95-98.

6. *Bandow, Shunji, Rao, A.M., Williams, K.A., Thess, A., Smalley, R.E., Eklund, P.C.* Purification of single-wall carbon nanotubes by microfiltration. *Journal of Physical Chemistry B* Volume 101, Issue 44, 1 January 1997, Pages 8839-8842.

7. *Paredes, J.I, Burghard, M*. Dispersions of individual single-walled carbon nanotubes of high length. *Langmuir* Volume 20, Issue 12, 8 June 2004, Pages 5149-5152.

8. *Duesberg, G.S., Muster, J., Krstic, V., Burghard, M., Roth, S*. Chromatographic size separation of single-wall carbon nanotubes. *Applied Physics A: Materials Science and Processing* Volume 67, Issue 1, 1998, Pages 117-119.

9. *Sáfar, G.A.M. , Ribeiro, H.B., Malard, L.M., Plentz, F.O., Fantini, C., Santos, A.P., de Freitas-Silva, G., Idemori, Y.M*. Optical study of porphyrin-doped carbon nanotubes. *Chemical Physics Letters* Volume 462, Issue 1-3, 1 September 2008, Pages 109-111.

10. *Tan, Y., Resasco, D.E*. Dispersion of single-walled carbon nanotubes of narrow diameter distribution. *Journal of Physical Chemistry B* Volume 109, Issue 30, 4 August 2005, Pages 14454-14460.

11. *Zhang, X., Sreekumar, T.V., Liu, T., Kumar, S*. Properties and structure of nitric acid oxidized single wall carbon nanotube films. *Journal of Physical Chemistry B* Volume 108, Issue 42, 21 October 2004, Pages 16435-16440.

12. *Zhang, Y. , Shi, Z., Gu, Z., Iijima, S*. Structure modification of single-wall carbon nanotubes. *Carbon* Volume 38, Issue 15, 2000, Pages 2055-2059.

13. Datsyuk, V., Kalyva, M., Papagelis, K., Parthenios, J., Tasis, D., Siokou, A., Kallitsis, I., Galiotis, C. Chemical oxidation of multiwalled carbon nanotubes. Carbon Volume 46, Issue 6, May 2008, Pages 833-840.

14. Kumar, I., Rana, S., Rode, C.V., Cho, J.W. Functionalization of single-walled carbon nanotubes with azides derived from amino acids using click chemistry. Journal of Nanoscience and Nanotechnology Volume 8, Issue 7, July 2008, Pages 3351-3356.

15. He, H., Zhang, Y., Gao, C. , Wu, J. Clicked' magnetic nanohybrids with a soft polymer interlayer. Chemical Communications Issue 13, 2009, Pages 1655-1657.

16. Rana, S., Kumar, I., Yoo, H.J., Cho, J.W. Assembly of gold nanoparticles on single-walled carbon nanotubes by using click chemistry.Journal of Nanoscience and Nanotechnology Volume 9, Issue 5, May 2009, Pages 3261-3263.

17. Campidelli, S. , Ballesteros, B., Filoramo, A., Díaz, D.D., De La Torre, G., Torres, T. , Rahman, G.M.A., Ehli, C., Kiessling, D., Werner, F., Sgobba, V., Guldi, D.M., Cioffi, C., Prato, M., Bourgoin, J.-P. Facile decoration of functionalized single-wall carbon nanotubes with phthalocyanines via "click chemistry. Journal of the American Chemical Society Volume 130, Issue 34, 27 August 2008, Pages 11503-11509.

18. Duc Anh Nguyen, Yu Rok Lee, Anjanapura V Raghu, HanMo Jeong, CheolMin Shin and Byung Kyu Kim, Morphological and physical properties of a thermoplastic polyurethane reinforced with functionalized graphene sheet, Polymer International, Volume 58, Issue 4, 2009, Pages 412 417.

19. Peter Steurer, Rainer Wissert, Ralf Thomann, Rolf Mu¨lhaupt, Functionalized Graphenes and Thermoplastic Nanocomposites Based upon Expanded Graphite Oxide, Macromolecular Rapid Communications, Volume 30, Issue 4-5, 18 February 2009, Pages 316-327.

20. Sun, Z., Kohama, S.-I., Zhang, Z., Lomeda, J.R., Tour, J.M, Soluble Graphene Through Edge-Selective Functionalization, Nano Research, Volume 3, Issue 2, February 2010, Pages 117-125.

21. Celik, C., Warner, S.B, Analysis of the structure and properties of expanded graphite-filled poly(phenylene ether)/atactic polystyrene nanocomposite fibers, Journal of Applied Polymer Science, Volume 103, Issue 2, 15 January 2007, Pages 645-652.

22. Mack, J.J., Viculis, L.M., Ali, A., Luoh, R., Yang, G., Hahn, H.T., Ko, F.K., Kaner, R.B, Graphite nanoplatelet reinforcement of electrospun polyacrylonitrile nanofibers, Advanced Materials, Volume 17, Issue 1, 18 January 2005, Pages 77-80.

23. Kyriaki Kalaitzidou, Hiroyuki Fukushima, Lawrence T. Drzal, A new compounding method for exfoliated graphite–polypropylene nanocomposites with enhanced flexural properties and lower percolation threshold, Composites Science and Technology, Volume 67, Issue 10, August 2007, Pages 2045-2051.

24. Jun Bian, Hai Lan Lin, Fei Xiong He, Xiao Wei Wei, I-Ta Chang, Erol Sancaktar, Fabrication of microwave exfoliated graphite oxide reinforced thermoplastic polyurethane nanocomposites: Effects of filler on morphology, mechanical, thermal and conductive properties, Composites Part A: Applied Science and Manufacturing Volume 47, Issue 1, 2013, Pages 72-82.

25. Hui Quan, Bao-qing Zhang , Qiang Zhao , Richard K.K. Yuen , Robert K.Y. Li, Facile preparation and thermal degradation studies of graphite nanoplatelets (GNPs) filled thermoplastic polyurethane (TPU) nanocomposites, Composites Part A: Applied Science and Manufacturing, Volume 40, Issue 9, September 2009, Pages 1506-1513.

26. G Carotenuto, S De Nicola, M Palomba, D Pullini, A Horsewell, T W Hansen, and L Nicolais, Mechanical properties of low-density polyethylene filled by graphite nanoplatelets, Nanotechnology, Volume 23, Issue 48, 7 December 2012, Article number 485705.

27. Xian Jiang, Lawrence T. Drzal, Multifunctional High Density Polyethylene Nanocomposites Produced by Incorporation of Exfoliated Graphite Nanoplatelets 1: Morphology and Mechanical Properties, Polymer Composites, Volume 31, Issue 6, June 2010, Pages 1091-1098.

28. Huang Wu, Lawrence T. Drzal, Graphene nanoplatelet paper as a light-weight composite with excellent electrical and thermal conductivity and good gas barrier properties, Carbon, Volume 50, Issue 3, March 2012, Pages 1135-1145.

29. Hyunwoo Kim, Yutaka Miura, and Christopher W. Macosko, Graphene/Polyurethane Nanocomposites for Improved Gas Barrier and Electrical Conductivity, Chemistry of Materials, Volume 22, Issue 11, 8 June 2010, Pages 3441-3450.

30. Yeh Wang, Huai-B. Tsai, Thermal, Dynamic-Mechanical, and Dielectric Properties of Surfactant Intercalated Graphite Oxide Filled Maleated Polypropylene Nanocomposites, Journal of Applied Polymer Science, Volume 123, Issue 5, 5 March 2012, Pages 3154-3163.

31. Tran Duy Thanh, Ludmila Kapralkova, Jirˇina Hromadkova, Ivan Kelnar, Effect of graphite nanoplatelets on the structure and properties of PA6-elastomer nanocomposites, European Polymer Journal, Volume 50, Issue 1, January 2014, Pages 39-45.

32. Yan Liua, Guisheng Yang, Non-isothermal crystallization kinetics of polyamide-6/graphite oxide nanocomposites, Thermochimica Acta, Volume 500, Issue 1-2, 10 March 2010, Pages 13-20.

33. Liu, W., Do, I., Fukushima, H., Drzal, L.T, Influence of processing on morphology and properties of exfoliated graphite nanoplatelet-polyamide nanocomposites, International SAMPE Symposium and Exhibition (Proceedings), Volume 54, 2009, 11p.

34. Kim, M., Hwang, S.-H., Park, Y.-B, Orientation effect of exfoliated graphite nanoplatelets on mechanical properties of nylon 6 composite fibers, International SAMPE Technical Conference , 2013, Pages 1875-1886.

Chapter 3

3. Experimental section

3.1. Materials

3.1.1. The polymeric matrix: polyamide-6 (PA6)

In this research the utilized polymer in order to compound with graphite, graphene oxide and carbon nanotube (CNT) was polyamide-6 (PA6) which is a techno-polymer and able to accept different kind of fillers to make the final nanocomposite.

The utilized polyamide-6 (PA6) in this research is a commercial polymer (Radilon S35 100 NAT, purchased from Radicinova, Italia) with an intrinsic viscosity (in sulfuric acid) 3.4 dl/g. The properties of utilized polyamide-6 are tabulated in (table 3.1).

Table 3.1) properties of PA6

Density (g/cm^3)	1.13
Strength at break (%)	78
Deformation at break (%)	50
Elastic modulus (MPa)	2000
Flexural modulus (MPa)	2500

3.1.2. Graphite

The applied graphite in this research as filler (flake graphite, very fine powder, grade: Ma-399, carbon content > 99%, flake size > 85%, finer than 45µm = 325 mesh) was purchased from NGS Naturgraphit.

3.1.3. Graphene oxide

Graphene oxide was obtained by a modified oxidation process based on "Marcano's method" that will be described in "graphene oxide preparation" section.

3.1.4. Carbone nanotube (CNT)

Multiwall carbon nanotube (MWCNT, carbon content > 95%, diameter = 6-9 nm, length > 1 μm) was purchased from sigma aldrich.

3.2. Graphene oxide preparation

For this method, a 9:1 mixture of concentrated H2SO4/H3PO4 (360:40 mL) was added to a mixture of graphite flakes (5 g) and KMnO4 (30 g), producing a slight exotherm to 35_40 °C. The reaction was then heated to 50 °C and stirred for 18 h. The mixture was cooled to room temperature and poured onto ice bath (~400 mL), with 30% H2O2 (3 mL) and then filtered through polyester fiber (0.22 μm). The filtrate then was centrifuged (5500 rpm for 15 min each time), and the supernatant was removed out. The remaining solid material was then eluted in succession with distilled water (20 ml), HCl 30% (200 ml), and ethanol (200 mL) (2×). The solid remained on the filter was vacuum-dried overnight at room temperature. A mixture of HCl 30% (162 ml) and distilled water (38 ml) was added to as dried material and sonicated for 5 minutes to break down the concreted solid materials. In continue the mixture was centrifuged (5500 rpm for 15 min each time) and after finishing and gathering precipitated particles, distilled water was added to wash the material and repeated the centrifuge procedure again to remove the presence of distilled water. For the last time operation of washing and centrifuge by ethanol (2×) was repeated and then, remained material was dried in the oven (80°C). One day later remained material was dissolved into ether (100 ml) and then the suspension was put onto the vacuum-filtrate. 5 days later the remained material on the filtrate was gathered.

3.3. Nanocomposites preparation

3.3.1. Processing

In order to prepare nanocomposites three different methods including 1.melt blending, 2.solvent castiong and 3.solvent/melt blending method (consist of solvent pretreatment and melt blending method in continue) were followed.

A. Solvent casting method

In the first step polyamide-6 (15g) was dissolved within acid formic (100mL) under heating (100°C) and magnetic stirring (5rpm) conditions in a flask. In the same time graphene oxide (0.075g) was exposed to formic acid and tried to break down the agglomerated graphene oxide particles and obtaining a homogeneous mixture by ultrasonication (30 min) in the other flask. After dissolving the whole of polyamide-6 within acid formic, the mixture of acid and polymer was poured into the other flask containing graphene oxide and formic acid mixture and ultrasonicated for the second time (30 min).

The final ultrasonicated mixture of formic acid/ polyamide-6/ graphene oxide was poured into the crystallizer flask, heated (100°C) and stirred magnetically over night. In order to remove all residual acid, rinsing step was started inside the crystallizer under magnetic stirring within distilled water just after evaporating formic acid and remaining the composite of polyamide-6/ graphene oxide at the bottom of crystallizer. This step (rinsing with distilled water) was repeated every 15 minutes by discarding water and adding clean water. In the end by measuring the PH of the last discarded distilled water after 48 hours we became sure that nanocomposite must be clean of formic acid.

B. Melt blending method

The blends were done in a discontinuous internal mixer (Brabender, model PLE 330) that posse a mixing box with 50 cm^3 volume capacity (figure 3.1). The temperature in two area are monitored consist of interior and

exterior walls. During the process, applied torque was measured by two rotational screws and allowed us to have information about melt viscosity and any modified products of the process such as (melting, ramification, degradation, etc.). By linking the system to a computer we were able to have the graphics consisting of processing time, processing temperature and applied torque. The principal parameters in order to set up the processing are: temperature, time, the velocity of blending that is a function of screws rotating speed and the ratio of loading the blending box. In order to investigate the effect of processing time and the consequences of that over the final product, four different processing times (4, 6, 9 and 15 minutes) were applied. The processing temperature was set up on 240°C for polyamide-6 and velocity of the screws also was fixed on 100 rpm.

After reaching the temperature 240°C, the screws velocity was tuned on 20 rpm and the blending box slowly was loaded by polyamide-6 and then the rotational speed of the screws was increased in 100 rpm and at the end, the inlet of the blending box was closed. At the end of first minute the screws velocity was lowered to 20 rpm and filler (graphite, MWCNT, graphene oxide) or PA6/graphene oxide was inserted into the blending process and again the velocity was increased to 100 rpm. In order to avoid of thermal degradation, after finishing the process there was just about 2 minutes time to remove the whole of molten nanocomposite from the blending box.

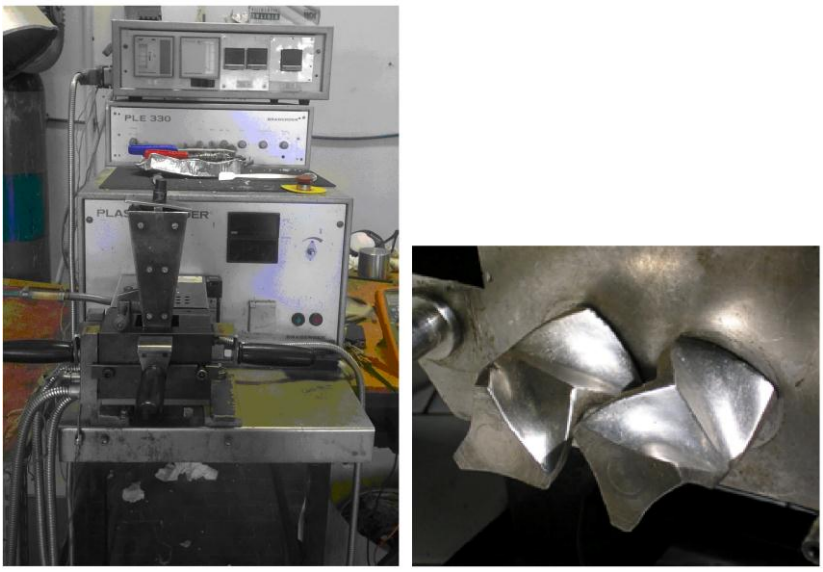

Figure 3.1) Discontinuous internal mixer (brabender) and its twin screws

C. Solvent/ melt blending method

This method was a combination of above mentioned methods and in the first step started with preparing a masterbatch based on solvent casting method and was followed with melt blending method. In the second step polyamide-6 was molten in the internal mixer and then at the end of first minute as prepared masterbatch was added into the internal mixer (containing molten polyamide-6). In continue processing time was followed without change.

All the prepared composites regarding their processing method, time, filler type and percentage are listed in (table 3.2-4)

Table 3.2) PA6/graphite preparation conditions

The composite	Processing time (minute)	Processing method
1. PA6/graphite (0.5%)	4	Melt blending
2. PA6/graphite (0.5%)	6	Melt blending
3. PA6/graphite (0.5%)	9	Melt blending
4. PA6/graphite (0.5%)	15	Melt blending
5. PA6/graphite (1%)	6	Melt blending
6. PA6/graphite (2%)	6	Melt blending

Table 3.3) PA/GO preparation condition

The composite	Processing time (minute)	Processing method
1. PA6/GO (0.5%)	4	Melt blending
2. PA6/GO (0.5%)	6	Melt blending
3. PA6/GO (0.5%)	9	Melt blending
4. PA6/GO (0.5%)	15	Melt blending
5. PA6/GO (0.75%)	6	Melt blending
6. PA6/GO (1%)	6	Melt blending
7. PA6/GO (2%)	6	Melt blending
8. PA6/GO (5%)	6	Melt blending

The composite	Processing time (minute)	Processing method
1. PA6/GO (0.5%)	-	Solvent casting
2. PA6/GO (2%)	-	Solvent casting
3. PA6/GO (5%)	-	Solvent casting

The composite	Processing time (minute)	Processing method
1. PA6/GO (0.5%)	6	Solvent/melt
2. PA6/GO (0.75%)	6	Solvent/melt
3. PA6/GO (1%)	6	Solvent/melt
4. PA6/GO (2%)	6	Solvent/melt
5. PA6/GO (5%)	6	Solvent/melt

Table3.4) PA6/MWCNT preparation condition

The composite	Processing time (minute)	Processing method
1. PA6/MWCNT (0.5%)	4	Melt blending
2. PA6/MWCNT (0.5%)	6	Melt blending
3. PA6/MWCNT (0.5%)	9	Melt blending
4. PA6/MWCNT (0.5%)	15	Melt blending
5. PA6/MWCNT (1%)	6	Melt blending
6. PA6/MWCNT (2%)	6	Melt blending

3.3.2. Compression molding and sample preparation

The obtained composites from Brabender was milled and sieved to become uniform in size and easy for compression molding (figure 3.2). The compression consists of two plates which are able to be tuned to have desired temperate (240°C) by electricity and that is where the cast (with different shapes) containing material was settled there (figure 3.3). In order to make easy the operation of extracting the compressed material from the cast, it was used two Teflon sheets over on the both sides of the cast in

contact with mediator plates (between the compression plates and the cast). The compressing time also was set about 2 minutes to avoid of any probable thermal degradation and having enough time to shape the samples. It must be reminded that, because of the hydrophilic nature of polyamide-6, putting into the oven for 12 hours before compressing operation is necessary (figure 3.4).

Figure 3.2) Electrical mill

Figure 3.3) Compression molding

Figure 3.4) Vacuum oven

3.4. Characterization

3.4.1. Raman analysis

Raman microscopes are more widely used to characterize elementary structure of the materials respect to other types of Raman instruments. Raman microscopes are able to examine the surface of different materials by focusing the laser beam and do not need to any special sample preparation and the surface is enough to be just pollution free. In fact Raman microspectroscopy (often called micro-Raman), is a dispersive instrument like other kinds of Raman instruments. Raman microscopy needs to collect spectrum for each wavenumber individually. Raman instruments include the following elements:

- Laser source
- Sample illumination and collection system
- Spectral analyzer
- Detection and computer control and processing system

There is a laser source that can provide monochromatic light for Raman microscopy. The laser source generates continues wave-laser and it differs from pulsed-laser. The laser source must generate laser beam in visible light range or at least near to this range. Both sample illumination and collection steps are done in the microscope. The Raman spectrum in this microscope is obtain by the optical system and this is the difference between the micro-Raman and conventional Raman instrument.

- Laser Source:

The most common laser sources nowadays are gas continuous-wave lasers such as Ar+, Kr+ and He–Ne. these types of laser sources have the capability to generate beams in multiple wavelengths. 515.4, 488.0 and 350.7 nm is the highest intensity wavelengths which are applicable. Therefore, it is necessary to filter out other wavelengths. Both on the other

side, the He Ne laser, generate beams with mor narrow wavelength (632.8 nm). Gas laser sources are capable to generate high laser power, but the laser power reaching the microscopic area of the sample must be just about a few mW.

- Microscope System:

The emitted laser beams from the beam source at first are filtrated to obtain a monochromatic wavelength and then, a pinhole spatial filter purifies it with removing noises from around the focused spot to have a clean point laser beam to illuminate the sample. this technique ensures that the only light coming from the microscopic area and sample will be transmitted to the detector . Two pinhole spatial filters play important roles sample illumination and Raman light collection. The pinhole spatial filters do it by eliminating stray light and noises coming from out of the sample. In confocal arrangement of the filters, it is possible to reach 1μm spatial resolution once a 100 × objective lens is exerted.

- Prefilters:

The emitted light from the microscope pass through special filters just before reaching the spectral analyzer to get purified more. In and ideal case the filter consists of a ‘notch’ feature that is zero transmission in a narrow wavenumber range located on an exciting laser wavenumber.

- Diffraction Grating:

This part is the most important part of the spectral analyzer in the Raman microscope and disperses Raman scattered light based on its wavenumbers. The diffraction grating disperses the scattered light by diffracting in a discrete direction. In some models one diffraction grating is able to a wide range of 1000 wavenumbers. In a modern Raman microscope, the diffraction grating rotates constantly with respect to the scattered light and in the same time separates the wavenumbers.

- Detector:

A detector made from photoelectric materials separates the Raman scattered light respect to its wavelength. The task of the detector is converting photon signals to electric signals. Nowadays this part of the Raman microscopes is often multi-channel and solid-state. The most commonly used detector in current Raman microscopes is the charged-coupled device (CCD) which is a silicon-based semiconductor. Light intensity of discrete wavelengths is detected and recorded by a one-dimensional array of a CCD. Computer processing is responsible for calculating and plotting the Raman shift versus wavenumber in the spectrum.

This is normal and in fact usual that or impurities in samples absorb laser radiation and then emit it again as fluorescence. For example the intensity of fluorescence in some cases is as much as 104 times higher in comparison with a Raman scattered light. The fluorescence problem is the main bug in using Raman spectroscopy and can completely mask the Raman spectroscopy.

Raman spectroscopy can be considered as an interesting characterization technique to examine ceramics and polymers because its ease to examine them by illuminating the samples surface and thickness or even form of the sample are not important parameters.

Raman microscopy is used for materials characterization, including:

- Phase identification of polymorphic solids;
- Polymer identification
- Composition determination
- Determination of residual strain
- Determination of crystallographic orientation

In this research Raman spectra were obtained by a micro Raman spectrometer Bruker SENTERRA at the room temperature with excitation in the visible band. The laser source worked with frequency diode of ν_0 = 532 nm that was companied with maximum potential 20 mW. The exerted

parameters for obtaining the spectra of graphite and graphene oxide are: lens 20x, small split 50x1000μm, spectra resolution 9-15 cm^{-1}, power 20 mW. The time of investigation of CCD was defined from time to time.

3.4.2. X-ray spectroscopy (XPS) analysis

XPS spectra were recorded by an instrument of Perkin-Elmer PHI 5600 that utilizes one standard A1 source with power 300mW and applied voltage 15 kV. The pressure during the experiment was about 3-4 x 10^{-9} mbar.

The circumstance of preparing a photoelectron spectrometer is briefly introduced in the following way: the ionization source (in this case source X-ray) is utilized to irradiate the sample. Because of the nature of this process (ionization), the sample starts emitting electrons through an appropriate slit to reach to an electrostatic analyzer of kinetic energy. The selected photoelectrons by analyzer are introduced to another slit in detector where amplifiers that into the stranger electronic signals for exhibiting by a software. All the system works under ultra vacuum (10^{-9} Pa). High vacuum required for working is directly related to two facts: minimizing the problem of collision between emitted electrons and gas electrons (avoiding of loosing electrons and loosing sensibility consequently) and avoid of superficial pollution (in case of extra vacuum, required time for obtaining is much longer than operation of obtaining photoelectronic signals). The instrument consists of:

- an X-ray source
- Mg and Al anodes
- an enclosure for the sample
- detector (hemispherical analyzer)
- ion source for sputtering and the pumping system

The spectrometer was calibrated by assuming the binding energy (BE) of Au peak 4f7/2 84.0 eV respect to Fermi level.

The extended spectra were recorded in an energy interval equal to 0-1350 eV, 0.025 s.step^{-1} (needed time for obtaining each canal). Spectra detail in high resolution were obtained for each single region with the following parameters: 11.75 eV pass energy, 0.2 eV step, 0.1 s.step^{-1}; in extra resolution with the following parameters: 5.75 eV pass energy, 0.05 eV step, 0.2 s.step^{-1}. Determined standard deviation for the values of BE of XPS spectra, by measuring cooper are equal to 0.05 eV. The atomic percentage was calculated by the factors of sensibility PHQ after subtraction. At the end the fitting of experimental data was performed by functions of Voight.

3.4.3. X-ray diffractometry (XRD)

X-ray diffractometry (XRD) is the most common X-ray diffraction technique in materials characterization and principally is used to examine the crystal structure of samples; therefore it is called commonly X-ray powder diffractometry. By a constant change in the emitted angle of the X-ray beam, we can obtain a spectrum of diffraction intensity versus the angle. It must be mentioned that this angle is between incident and diffraction beam is recorded.

- Bragg's law:

Crystallographic planes crystalline solid diffracts incidences X-ray beams. Beam 1 and beam 2 as two in-phase incident (phase difference of $n\lambda$ between two light waves with the same wavelength and in the same moving direction) waves, are deflected by two crystal planes (A and B). It must be considered that, the deflected waves will not be in phase except when below relationship is right.

$$n\lambda = 2d \sin\theta \quad \text{equation (3.1)}$$

Equation (3.1) must be looked as the basic law of diffraction called *Bragg's Law*. Bragg's Law is obtained by a simple calculation of the path

differences between the two beams. The path difference also depends on two other variables: the incident angle (θ) spacing between the parallel crystal planes (d).

- Instrumentation:

Detecting X-ray diffraction in materials is the main task of diffractometer that just does it by recording the diffraction intensity as a function of the diffraction angle (2θ). An X-ray tube generates the radiation and passes that through some special slits that must collimate the beam. Mostly soller slits are used in the laboratory diffractometers. soller slits usually consist of thin metal plates parallel to the figure plane to preserve beam in the right direction perpendicular to the figure plane. In fact a divergent beam strikes the specimen right after passing through the slits. The physical state of specimen must be in the flat form and fixed on specimen table X-rays are diffracted by the striked specimen that in continue make a convergent beam at receiving slits just before reaching to the detector. A detector can receive the diffracted beam in condition that beam past earlier through a monochromatic filter. It must be mentioned that usually, the monochromatic filter location is in the diffracted beam path. The main reason of this arrangement is filtering wavelengths out of Kα radiation and also minimizing the background radiations which come from the specimen. Nowadays diffractometers usually consist of a graphite crystal monochromator that is specified for diffracting a single wavelength that works in function of Bragg's Law. In order to record diffraction intensity in the desired range of 2θ it is necessary to have a relative movement in X-ray tube, fixed specimen on the path and the detector. *Bragg–Brentano arrangement* is the most common arrangement between diffractometers that insteat of the X-ray incident beam rotating, the sample stage rotates around the axis perpendicular to the figure plane and it provides the incident angle change.

A diffractometer records changes of diffraction intensity with 2θ. The starting point for recording of diffraction intensity usually is a very low 2θ

angle about 5° and the ending point is about 65°. Nowadays, all the operation of data acquisition/treatment and spectra drawing are majorly done by a computer.

In this research a SIEMENS D-500 diffractometer with an internal angle between 50-60°C and variation (5°/min) was exerted for examining the crystal structure of graphite, graphene oxide, polyamide-6 and other nanocomposites.

3.4.4. Morphological analysis (SEM)

Morphological analysis on the nanocomposites was performed via a scanning electron microscopy (SEM) FEI Quanta 200 ESEM. The specimens were prepared by putting into the liquid Nitrogen and making them fragile enough to break and reach to a smooth plane.

The scanning electron microscope (SEM) is the most common microscope to observe the microscopic structure of the materials. SEM investigates microscopic structure by scanning the surface of materials with high resolution and depth of field in comparison with confocal microscopes. In order to form a SEM image the specimen surface must be scanned by focused electron beam. Because of large depth of field in sample scanning we can have three dimensional images from specimens. For example, this is normal that the depth of field reaches to tens of micrometers at 103 × magnification and in the same time the order of micrometers at 104 × magnification. We can obtain chemical information from a specimen by using some kind of techniques, which consist the X-ray energy dispersive spectrometer (EDS) we can.

- Instrumentation:

Electron gun and a series of electromagnetic lenses are the main parts of a scanning electron microscope. The emitted electrons must be first condensed to a fine probe for surface scanning. In some SEMs it is preferred to use a field emission gun because of its advantage in beam

brightness. In current SEMs the regular acceleration voltage of 1–40 kV is applied to generate an electron beam. Condenser lenses and one objective lens all perform the optical path of a SEM. the condenser lenses are responsible to lower the crossover diameter of the electron beam; and then, the objective lens focuses the electron beam with a nanometer scale. In order to have Probe scanning it is necessary to have a beam deflection system incorporated within the objective lens in the optical system of SEM. The probe is moved by the deflection system on the surface of specimen in a straight line and then moves the probe to a coordinate on the next line to scan; therefore a rectangular raster is created on the surface of specimen. The detector collects and amplifies the emitted signal electrons from the specimen and at last use used to reconstruct an image. In order to have a point-to-point image on the display screen the electron signals coming from each pixel of the raster must be collected by the detector.

3.4.5. Mechanical analysis (tensile test)

Tensile test deals with elastic modulus, strength and deformation at break. Tensile test was performed on the prismatic samples with rectangular section, with length of 90 mm, width of 10 mm and thickness of 0.3-0.5 mm by an Instron 3365 apparatus (figure 3.5). In this experiment the optimum distance between the both upper and lower grips must be 30 mm and it equals to having exactly 30 mm of the sample in each grip. The test is started with an initial velocity of 1 mm/min and ended by sample breaking while velocity has been reached to 100 mm/min. each test was repeated between 10-15 times on each material to guarantee the accuracy of the later calculations.

Figure 3.5) tensile test instron 3365 apparatus

3.4.6. Dynamic mechanical thermal analysis (DMTA)

Dynamic mechanical thermal analysis (DMTA) is an efficient examining instrument that permits evaluating the mechanical respond of a viscoelastic material under a sinusoidal deformation. In fact, this technique allows measuring of the intrinsic properties of materials, such as: tendency of the elastic modulus in function of temperature, the temperature of glass transition corresponding to other molecular movement resulted from the molecules mobility in presence of other molecular groups. The fundamental of the analysis is based on this fact that, whenever polymer is under dynamic-mechanical analysis, in response to each relaxation phenomenon expresses a specific molecular motion that dissipates the mechanical energy. Loss modulus E", and tan δ exhibit the maximum, but storage elastic modulus E' is a moment component.

In this research dynamic mechanical thermal analysis (DMTA) was done by a DMTA V RHEOMETRIC SCIENTIFIC (figure 3.6). This instrument was selected to test the nanocomposites based on PA6 for dynamic flexural test

in single cantilever mode. The samples (thickness 4mm, length 35 mm, width 8 mm) were mounted inside both mechanical grips with a slight traction. After putting the sample inside the grips we can close the entrance of enclosure and let the Nitrogen to get into the enclosure and isolate that thermally from the outer ambient. Experiment was carried out in *temperature sweep* mode with temperature from 30 and 180°C with heating rate 5° C/min. the maximum applied deformation on the sample was 0.1%, frequency was set on 1 Hz (6.28 rad/s). Tendency of conserved modulus E' and tan δ were transported in a graphic in function of temperature.

Figure 3.6) Dynamic mechanical thermal analysis (DMTA) apparatus

3.4.7. Differential scanning calorimetry (DSC)

Differential scanning calorimetry (DSC) is considered as the most regular thermal analysis technique. With this technique we can monitor thermal events in a material without any mass exchange by heating and cooling. Four different thermal events are examined by DSC such as: solid phase transformation, glass transition, crystallization and melting. By 'differential' we mean analysis is based on differences between sample material and a reference material in which does not have any thermal event.

There are two common DSC systems including: the power-compensated DSC and flux DSC and the. The heat flux DSC measures the temperature difference directly and then converts it to heat flow difference and that is why this type of DSC is known ‘quantitative DTA’ . An algorithm in computer software accomplishes this conversion. But in the other hand the power-compensated DSC directly measures the enthalpy change of a sample during heating and cooling. There are two separate chambers (power-compensated DSC), to put the sample and reference and each chamber possess a separate heat element to control temperature.

The equipment always keep a state with thermal null ($\Delta T=0$). Whenever there is a thermal event in the sample, a different applied power is required for heating element to keep the sample temperature in the same state with reference. When the sample starts to earn more heat, the system must apply more energy and we have an endothermic event while for cooling the sample lower energy must be applied by the system and it means an exothermic event. There is a proportion between the amount of power change energy of heat flow to compensate that must be equal for the heat release or gain of the sample.

Sample preparation: Samples for DTA or DSC should be in the form of dense powder or small discs. Film, sheets and membranes are often cut into discs fitting into the sample pans.

Effects of Scanning Rate: DSC equipment works usually are with a temperature range with a constant heating or cooling rate because thermal events measurement is under influence of the rate of scanning through a temperature range and more scanning rate can change the curve position and style and characteristic temperature included in a curve.

Transition Temperatures: Measuring transition temperatures is the first objective of DSC. The most known transitions are glass transition, melting and crystallization.

Measurement of Enthalpy Change: peak area of a DSC curve is important to measure the enthalpy change of phase transformation.

- Applications:

This technique is so useful to characterize polymeric materials, as well as characterization of inorganic materials. But there are two main applications for this technique including:

1. Determination of Heat Capacity
2. Determination of Phase Transformation and Phase Diagrams

In this research a PERKIN ELMER Differential Scanning Calorimetric DSC7 equipped with a thermal Analysis Controller TAC 7/DX was utilized to analyze thermal respond of nanocomposites (figure 3.7). The heating and cooling cycles were arranged on 4 cycles including two heating and cooling cycles. The operation is started from 30°C and is concluded at 250°C, then temperature decreases to reach to the initial temperature (30°C) and then again this cycle is repeated. It must be mentioned that heating rate in his test is 10 °C/min. having two cooling and heating cycles is recording the real response of the polymer.

Figure 3.7) Differential scanning calorimetric (DSC) apparatus

3.4.8. Rheological analysis

Rheological characterization was performed with by measuring complex viscosity, storage modulus G' and loss modulus G". For this aim, a rotational rheometer with two parallel plates with 25 mm diameter for each plate was utilized. In the rheometer the upper plate is in direct contact with the engine that imposes a rotational movement with different frequencies on the plate (and the sample consequently) while the other plate is fixed in its place and is inked to torque and normal strength transducer. Sample and holder are kept inside an enclosure made of ceramic which allows imposing a specific temperature and having a thermal cycle (figure 3.8).

Viscosity is obtainable from the required torque to maintain the rotation of the first plate. Along forming the molten thickness of the polymer, as a result of dragging motion, a straight velocity profile is created that comes from the fixed plate to the rotating plate and results to a velocity gradient of deformation. By conducting the test in an area with different frequencies we can calculate the tendency of viscosity at varying shearing rate. The flow curvature permits obtaining important information about molecular characteristics of the polymers.

The experiment was performed with a rheometer G2 ARES in the following mode: oscillation frequency, applied temperature 240°C, strain 10.0%, angular frequency 0.1-500.0 rad/s, points per decade 5.

Figure 3.8) Rheological analyzer apparatus (G2 ARES)

3.4.9. Artificial weathering (Q-UV) experiment

Artificial weathering is an efficient technique that simulates natural degradation of the polymers in terms of duration and time stability of the samples. Pure polyamode-6 and nanocomposites of polyamide-6/ graphene oxide prepared with different methods were subjected to Q-UV test for 0, 10, 24, 48 and 96 hours. This experiment was conducted in a special instrument (Q-UV panels) which copies artificially atmospheric phenomena that are mainly important in film degradation (figure 3.9). The damage caused by exposure to the solar light is simulated by means of eight fluorescent lamps which emit UV-B radiations (280-320 nm) arranged in two series by four sides of the radiation chamber. Raining and other involved phenomena in natural condensation, are simulated by a mechanism of artificial condensation obtained by water evaporation from a tank which is heated by UV lights and after evaporation provides the relative humidity of the chamber. The machine performs an accelerated aging at controlled temperature and UV exposure in 24 hours cycles. UV frequency, in

particular UV-B was constituted about 5% of the entire solar spectrum is very harmful and responsible in fact for photochemical damages and leads to degradation of the films. Therefore exclusive utilization of UV-B radiations provides a more critical condition for the samples respect to solar radiation and in just few days or weeks the damage that the weather outside cause in months or years. The samples were arranged by means of special frames at a distance of about 5 cm from the lamps on the wall of the room. One side of the sample was exposed to the temperature of the room and the rear was exposed to the ambient temperature allowing cooling the sample surface by a few degrees below the temperature of the steam. This temperature difference provokes the condensation of vapor on the surface of the samples.

The weathering conditions were 8 h of light at T=55°C and 4 h of condensation at T=45°C.the specimens were exposed up to about 96 h.

Figure 3.9) Accelerated weathering test apparatus

3.4.10. Attenuated total reflectance infrared spectroscopy (ATR-FTIR)

Infrared (IR) spectroscopy is an extremely reliable and well known fingerprinting method that is able to be used for characterization, identification and also quantification of many substances. IR is able to use an analytical technique to obtain spectra from a very wide range of solids, liquids and gases however in many cases some form of sample preparation is required in order to obtain a good quality spectrum. Traditionally IR spectrometers have been used to analyze solids, liquids and gases by means of transmitting the infrared radiation directly through the sample. Where the sample is in a liquid or solid form the intensity of the spectral features is determined by the thickness of the sample and typically this sample thickness can not be more than a few tens of microns. The technique of Attenuated Total

Reflectance (ATR) has in recent years revolutionized solid and liquid sample analyses because it combats the most challenging aspects of infrared analyses, namely sample preparation and spectral reproducibility.

Principles of ATR:

An attenuated total reflection accessory operates by measuring the changes that occur in a totally internally reflected infrared beam when the beam comes into contact with a sample.

An infrared beam is directed onto an optically dense crystal with a high refractive index at a certain angle. This internal reflectance creates an evanescent wave that extends beyond the surface of the crystal into the sample held in contact with the crystal. In regions of the infrared spectrum where the sample absorbs energy, the evanescent wave will be attenuated or altered.

The attenuated energy from each evanescent wave is passed back to the IR beam, which then exits the opposite end of the crystal and is passed to the detector in the IR spectrometer. The system then generates an infrared

spectrum. For the technique to be successful, the following two requirements must be met:

- The sample must be in direct contact with the ATR crystal, because the evanescent wave or bubble only extends beyond the crystal 0.5 μ - 5 μ.
- The refractive index of the crystal must be significantly greater than that of the sample or else internal reflectance will not occur – the light will be transmitted rather than internally reflected in the crystal.

Chapter 4

4. Results and discussion

4.1. Graphene oxide structural analysis

4.1.1. X-ray diffractometry (XRD) analysis

Graphite flakes showed a sharp and intensive peak (2θ= 26.7°) corresponding to an interlayer spacing (0.342 nm) and other weak peak is attributed to an interlayer spacing (0.169 nm) this assure us that graphite flakes have a crystal structure that consist of a lot of graphene layers which are on each other (figure 4.1). But after oxidation the peak was shifted to lower degree (2θ= 10.6°) that is attributed to interlayer spacing improvement (~0.94 nm) and proves a successful expansion which happened among graphene layers, because of functional groups and also this expansion decrease the degree of crystallinity in lattice structure. XRD pattern of GO shows very less intense peak (~24.4°), indicates the distorted graphite structure and hence suggests the formation of graphene sheets. All these changes are corresponded to the results of previous studies on graphite oxidation [1-6].

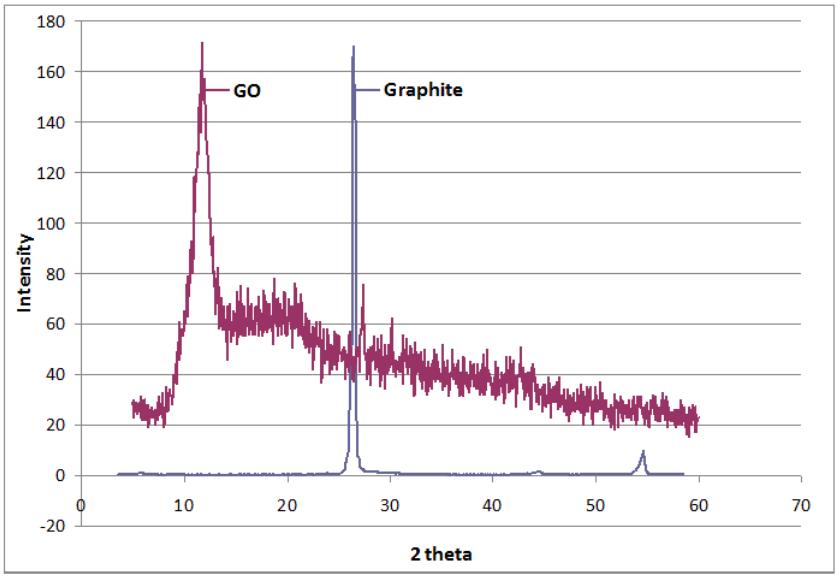

Figure 4.1) XRD patterns of graphite (blue), GO (red)

In continue and after fabricating the composites of polyamide-6 and different fillers such as graphite flakes and graphene oxide via different preparation techniques such as melt blending, solvent casting and solvent/melt blending, XRD characterization was repeated to discover the effect of preparation method and filler type on the crystalline structure of polymer. Polyamide-6 is known as a semicrystalline polymer which consists two α and ɣ-form crystals with different percentages depending on the filler contents and preparation methods. XRD results prove that pure polyamide-6 contains two obvious peaks first α-form crystal containing $\alpha_{(200)}$ $2\theta=20.4°$, $\alpha_{(002,\ 220)}$ $2\theta=23.8°$ peaks and second, ɣ-form crystal containing $\gamma_{(100.010)}$ $2\theta=21.45°$ and $\gamma_{(002)}$ $2\theta=10.8°$ which appear not here (figure 4.2). Practically α crystalline phase is thermodynamically more stable whereas ɣ crystalline phase is kinetically favored and this is supposed because to be in influence of polymer chains which in α –form is folded while in ɣ-form is not. As it seems pure polyamide-6 exhibit more α crystalline phase and the presence of ɣ-form crystals are not evident. In the composite prepared by melt blending technique of polyamide-6 and graphite with 0.5 vol%, graphite content inside the polymer exhibits its sharp and intensive peak ($2\theta= 26.7°$) corresponding to an interlayer spacing (0.342 nm) and it confirms that multilayer structure of graphite remained totally untouched. On the other hand in nanocomposites of polyamide-6 and graphene oxide with the same volume filler content prepared via either melt blending, solvent casting and solvent/melt blending techniques, expanded structure of graphene oxide was disrupted and graphene oxide sheets successfully dispersed within matrix. It must be mentioned that presence of either graphite or graphene oxide in 0.5 vol% does not influence the crystalline form of polyamde-6 and α-form crystals are still dominant and theses results are in agreement with other layered nanofillers in other similar researches and it will confirm in continue with DSC results[7-9].

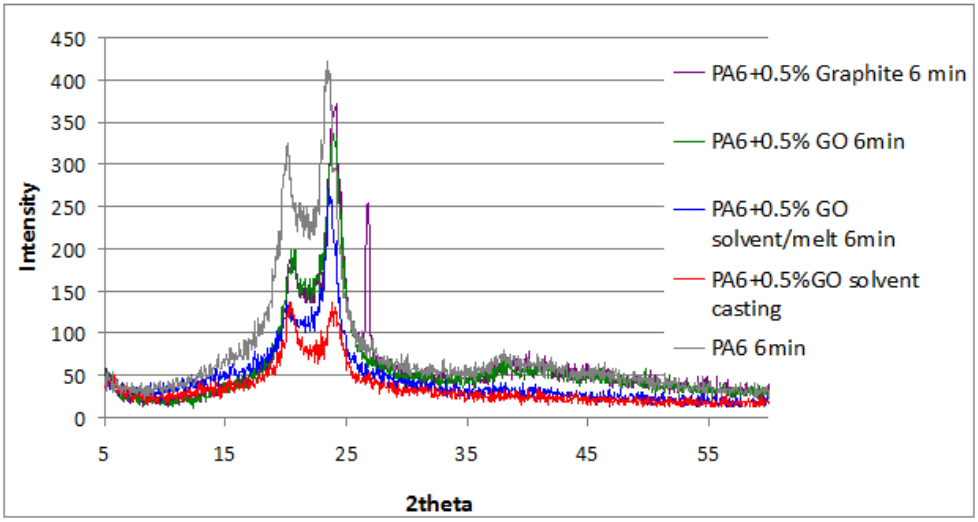

Figure 4.2) XRD spectra of pure PA6 and its composites in composition with graphite and graphene oxide via different preparation methods.

4.1.2. Raman analysis

As it seems, graphite band consists of G (1570.5 cm-1), D (1355 cm-1) and 2D (2713.5 cm-1) peaks which are attributed to SP^2 covalent C=C bonds in 2D lattice structure, SP^3 oxygen containing functional groups respectively and in case of 2D peak there is no clear reason (figure 4.3). A standard graphite band must have a sharp and intense G peak and in contrast, wide and weak D peak that all are clear in the presented graphite band. On the other hand D peak has become extremely intensive (almost 10 times more intensive) and obvious with an improvement at ID/IG consequently. This improvement proves an oxidation and presence of carboxyl, hydroxyl, epoxide and other oxygen containing functional groups which were inserted between the graphene layers. As we know functional groups are main reason of any disorder and defects in graphite structure but in the mean time presence of these groups caused to an interlayer expansion and it probably explain an intense D peak in GO. These results are corresponded to other studies by chemical oxidation methods [5, 10-15].

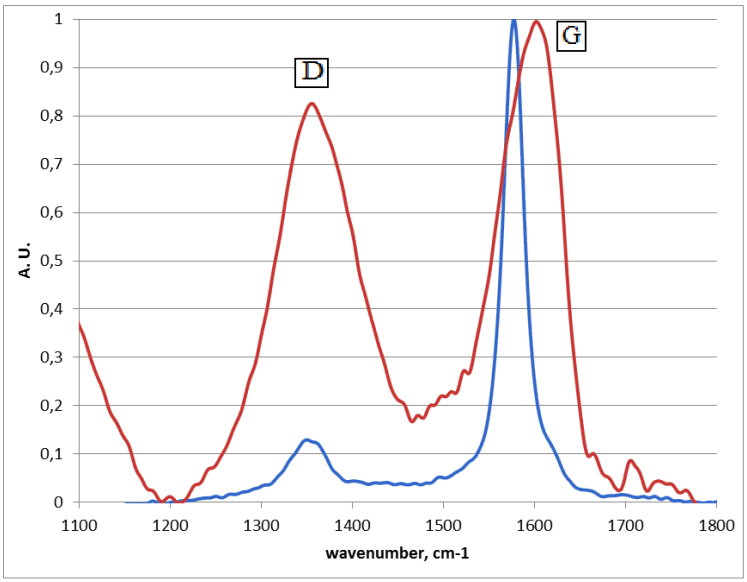

Figure 4.3) Raman spectra of graphite powder (blue), GO (red).

4.1.3. X-ray spectroscopy (XPS) analysis

XPS reveals strong presence of oxygen in graphene oxide while this peak is slightly observable in graphite which is the only difference between them. Graphitic carbon C 1s (C=C) has been located at 284.5 eV. Graphene oxide presents wider peak at 286.6 eV that refers to single bond carbon with oxygen (C-O) and on the other hand the peak at 289.5 eV refers to double bond carbon with oxygen (C=O) and at the end there is a very small peak at 532.2 eV at graphite, that refers to O 1s (ethereal oxygen). Noted results suggest $C_{95}O_5$ formula for graphite and $C_{71}O_{29}$ for graphite oxide that reveal a high level of oxidation which faced on the graphite and confirm the results of EDAX and Raman experiments and also other works (figure 4.4) [8, 12, 16-19].

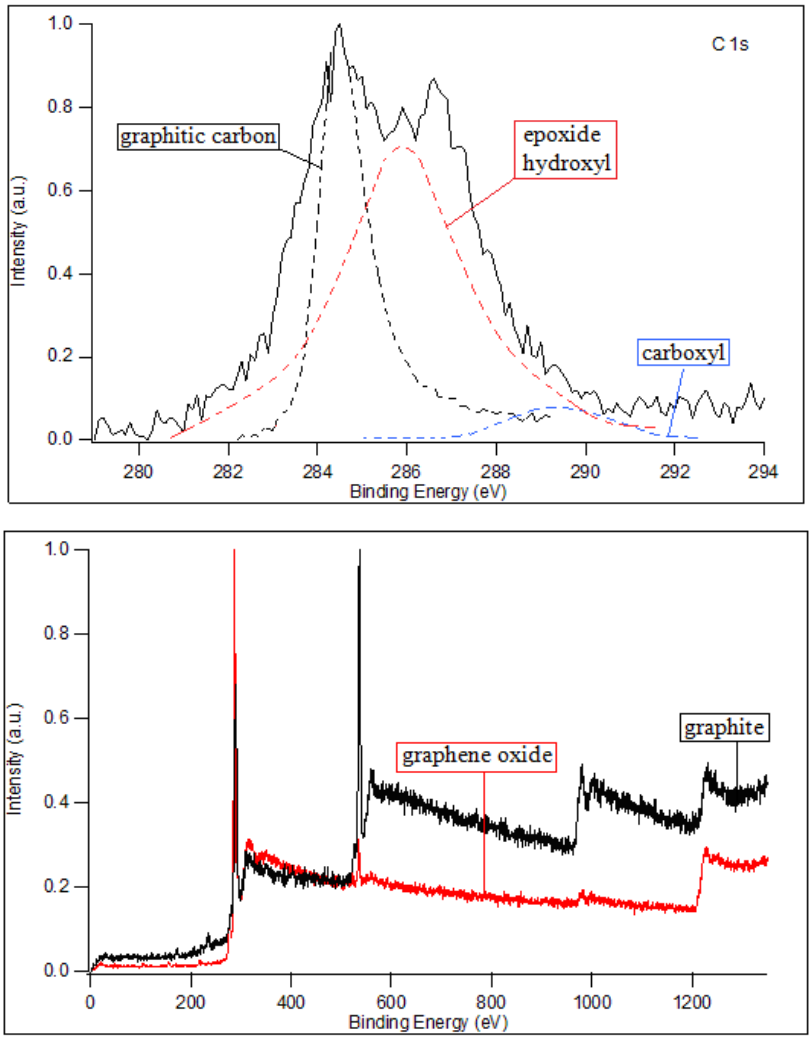

Figure 4.4) XPS curves: Top, Carbon C1s XPS profiles of raw GO, sum (continues black), graphitic carbon (dotted black), epoxide and hydroxyl (dotted red), carboxyl (dotted blue). Bottom, graphite (red) and graphene oxide (black)

4.2. Nanocomposite mechanical analysis (tensile test)

4.2.1. Effect of preparation methods

The mechanical results of tensile test is reposted in (figure 4.5) which shows the effect of filler concentration and different preparation methods on Young's modulus, strength at break and deformation at break. As it is obvious, adding graphene oxide results in an enhancement in elastic modulus and strength at break of polyamide-6 nanocomposites. first we turn our attention to the solvent casting method, adding just 0.5% graphene oxide caused to 13 vol% increase in elastic modulus but in higher percentage it can be observed about 36% when exactly graphene oxide content is increases to 2 vol%. In the second step we have melt and solvent/melt blending methods which show higher values of elastic modulus and in just 0.5 vol% they both exhibit 45% improvement in elastic modulus. In continue, this increscent in 0.75 and 1 vol% graphene oxide content remains stable for melt and solvent/melt blending method. In 2% graphene oxide content melt and solvent/melt blending methods exhibit two different values of elastic modulus increasing which is still 45% for melt blending method but in solvent/melt blending method this is 64% respect to pure polyamide-6, and it means about 19% difference between these two methods that it practically proves solvent/melt blending method is the best method to prepare nanocomposites. These results are interesting when compared with strength at break and deformation at break which show more or less similar trend in nanocomposites.

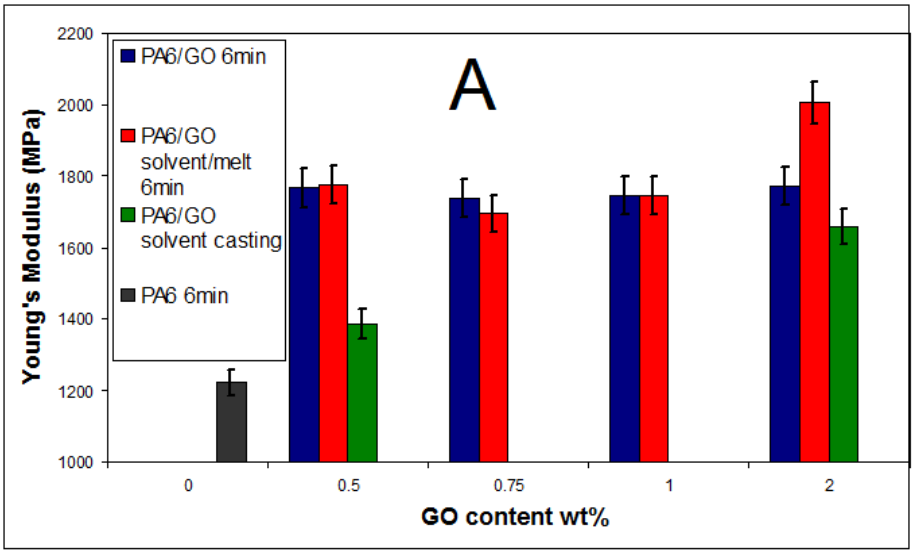
A
PA6/GO 6min
PA6/GO solvent/melt 6min
PA6/GO solvent casting
PA6 6min
Young's Modulus (MPa)
2200
2000
1800
1600
1400
1200
1000
0
0.5
0.75
1
2
GO content wt%

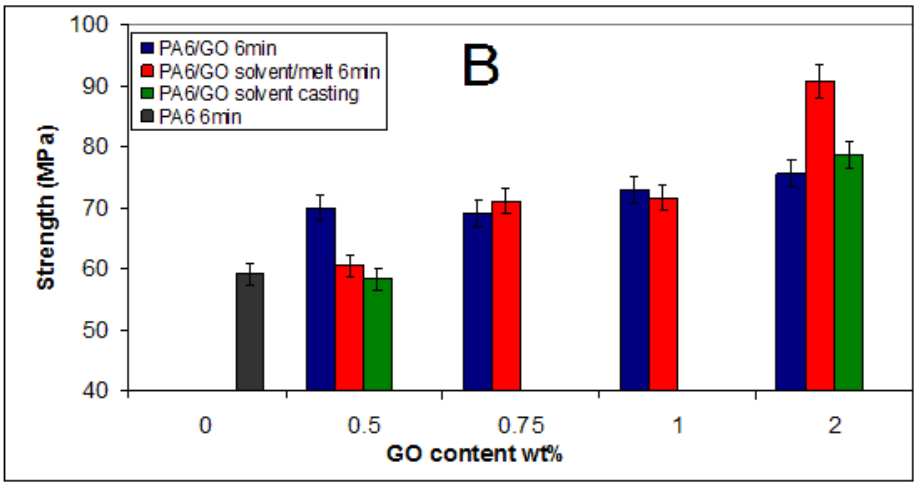
B
PA6/GO 6min
PA6/GO solvent/melt 6min
PA6/GO solvent casting
PA6 6min
Strength (MPa)
100
90
80
70
60
50
40
0
0.5
0.75
1
2
GO content wt%

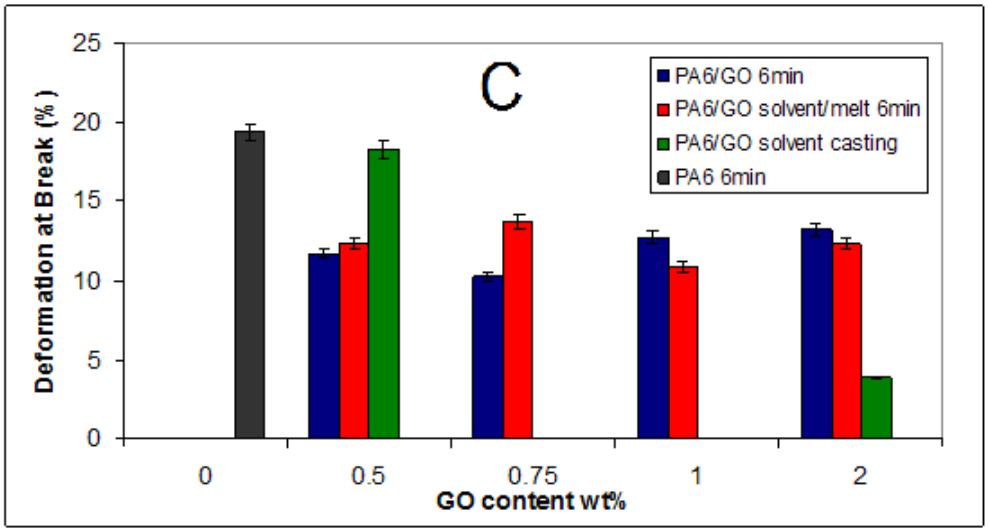

Figure 4.5) effect of GO concentration on A) Young's modulus B) strength at break C) Deformation at break

It is known that solvent casting method is an efficient method to disperse nanofillers within a solution of polymers and in this case we can observe a mechanical properties enhancement but in the mean time suffers from some disadvantages such as residual solvent that influences deformation at break and toxicity which are in accordance with other studies with other kinds of polymer and graphitic carbon materials different geometrical shapes [20-22]. It must be considered that in this research graphene oxide is produced from graphite flakes by an oxidation method that for sure causes some aggregations that prevent us from having a fine dispersion, therefore solvent casting method exhibit all its potential to overcome this problem and shows just 13 vol% increscent in elastic modulus.

On the other hand in the same graphene oxide volume content melt blending method exhibits higher elasticity, strength at break and rather lower deformation respect to solvent casting method which is related to its innate features. It is believed that melt blending method has some key features that make that more efficient. During melt blending there is continues movement of molten polymer which consists of two heat and

friction parameters. It is supposed, friction between molten polymer surface and graphene oxide agglomerations results in graphene oxide exfoliation which is companied with 240°C temperature for 6 minutes that also serves to have better exfoliation. It must be mentioned that melt blending method has also some negative aspects such as thermal degradation in polymer and the probability of graphene oxide damaging during the process but as it seems, in all levels of graphene oxide content elastic modulus remains stable [20, 23, 24].

In the third method (solvent/melt blending) there is the same mechanical response to the graphene oxide which was used in melt blending method but, in 2 vol% higher elastic modulus was exhibited. Young's modulus value is about 13% and it means 21% higher than melt blending and solvent casting method respectively. It can be explained by having the positive aspects of both solvent and melt blending methods and it shows that solvent casting as a pretreatment step causes to have better graphene oxide distribution within molten polyamide-6 which is confirmed with the results obtained from strength at break.

We can conclude that solvent/melt blending method is the best composite preparing method and 2 vol% filler content is mechanical percolation threshold.

4.2.2. Effect of processing time

The mechanical results of tensile test is reported in (figure 4.6) which shows effect of processing time on elastic modulus, strength and deformation at break of melt blended composites with three different filler including graphene oxide, graphite flakes and MWCNT.

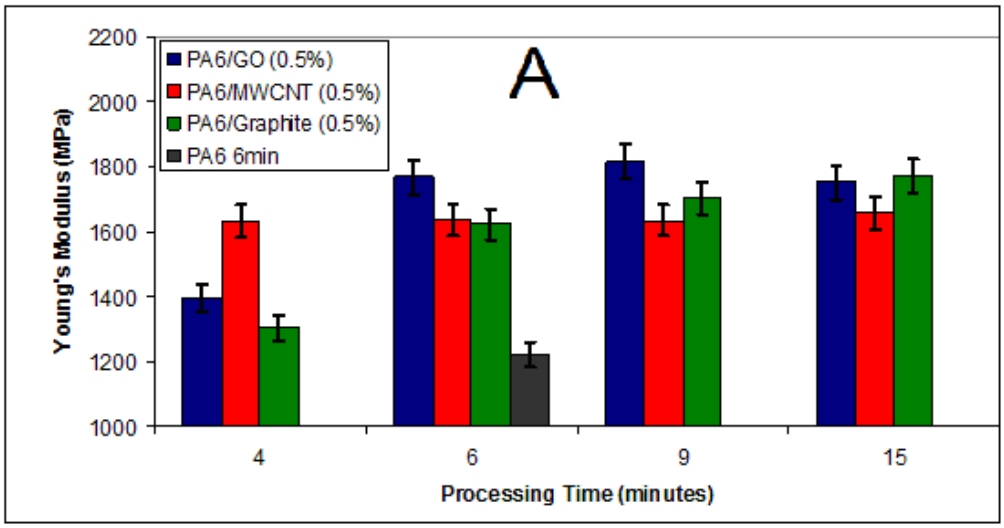
A
PA6/GO (0.5%)
PA6/MWCNT (0.5%)
PA6/Graphite (0.5%)
PA6 6min
Young's Modulus (MPa)
2200
2000
1800
1600
1400
1200
1000
4
6
9
15
Processing Time (minutes)

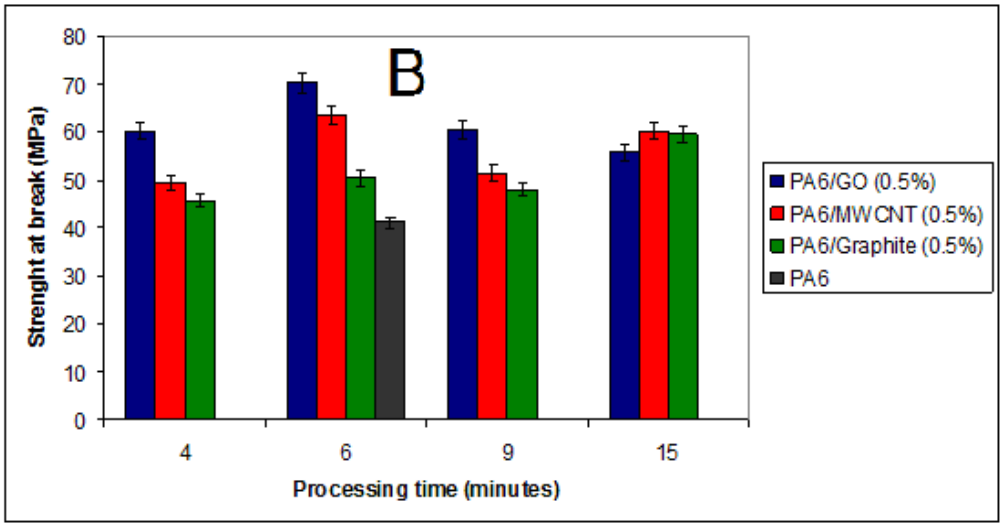
B
Strenght at break (MPa)
80
70
60
50
40
30
20
10
0
4
6
9
15
Processing time (minutes)
PA6/GO (0.5%)
PA6/MWCNT (0.5%)
PA6/Graphite (0.5%)
PA6

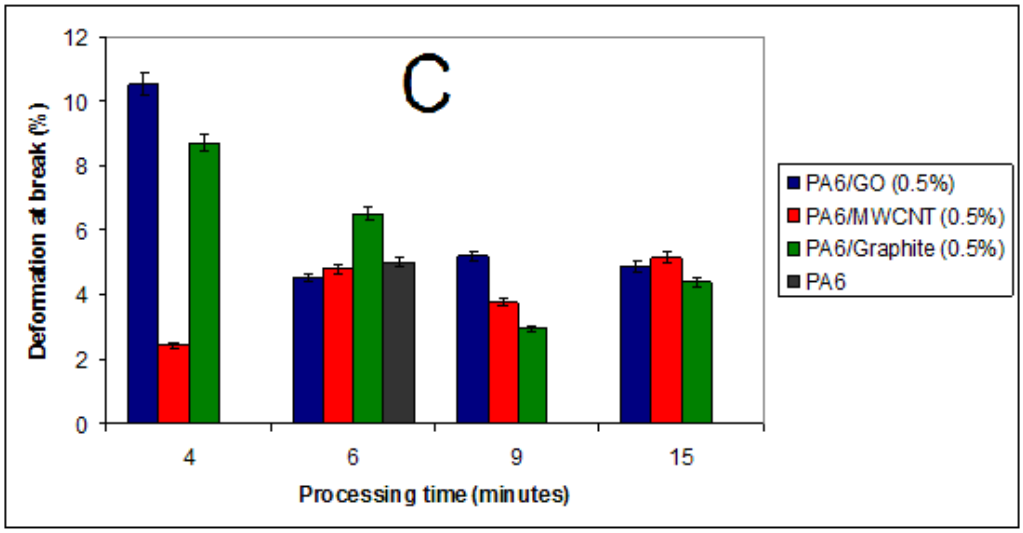

Figure 4.6) effect of processing time on A)Young's modulus in different composites B) strength at break C) deformation at break.

Generally we can look at these three kinds of filler contents as 2D materials including graphite and graphene oxide and 1D material including MWCNT. The other way of categorizing these filler contents is polarity consideration which divides these three fillers to two groups including polar (graphene oxide) and non-polar (graphite, MWCNT) materials. As it is obvious in nanocomposite made by MWCNT there is no difference in Young's modulus and strength between the samples with different processing time from 4 to 15 minutes. This phenomenon is explainable by considering the geometry of MWCNT as 1D material with very high aspect ratio and the ease of dispersion within the matrix. All evidences indicate, 4 minutes is enough to disperse MWCNT homogenously within the matrix and making a network of nanotubes inside the matrix but extending this time dose not help and even can result in polymer thermal degradation or disrupting the carbon structure in MWCNT. Thus the obtained mechanical properties results are in accordance with the previous studies in this area [25-27].

In composite made by graphite, increasing processing time generally has a positive effect on both Yong's modulus and strength at break and extending

processing time from 4 to 6 minutes caused to 20% increscent in Young's modulus but, after 6 minutes there is no significant improvement in mechanical properties of the composite. On the other hand this time extending slightly influences strength at break. In order to explain this phenomenon it is necessary to have a comparison between graphite and MWCNT. In the same percentage, graphite is obviously less bulky with MWCNT that is related to 2D geometry of stocked graphene sheets on each other. Melt blending that imposes friction on the graphite surface is caused to partial exfoliation in graphene sheets and better distribution within the matrix as well. Dense and bulky graphite flakes need to more time for being distributed within the matrix and that is why there is 24.5% difference between 4 and 6 minutes processing time [28].

In the last composite made by graphene oxide, mechanical response to the various processing time is different. As it was discussed before, graphene oxide was produces directly from graphite flakes via chemical oxidation process and the main difference between graphite flakes and graphene oxide particles is polarity, hydrophilic nature and bulk aggregations of graphene sheets. In this research hydrophilic nature of graphene oxide serves to have better dispersion within the polar matrix (PA6). But aggregation of graphene oxide is an impediment in dispersion and requires more processing time to overcome. For sure melt blending features such as friction and heating plays positive role in this way and results in graphene oxide exfoliation inside the polymer and on the other hand, partial thermal reduction in graphene oxide sheets decreases polarity of the filler and must be also considered. Graphene oxide exfoliation has a positive effect on dispersion of nanosheets but extending processing time can also cause to polymer thermal degradation and lattice distortion in graphene oxide sheets which are more sensible respect to two other fillers (graphite and MWCNT). As this is observable Young's modulus in the composite made by graphene oxide with 4 minutes processing time is about 7% higher than composite made by graphite and this trend remains sustainable in 6 minutes.

Extending processing time from 4 to 6 minutes causes to an improvement in Young's modulus and strength by 25.6% which is explainable by earlier explanations about the effect of friction and processing time on the graphene oxide dispersion within the polymer. After exceeding the sixth minute there is a plateau in Young's modulus and strength that exhibits no reaction to the processing time [29].

At the end we can conclude, because of difference in geometry and polarity in these three types of filler contents, their response to processing time varies from each other however this response in graphene oxide and graphite flakes is rather similar and confirm 6 minute processing time a the optimum processing time to achieve to the optimum dispersion of filler within the polymer.

4.2.3. Effect of photo oxidation

The mechanical results of tensile test on the UV exposed samples are reported in (figure 4.7) that shows the effect of UV exposure time on elongation at break and tensile stress in the nanocomposites regarding their preparation method. As it was expected as once polyamide-6 is exposed to UV radiation starts to extremely lose its mechanical resistivity and decreasing elongation at break which is directly related to photo oxidation phenomenon. After just 10 hours from polyamide-6 exposing to the UV light, elongation at break extremely decreases by 40% and it reaches to 82% at the end of 96^{th} hour. This response confirms other explanations about chain degradation and sensibility of polyamide-6 against photo oxidation (figure 4.8) [30-33].

In other samples such as nanocomposites made by graphene oxide via melt, solvent casting and solvent/melt blending methods we observe totally different trends. Elongation at break remains constant after 48 hour for all nanocomposites in 0.5 vol% and 1 vol% of graphene oxide but after this point polyamide-6 graphene oxide prepared by melt blending method starts to show an intensive decrease by 60%.

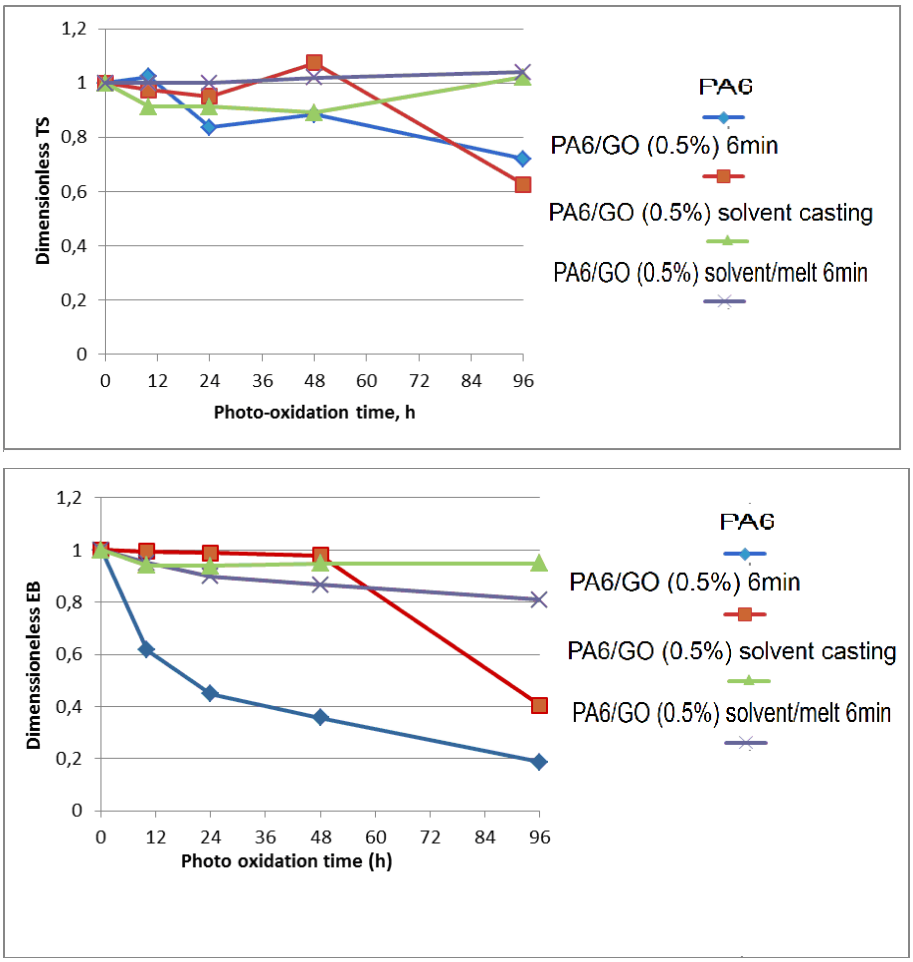

Fig 4.7) effect of UV radiation on dimensionless tensile strength (Top) and dimensionless elongation at break (Bottom) in nanocomposites.

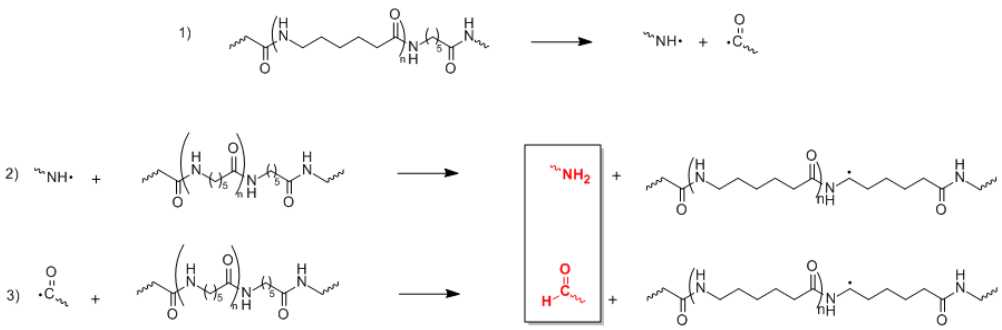

Figure 4.8) photo oxidation process in polyamide-6

Based on the results, presence of graphene oxide generally caused to decrease in polyamide-6 photo oxidation and in some cases stopped that just like other nanoparticles [34,35]. This effect could be because of photo-stabilization effect of graphene oxide nanoparticles and ultraviolet absorption which is not proved up to now by any other similar researches. Based on the previous experiments melt blending companied with solvent casting has the best mechanical result and graphene oxide dispersion. Here also the most photo oxidation resistance was observed in specimens that were prepared based on melt blending and solvent casting/melt blending method. But the most gained decrease in elongation at break was observed when melt blending method was used in 0.5% graphene oxide level after 96 hours. We believe better dispersion of the filler caused to better ultraviolet absorption and saving the polymer chain of degradation consequently, as it was discussed before neither solvent nor melt blending methods are able to reach to the optimum graphene oxide dispersion within the matrix and just using solvent casting as a pretreatment step for melt blending method can assure us about it.

4.3 Attenuated total reflectance infrared spectroscopy (ATR-FTIR) analysis

Generally UV irradiation results in N-C bond breaking down and forming free radicals which cut the polymer chains consequently. ATR-FTIR test was performed on the PA6/GO (0.5%) sample prepared via solvent/melt blending method on both exposed and unexposed sides, before and after exposing to UV radiation (figure 4.9). After looking precisely in IR spectrum, we can divide that into four zones including:

1. Spectral range investigated 3700-3100 cm^{-1} peaks detected: 3200 cm^{-1} (absorbance of -NH_2 (amine)) and 3400 cm^{-1} (absorbance of –CHO (aldehyde)). In this zone the variation of absorbance at 3200 cm^{-1} and at 3400 cm^{-1} are evidence of unoxidized samples.

2. Spectral range investigated 1700-1730 cm^{-1} that in this range variation of the absorbance at 1710 cm^{-1} belongs to formation carboxyl.
3. Peaks detected at 1538 cm^{-1} (C-N deformation and CO-N-H angular deformation) belonging to amide I and 1640 cm^{-1} (C=O axial deformation), belonging to amide II. In this range intensity ratio of the band located at 1640 cm^{-1} to the band centered at 1538 cm^{-1} (I_{1640}/I_{1538}) directly proportional to the chain length.
4. The bands at 930 and 1124 cm^{-1} were used to obtain the α-crystalline and amorphous orientation respectively (Table 4.1) [30].

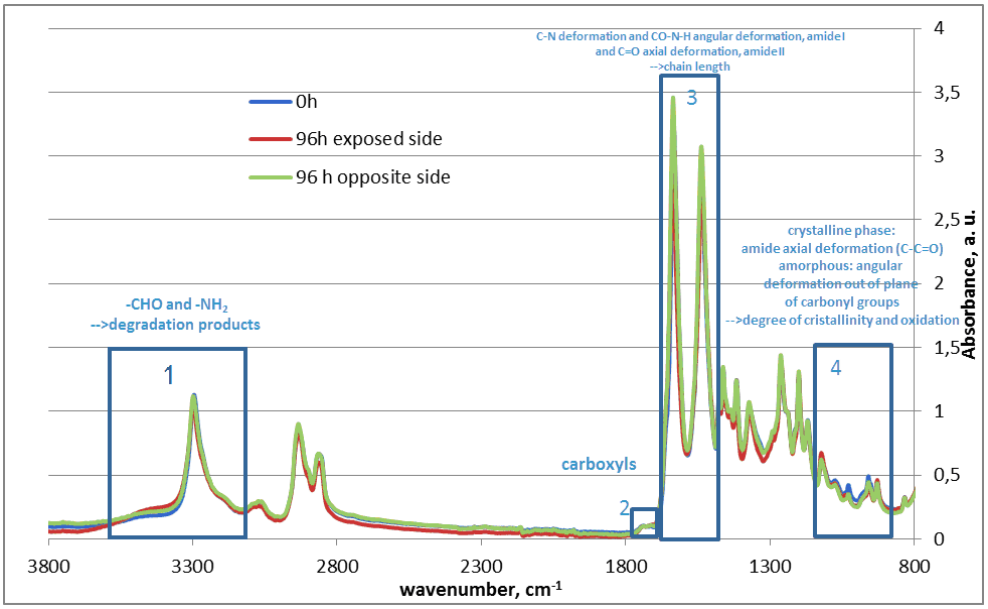

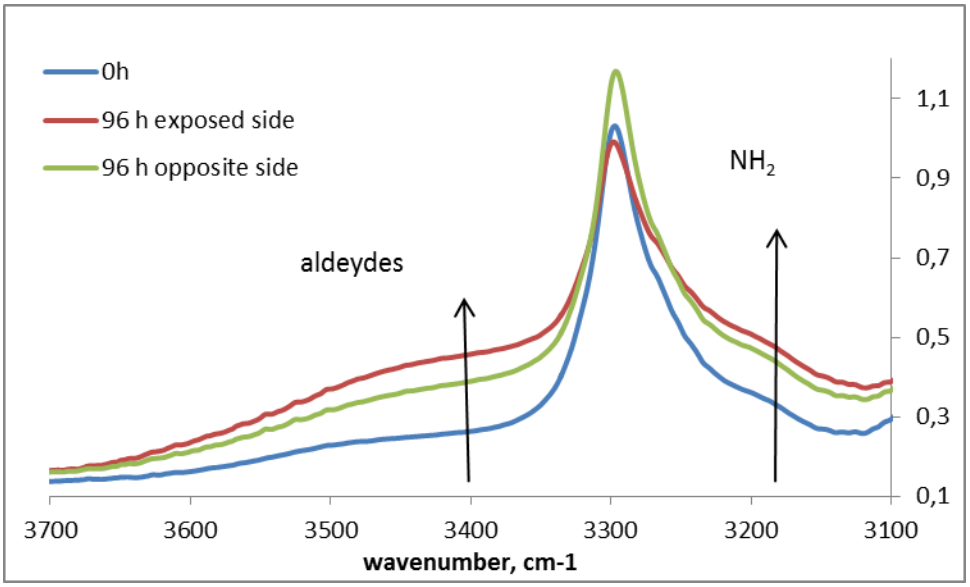

Figure 4.9) ATR-FTIR absorption curves of PA6/GO (0.5%) solvent/melt 6min.

Table 4.1) ATR-FTIR absorption curves of PA6/GO (0.5%) solvent/melt 6min, phase and chemical bonds identification

Wave Number (cm^1)	**Phase**	**Transition Moment**	**Assignment**
930	α-Crystalline phase	Parallel to the chain axis	CONH in plane
1124	Amorphous	Parallel to the chain axis	C—C stretching
1170	Reference	Unknown	CH_2 twisting or wagging

It is evident that photo-oxidation time has direct influence on aldehyde and amide groups forming which confirms facing photo-oxidation in PA6. By observing graphene oxide shielding effect at 3400 cm^{-1} by calculating the absorbance difference between exposed side and opposite side of the samples ((D Abs 3400 cm-1) exposed side - (D Abs 3400 cm-1) opposite side) and variations in the absorbance at 1710 cm^{-1} we can conclude about the role of graphene oxide nanosheets photo-oxidation experiment (figure 4.10-11). First, there is a small difference between the exposed and

unexposed sides of the samples that shows the intensity of photo-oxidation on the surface of the samples and in the depth. As it was expected by starting UV exposing, PA6 shows higher absorbance that achieves to the maximum intensity at the end of 96th hour. After comparing these results with nanocomposites prepared by different preparation methods it was realized that presence of GO resulted in carboxyl and aldehyde peaks restriction. But each preparation method showed its specific effect on carboxyl formation in PA6 that is due to its efficiency in dispersing GO through the matrix. Sample prepared by solvent/melt blending method exhibits the best results by showing the minimum intensity of carboxyl groups at the end of 96th hour that it proves the minimum level of photo-oxidation faced. In the second step solvent casting method and then melt blending methods showed the minimum intensity of carboxylic peak in the nanocomposites. In fact ATR-FTIR test results are in accordance with other experiments such as mechanical, rheological, and DMTA tests an also prove the photo-oxidation shielding effect of graphene oxide nanosheets.

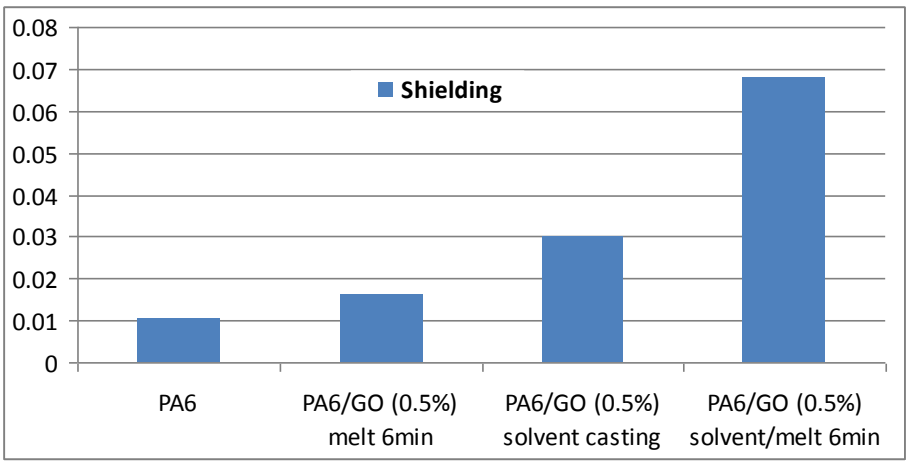

Figure 4.10) GO shielding effect on PA6 nanocomposites at 3400 cm^{-1}

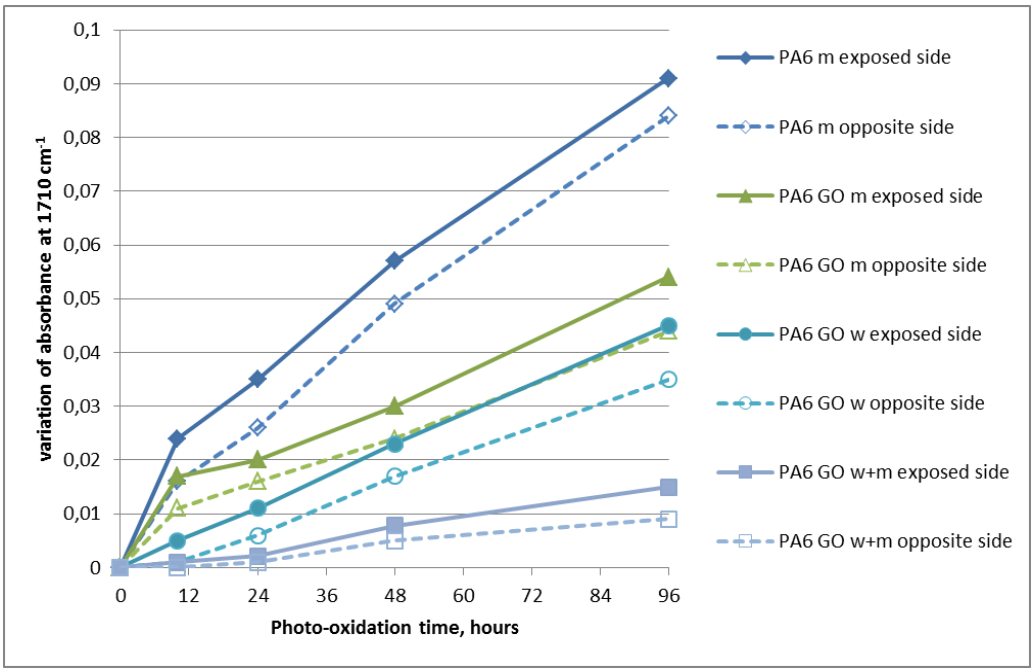

Figure 4.11) - Variations in the absorbance at 1710 cm^{-1} of PA6 and PA6/GO (0.5%) nanocomposite films prepared via melt blending (m), solvent casting (w) and solvent/melt blending (m+w) methods at various stages of photo-oxidation at 254 nm

4.4. Dynamic mechanical thermal analysis (DMTA) analysis

From DMTA experiment two fundamental quantities are derived: storage modulus E' and loss factor (tan δ**)** that provide some information about elasticity of the material (real component of complex modulus E*) and the relationship between the maximum dissipated energy and potential energy preserved for each cycle.

Dynamic mechanical thermal results related to storage modulus in function of temperature for the samples prepared with melt blending method and different processing time are reported in (figure 4.12).

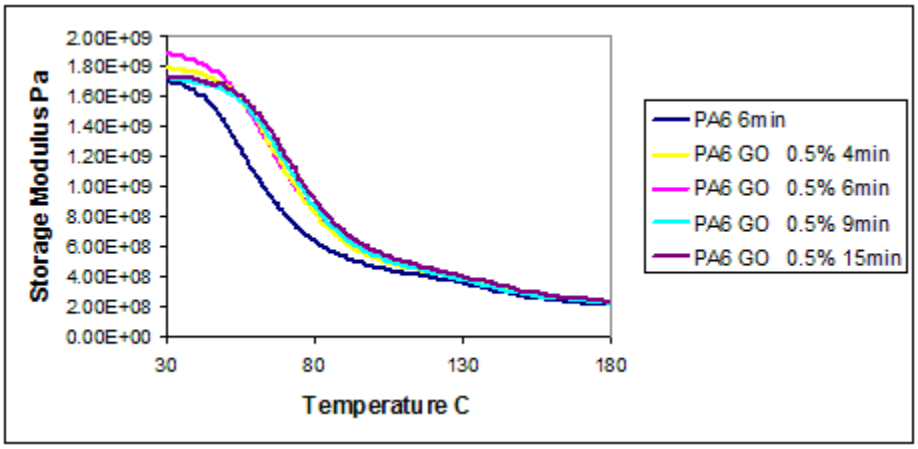

Figure 4.12) storage modulus E' in function of temperature for nanocomposites prepared with melt blending method and different processing time

As it seems in all materials loaded with graphene oxide there is an improvement in storage modulus (E') respect to pure polyamide-6. Increasing processing time from 4 to 6 minute shows an enhancement in storage modulus (E') in nanocomposites with the same 0.5 vol% graphene oxide content but after this point the trend changes and starts to show lower values. Till now these results are in accordance with tensile test results and confirm that 6 minute processing time as the optimum processing time in terms of graphene oxide dispersion within polyamide-6 (respect to 4 minute processing time) and lowering the possibility of thermal degradation in the matrix (in comparison with 15 minute processing time).

Dynamic mechanical thermal results related to storage modulus in function of temperature for the samples prepared with different graphene oxide filler content are reported in (figure 4.13).

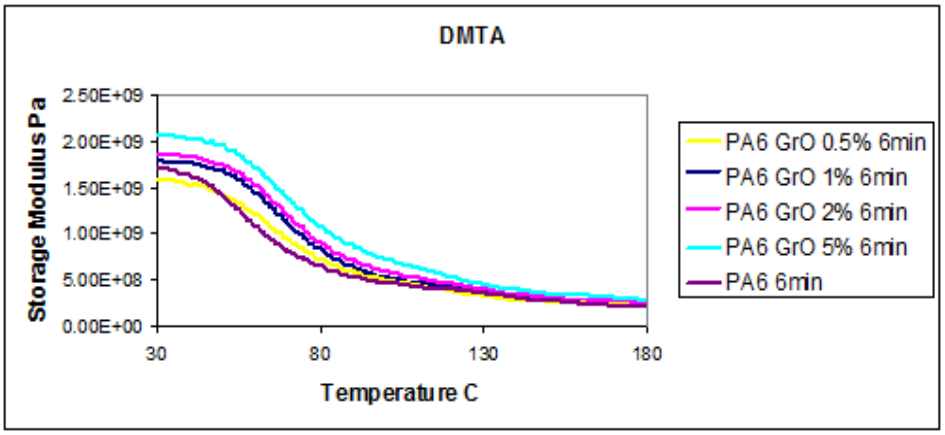

Figure 4.13) storage modulus E' in function of temperature for nanocomposites prepared with melt blending method and different graphene oxide content volumes

In general increasing the percentage of graphene oxide content results in a storage modulus enhancement and this is observable in both low and high temperature. In this experiment pure polyamide-6 showed the lowest storage modulus and then, nanocomposite of polyamide-6 with 0.5 vol% graphene oxide exhibited rather more values that this trend is followed over 1, 2 and 5 vol%. By increasing the filler content from 2 to 5 vol% we can observe an intensive storage modulus (10%) that is notable when is compared with 1 to 2 vol% graphene oxide content loading (4%). In both low and high temperature measuring there is in accordance between DMTA and tensile test results and clearly we can conclude presence of graphene oxide is caused to mechanical and dynamic mechanical thermal properties of nanocomposites and this is also in accordance with other similar researchs on multilayer nanofillers [36-38].

Dynamic mechanical thermal results related to storage modulus in function of temperature for the samples prepared with different preparation method are reported in (figure 4.14)

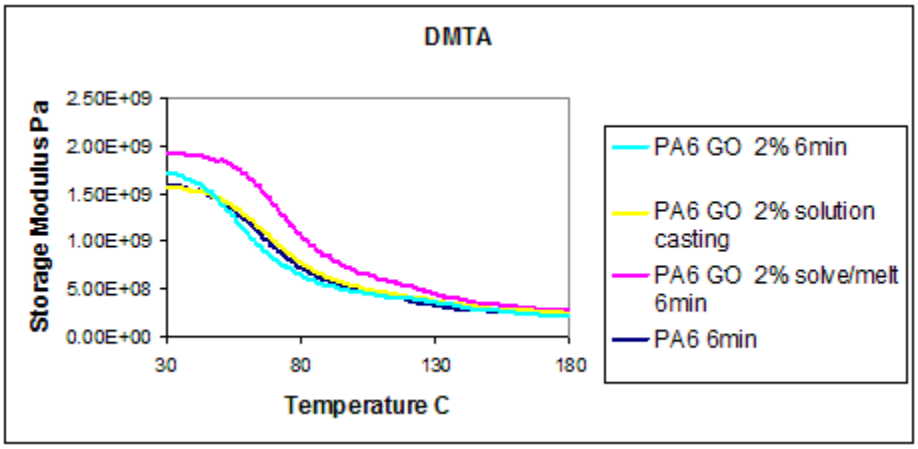

Figure 4.14) storage modulus E' in function of temperature for nanocomposites prepared with different preparation methods

As it seems the highest storage modulus obtained at 30°C and 2 vol% graphene oxide content belongs to solvent/melt blending method and then melt blending, solvent casting and pure polyamide-6 are in the next steps subsequently. These results confirm again mechanical results of tensile test that proves the superiority of this method in graphene oxide dispersion within the polyamide-6 and enhancing mechanical properties of the produced nanocomposites. It must be noticed that the superiority of this method remains stable in high temperatures however by increasing the temperature in other nanocomposites the response become more similar to the pure polymer.

Dynamic mechanical thermal results related to storage modulus in function of temperature for the samples prepared with melt blending method and different filler content are reported in (figure 4.15)

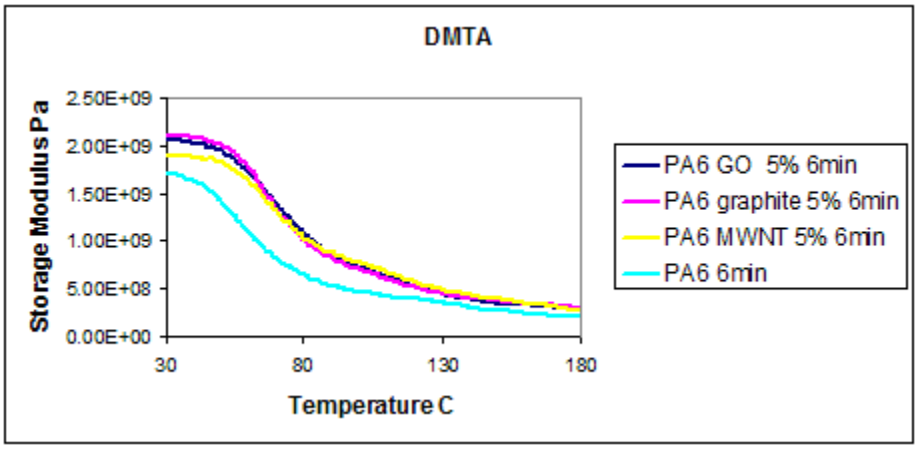

Figure 4.15) storage modulus E' in function of temperature for nanocomposites prepared with different filler content

Nanocomposites loaded with graphene oxide and graphite show really similar response to the thermo dynamic mechanical stress imposed by the experiment and they overlap each other. This response is interpretable by considering their geometry and the way that they are dispersing through the matrix. However this is little far from our expectation that graphene oxide by exceeding 2 vol% as its mechanical percolation threshold in the composite had to show much higher values of storage modulus respect to graphite flakes. The only interpretation for this phenomenon is the possibility of graphene oxide agglomeration in higher volumes because of its hydrophilic nature and strong tendency to restocking and this problem can impede the efforts to load nanocomposites with higher volumes. On the other hand nanocomposites prepared with MWCNT show lower values of storage modulus but by reaching the higher temperatures than 65°C the mechanical response starts to become similar to other composites. All these results are just evidence of better compatibility between graphene oxide nanosheets and matrix respect to hydrophobic MWCNTs which provides more homogenous composite of both filler and matrix phase however it needs more studies.

Dynamic mechanical thermal results related to loss factor (tan δ) in function of temperature for the samples prepared with melt blending method and different processing time are reported in (figure 4.16).

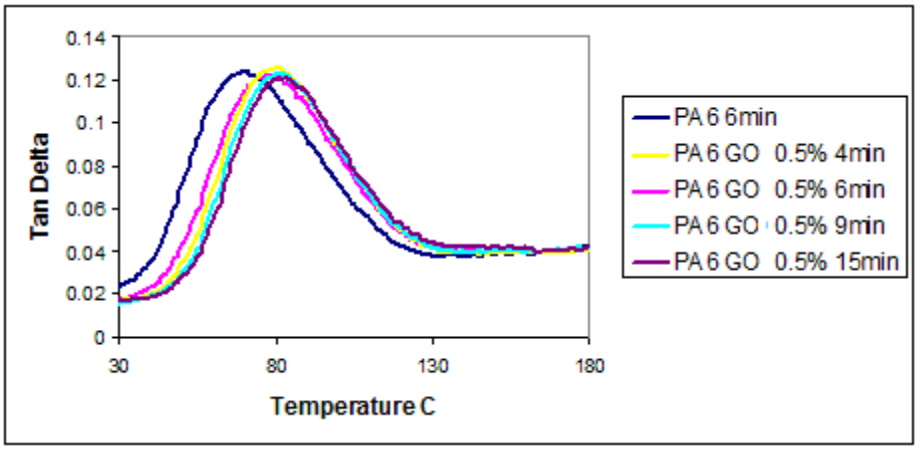

Figure 4.16) tan δ in function of temperature for nanocomposites prepared with melt blending method and different processing time

The results of tan δ show by adding graphene oxide into polyamide-6, tan δ peak shifts to the higher temperatures. This shift for 4 minute processing time is about 7°C while by extending it to 6 minute this value will be reach to 10°C and even more in 15 minute (13°C). based on other same researches polyamide-6 has two tan δ relaxation peaks that was observed just one of them at 79°C (α relaxation) and the other one in -60°C (β relaxation) that is not included in our plot. α relaxation is believed to be attributed to breakage of hydrogen bonding between polymer chain which induces long range segmental chain movement in the amorphous area and assigned to the glass transition temperature of polyamide-6 (T_g). It seems PA6 loading with graphene oxide results in T_g increasing and the more processing time, the more increase in T_g. this is believed this response is in direct relationship with the degree of graphene oxide dispersion within the matrix and it caused to graphene oxide intercalation by the matrix, better

compatibility and finally increasing the $T_{g.}$ it must be mentioned there is no significant change in the width of the composites in comparison with pure polyamide-6.

Dynamic mechanical thermal results related to loss factor (tan δ) in function of temperature for the samples prepared with melt blending method and different volume of graphene oxide content are reported in (figure 4.17)

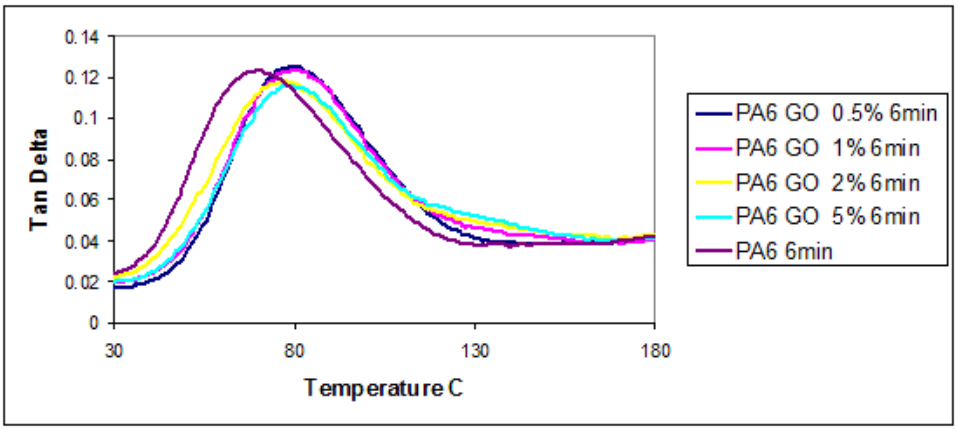

Figure 4.17) tan δ in function of temperature for nanocomposites prepared with melt blending method different volume of graphene oxide content

As it seems from the fig by adding just 0.5 vol% α relaxation peak shifts to the higher temperatures and Tg increases by 10°C and remains unchanged even at higher volume of the filler. This response is normal and the reason was explained before but by increasing the volume percentage of graphene oxide to the higher amounts, tan δ starts to go down and in the same time becomes wider. This phenomenon is explainable by just relating that to the free volume of polymer chemical bonds and trying to look at this phenomenon from the crystallinity point of view. Increasing the amount of graphene oxide resulted in both Tg increasing and widening the nanocomposites bands. We can conclude that graphene oxide results in higher volume of crystallinity in the matrix by exposing nucleation site for forming the crystals and this explanation confirms higher elastic modulus in

nanocomposites and this is in accordance with other researches with nanoclay fillers [39-41].

Dynamic mechanical thermal results related to loss factor (tan δ) in function of temperature for the samples prepared with different preparation methods are reported in (figure 4.18).

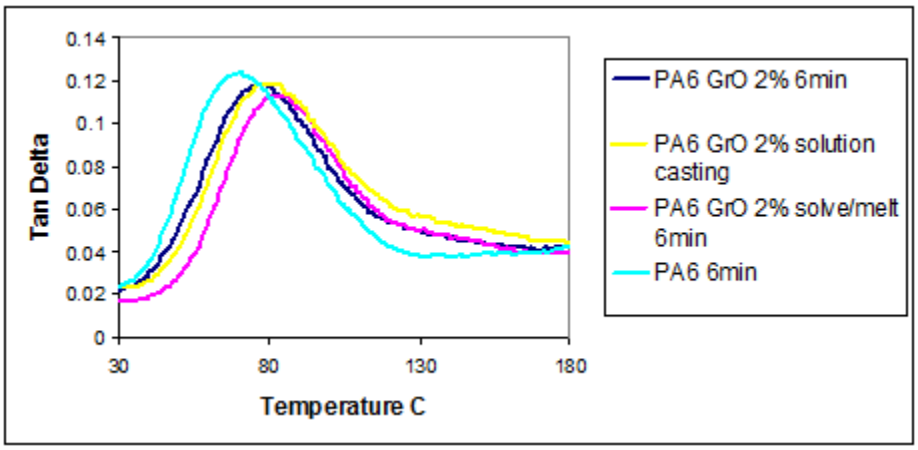

Figure 4.18) tan δ in function of temperature for nanocomposites prepared with different preparation methods

This is evident that adding graphene oxide to polyamide-6 by melt blending method results in 10°C increasing in Tg of the composite but by changing the method from melt blending to solvent casting and then solvent/melt blending method this shift continues and finally will reach to 14°C enhancement. The second rather clear evidence in these curves is the shape of bands that is under effect of preparation method and shows that solvent/melt blending preparation method posses a wider band respect to solvent casting and melt blending method. Both higher Tg and wider band are evidence of a better graphene oxide dispersion, compatibility between both filler and matrix phases and also more crystalline nanocomposite that is confirmed by elastic modulus results of tensile test experiment. This is

believed that exfoliated graphene oxide sheets in this way play a positive role to effect the crystallinity of the matrix.

Dynamic mechanical thermal results related to loss factor (tan δ) in function of temperature for the samples prepared with different filler are reported in (figure 4.19)

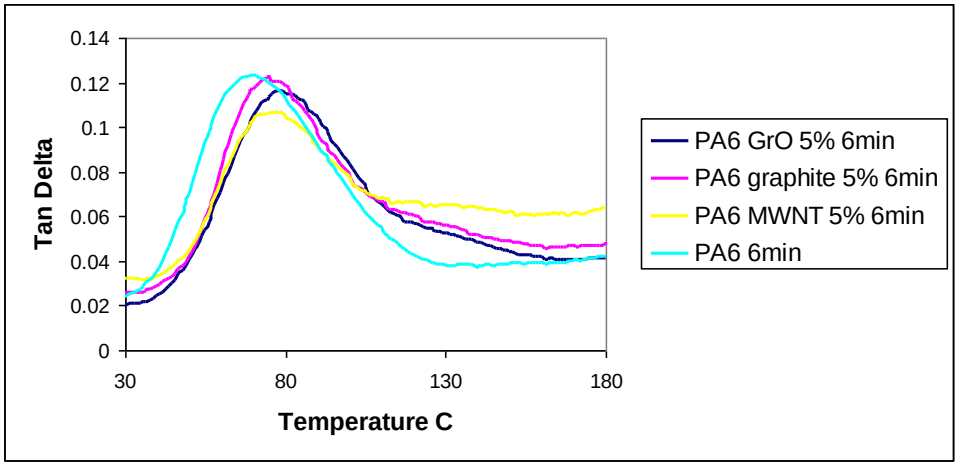

Figure 4.19) tan δ in function of temperature for nanocomposites prepared with different filler contents

The results of tan δ show by adding the filler into polyamide-6, Tg starts to shift to higher values and this is totally obvious by comparing with polyamide-6 glass transitional peak which is located at about 70°C. nanocomposites loaded with graphene oxide shows about 5°C shift and has rather high and sharp peak. On the other hand in the composite made by graphite filler, Tg shifting is even more than other nanocomposites and is stabled at about 80°C, while the curve starts to become wider and lower. At the end MWCNT nanocomposite shows the widest curvature with rather higher Tg respect to neat polymer at 78°C. It is supposed that adding nanoparticles by influencing on the crystalline structure of polyamide-6 and as it was discussed before this is related to the free volume of polymer chemical bonds. In fact MWCNT by exposing more nucleation sites to polyamide chains permit them to form easily and makes the polymer more

crystalline and rigid as well. These results are in accordance with DSC results and they will prove this interpretation.

4.5. Rheological analysis

Rheological test results related to storage modulus (G') and loss modulus (G") in function of angular frequency for the samples prepared by melt blending method in different processing time is reported in (figure 4.20).

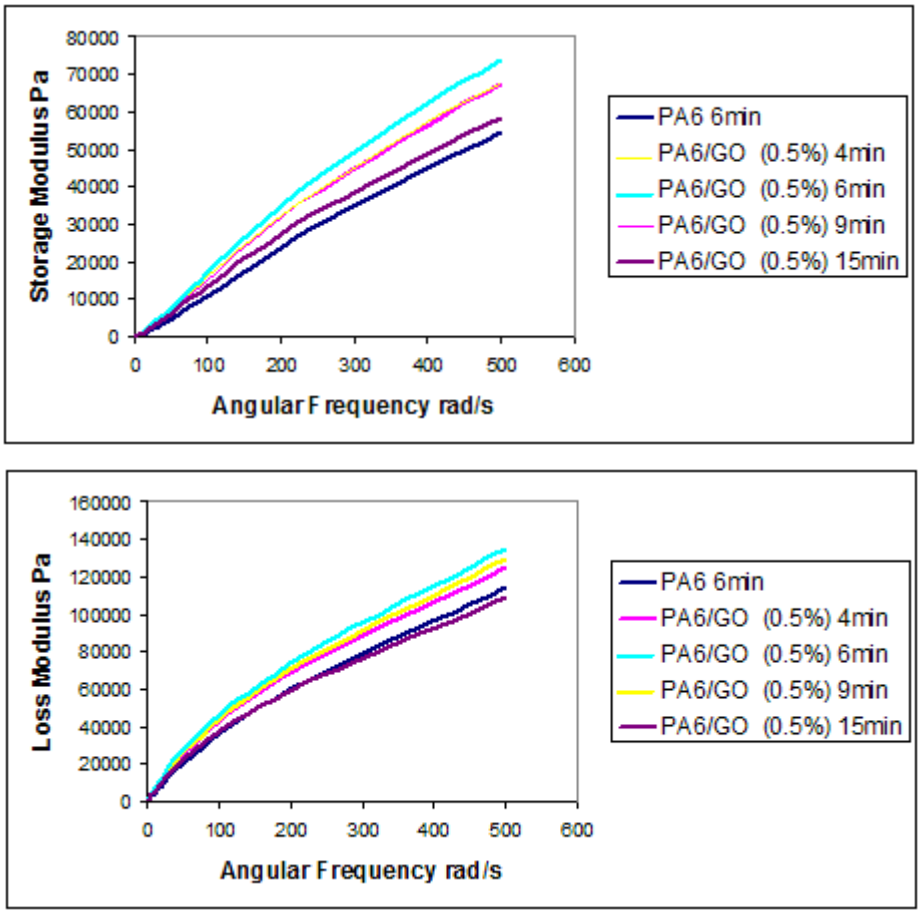

Figure 4.20) storage modulus (G') at top and loss modulus (G") at bottom in function of temperature for nanocomposites prepared with different processing time

This is apparent that extending the processing time in nanocomposites of graphene oxide and polyamide-6, storage modulus starts to increase and shows higher values respect to the pure polymer. It seems that there is no clear difference in the values of storage modulus between 4 and 9 minute while 6 minute processing time exhibits the optimum processing time to achieve to the highest value of storage modulus and 15 minute shows the lowest value which was expectable by the results of tensile test. On the other hand there are the same results in loss modulus (G") and longer processing time is caused to the higher values however the differences are not so evident. The lowest values are related to 15 minute processing time and the highest to 6 minute while there is a slight difference between 4 and 9 minute processing time and it differs from storage modulus graphics.

It must be considered, storage modulus and loss modulus represent elasticity and the viscous response of the materials. On the other hand a higher frequency in the dynamic mechanical analysis means a higher loading rate and a higher loading rate is known to cause a higher elastic modulus. Therefore this phenomenon is interpretable by looking at the results from dispersion standing point. Giving enough time to the process for blending graphene oxide within polyamide-6 leads to breaking down graphene oxide agglomerations, increasing the particles surface area and acting as higher filler volume subsequently. But in 15 minute processing time there is a paradox and this point is explainable just by considering the time as a destructive parameter in molten polymer and thermal degradation resulted from this fact that affects mechanical properties in nanocomposite.

Rheological test results related to storage modulus (G') and loss modulus (G") in function of angular frequency for the samples prepared with solvent/ melt blending method in different volume of graphene oxide content in (figure 4.21).

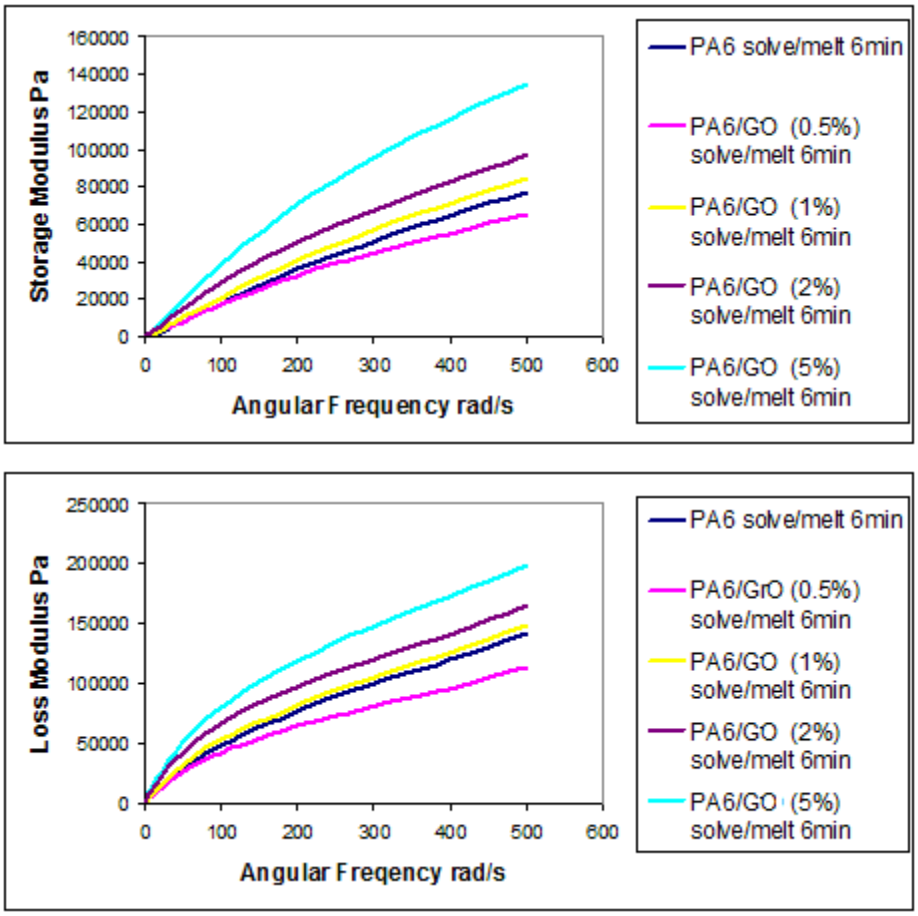

Figure 4.21) storage modulus (G') at top and loss modulus (G'') at bottom in function of temperature for nanocomposites prepared with different volume of graphene oxide content

As it seems from the storage modulus and loss modulus graphics, adding graphene oxide as nanofiller into the matrix results in an enhancement in the values and this is more evident once the frequency is at the highest level. This must be mentioned that based on the mechanical results of tensile test 2 vol% in nanocomposites prepared by solvent/melt blending method is mechanical percolation threshold point and the point where elastic modulus starts to enhance quickly. Here we can observe the same response and mush higher values in storage modulus (~40%) once graphene

oxide crosses 2 vol% to 5vol%. Increasing the graphene oxide content obviously will results in agglomerated particles (because of its hydrophilic nature) that naturally acts like lower filler content but here solvent/melt blending method exhibited an efficient way to overcome this problem and this is in agreement with other studies on nanocomposites prepared by layered nanofiller [42-44].

Rheological test results related to storage modulus (G') and loss modulus (G'') in function of angular frequency for the samples prepared with different preparation method and equal percentage of graphene oxide content in (figure 4.22).

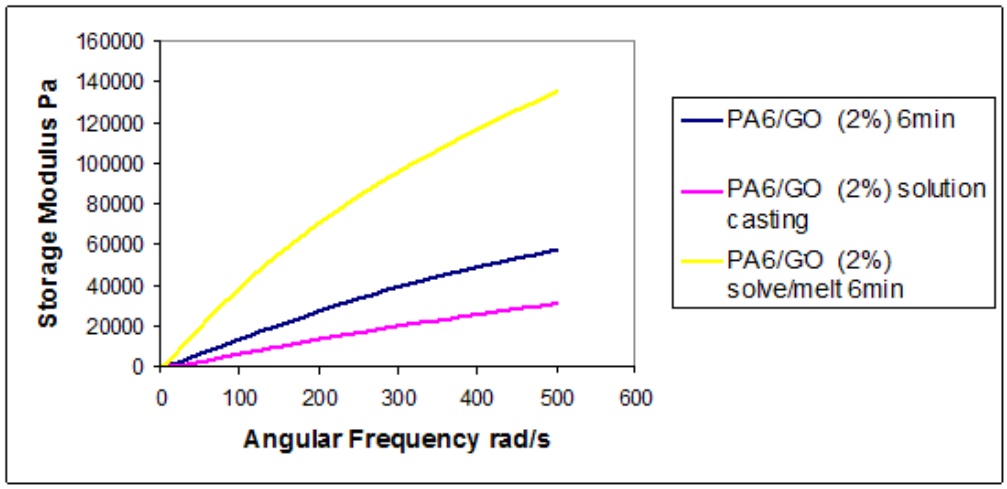

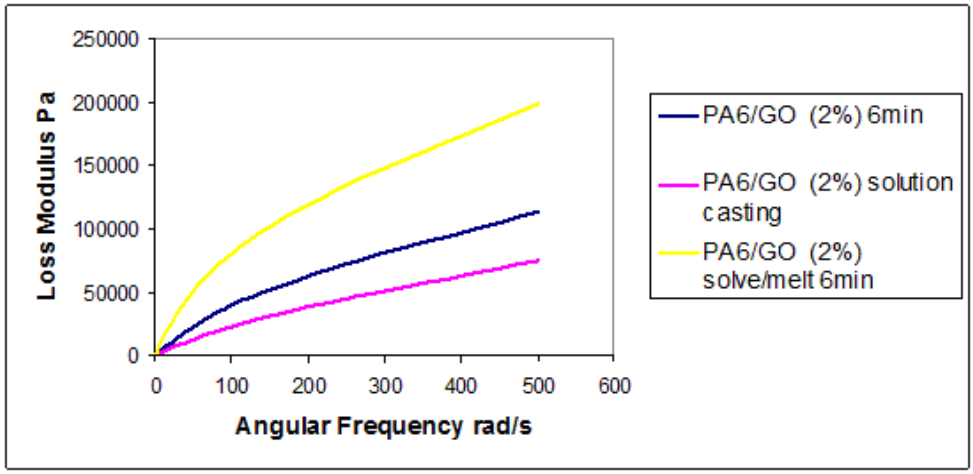

Figure 4.22) storage modulus (G') at top and loss modulus (G") at bottom in function of temperature for nanocomposites prepared with different preparation method and equal percentage of graphene oxide content

Here we can observe effect of nanocomposite preparation methods in the same graphene oxide content volume on storage modulus and loss modulus which exhibits a clear difference in the modulus. As it seems by increasing frequency both storage modulus and loss modulus show higher values and it confirms a strong interaction between graphene oxide and polyamide-6. These results are in accordance with the results of tensile test and again confirm the superiority of solvent/melt blending method in dispersing graphene oxide within the matrix. By changing the method from solvent casting to melt blending, storage modulus increases by about 85%. It must be mentioned having a plateau in low frequency is a sign of solid-like materials and by adding graphene oxide and using different methods we can claim that the composites have tendency to express solid-like behavior and it must be because of homogeneity of the composite of the filler particles and matrix.

Rheological test results related to storage modulus (G') and loss modulus (G") in function of angular frequency for the samples prepared with melt blending method and different fillers in (figure 4.23)

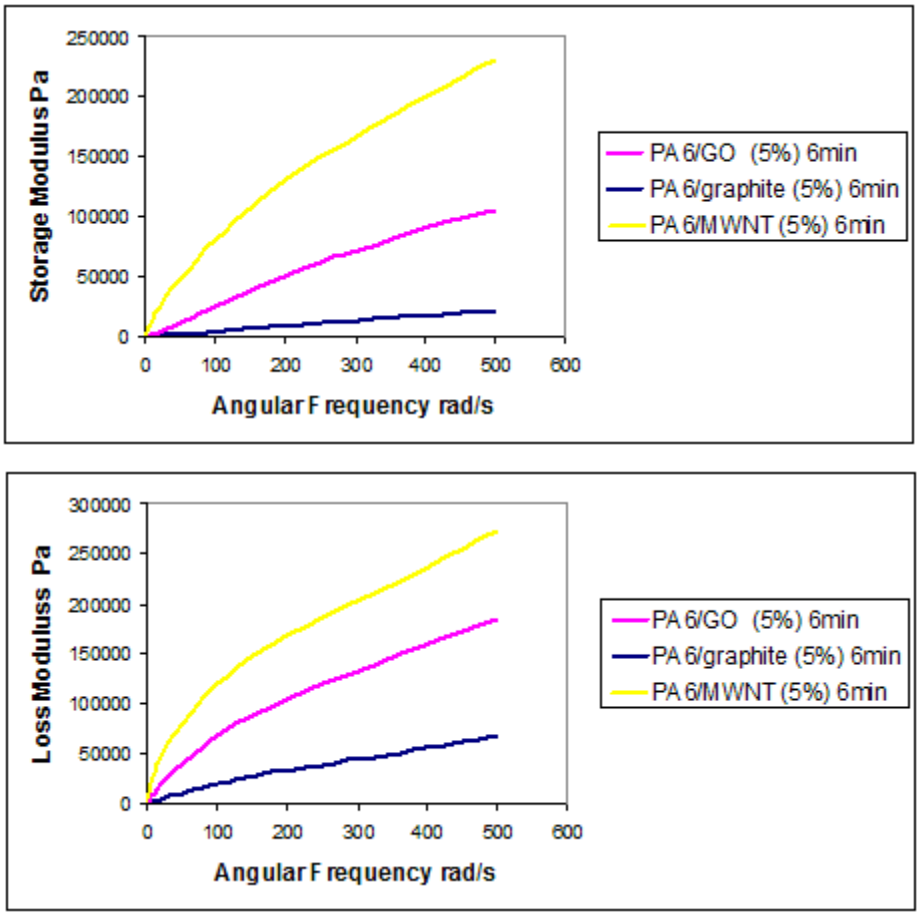

Figure 4.23) storage modulus (G') at top and loss modulus (G") at bottom in function of temperature for nanocomposites prepared with melt blending method and different fillers

Rheological experiment of nanocomposites prepared with graphene oxide, graphite and MWCNT contain some meaningful results. first In both storage modulus (G') and loss modulus (G") graphics, the lowest observed values are related to the composites prepared loaded with graphite flakes. In the second, nanocomposites of graphene oxide and polyamide-6 shows significantly higher values and at the end, MWCNT nanocomposite shows the highest storage modulus (G') and loss modulus (G") values.

But in order to interpret these results it is necessary to remind, storage modulus and loss modulus represent elasticity and the viscous response of the materials. On the other hand a higher frequency in the dynamic mechanical analysis is equal to higher loading rate and a higher loading rate is known to cause a higher elastic modulus. The difference between graphite and graphene oxide is explainable with considering their own polarity and thickness. Graphene oxide because of expanded graphene sheet and presence of oxygen containing functional groups on the surface is capable to result in a better dispersion and better compatibility with polymer chains [42-46]. But in MWCNT nanocomposite there is a different reason to explain why the values of both storage modulus (G') and loss modulus (G") is the highest. It must be reminded that both graphene oxide and graphite are two dimensional and layer substances that under mechanical stress and melt flow exhibit different behavior respect to MWCNT. But MWCNT is a one dimensional material with extremely high aspect ratio. In fact MWCNT does not need to long time of processing and is able to be easily dispersed through the matrix and make a strong network of the nanotubes that is proved with other similar studies [26, 47,48].

Rheological test results related to complex viscosity (η*) in function of angular frequency for the samples prepared by melt blending method and different processing time in (figure 4.24).

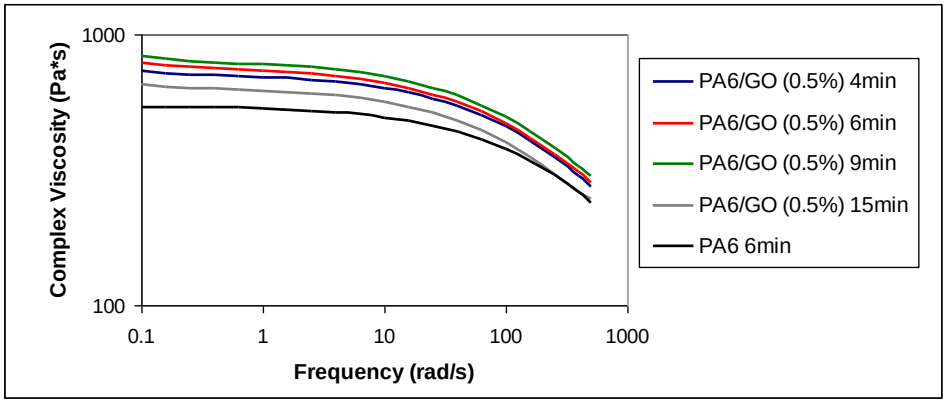

Figure 4.24) complex viscosity (η*) in function of temperature for nanocomposites prepared by melt blending method and different processing time

By a careful observation it is realized that presence of graphene oxide nano sheets in the matrix results in an increscent in the viscosity of nanocomposites and in this case extending processing time till 9th minute has a positive influence in increasing the viscosity. But after exceeding the 9th minute and does not play the same role and results to diminishing the viscosity. It must be remained that processing time is important to give enough time and energy subsequently to overcome to the problem of agglomeration in highly hydrophilic expanded graphene oxide sheets within polyamide-6. Breaking down the agglomerations obviously causes to increase the surface area in the filler, better dispersion, stronger interaction between the sheets and matrix, and more viscosity consequently. This phenomenon is explainable by looking at the role of these nanoparticles in the melt polymer as accelerators in energy dissipation. But after the 9th minute we can see a different response in the composites and it could be interpreted from thermal degradation point of view in both graphene oxide and polymer phases. These results are in accordance with the previous experiments results especially with mechanical results obtained from tensile test.

Rheological test results related to complex viscosity (η*) in function of angular frequency for the samples prepared with different volume of graphene oxide in (figure 4.25).

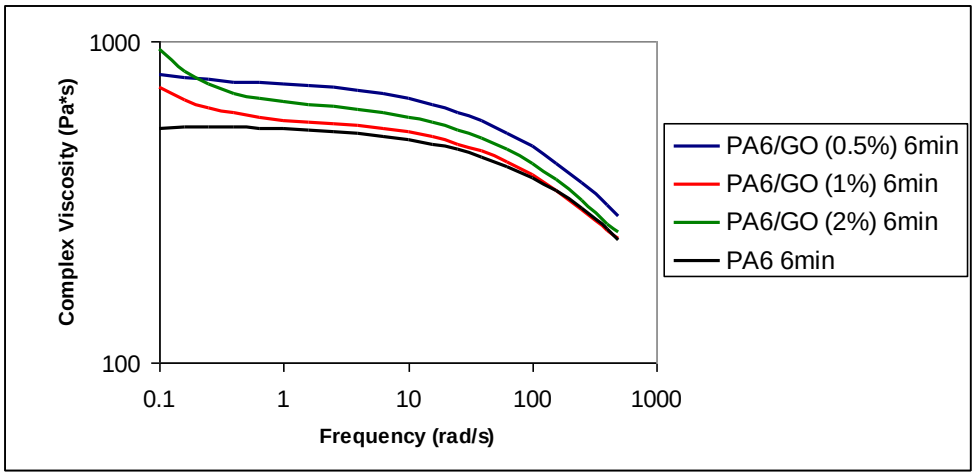

Figure 4.25) complex viscosity (η*) in function of temperature for nanocomposites prepared with different volume of graphene oxide

This is evident that presence of graphene oxide nanosheets within polyamide-6 results in viscosity enhancement and this is believed because of interaction between graphene oxide surface and polyamide-6 chains that increases energy dissipation and discussed before. But as it is clear the highest complex viscosity belongs to 0.5 vol%. Increasing the filler volume percentage in spite of our expectation does not aid to enhance viscosity and this phenomenon must be analyzed from dispersion point of view. We know expanded graphene oxide sheets have very strong tendency to restock on each other and particle agglomeration subsequently. This behavior is similar to utilize lower volume of graphene oxide and this is what exactly we observe here. Based on our previous results especially from tensile test, applying only melt blending method is not enough to overcome this problem. More or less there is a similarity between graphene oxide sheets

loaded nanocomposites and other kinds of nanocomposites loaded with layered nanoplatelets like nanoclay [41-44, 49].

Rheological test results related to complex viscosity (η*) in function of angular frequency for the samples prepared with different preparation methods in (figure 4.26).

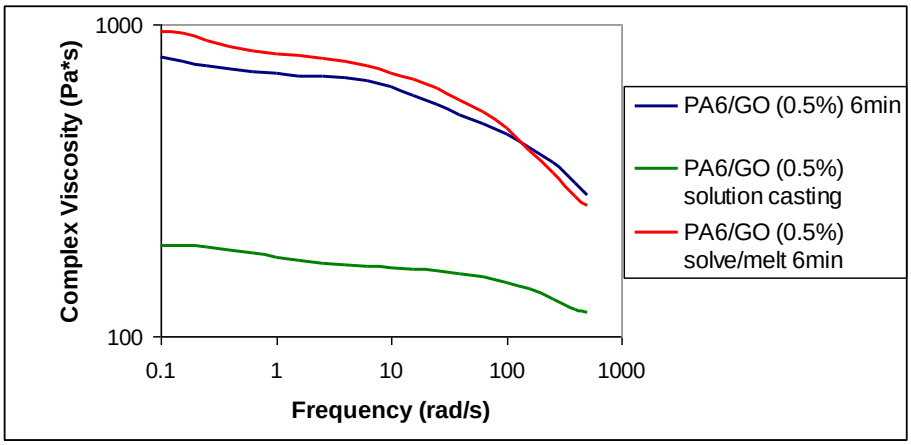

Figure 4.26) complex viscosity (η*) in function of temperature for nanocomposites prepared with different preparation methods

By having a careful look at the resulted complex viscosity from three different melt, solvent casting and solvent/melt blending methods we can claim that solvent/melt blending method superiority is still preserved in the rheological experiments and especially in enhancing the viscosity of nanocomposites. The most important factor in having high viscosity is transferring the response of nanocomposite to solid-like phase and this aim is achievable by having a strong interaction between the particle phase and matrix. In this case we have used the same volume of graphene oxide but viscose behavior of the composites confirms a clear different in this interaction. The lowest observed viscosity belongs to the solvent casting method that suffers from the problem of residual formic acid which has not been removed by the traditional distilled water rinsing procedure. On the

other hand melt blending method and solvent/melt blending method exhibit very close viscosity however as always this is solvent/melt blending method that shows the best values. All this results again confirm better performance of solvent/melt blending method to overcome the agglomeration problem in graphene oxide and resulting in a better graphene oxide dispersion and better intercalation between the sheets and polymer chains.

Rheological test results related to complex viscosity (η*) in function of angular frequency for the samples prepared with different filler content in (figure 4.27)

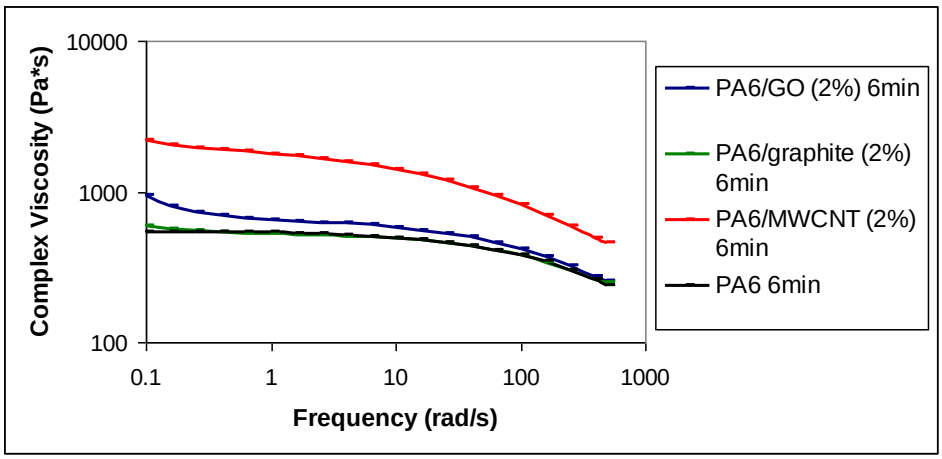

Figure 4.27) complex viscosity (η*) in function of temperature for nanocomposites prepared with different filler content

As we know adding filler nanoparticles in when obtaining a homogenous nanocomposite is desirable, will enhance the viscosity but in this case adding graphite flakes in 2 vol% to polyamide-6 does not cause to any significant change. On the other hand the same volume of graphene oxide exhibits rather higher viscosity in the nanocomposites. Finally, adding the same volume of MWCNT results in an extremely higher viscosity from both graphite and graphene oxide. Higher viscosity is the sign of better compatibility/interaction between filler and matrix but in this case it must be seen from the filler size and filler dispersion subsequently. This is

obvious that in the same volume, MWCNT because of its geometry has extremely higher aspect ratio and during the processing it helps to disperse the nanotubes and form an internal network inside the matrix. But on the other hand graphite consists of a lot of stocked graphene layers and it makes that denser and this fact plays a negative role in filler dispersion and making a homogenous composition. But graphene oxide because of passing chemical oxidation and expansion subsequently has this chance to become intercalated by polyamide-6 during the process and making smaller hydrophilic particles which aids to have a better dispersion and stronger interaction within the matrix phases [26, 47,48].

4.6. Differential scanning calorimetry (DSC) analysis

Differential scanning calorimetric experiment results including heating, cooling and numerical data in function of temperature for nanocomposites prepared with different processing time are reported in (figure 4.28).

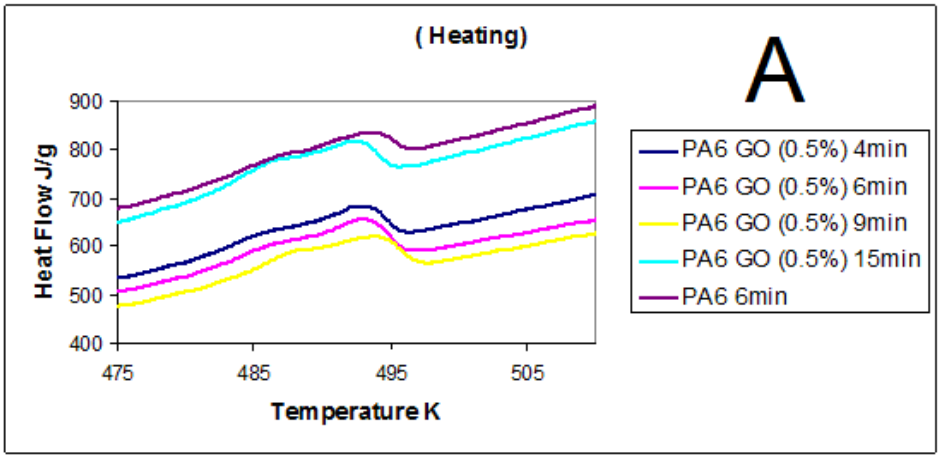

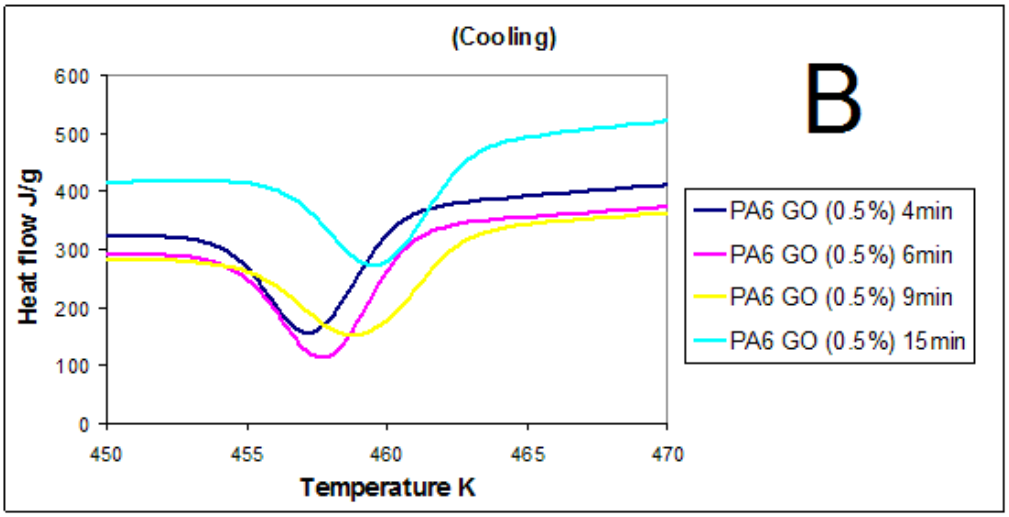

(C) Samples (cooling)	Area	Δ H (J/g)	Peak K
PA6/GO (0.5%) 4min	-428.65	-47.104	457.283
PA6/GO (0.5%) 6min	-493.954	-50.404	459.116
PA6/GO (0.5%) 9min	-568.867	-53.165	458.95
PA6/GO (0.5%) 15min	-469.822	-48.94	459.616

Figure 4.28) (A) DSC heating and (B) cooling curves obtained from the samples prepared with different processing time (C) numerical results obtained from cooling curves

Polyamide-6 because of its semicrystalline structure has two forms of crystals containing α and ɣ-forms. The α-crystal has more structural stability due to its shorter H-bond respect to ɣ crystal and is important in endowing better mechanical properties. Obviously this structural stability results in higher melting peak (~220-223°C) respect to less structural stable ɣ-crystal (~210-215°C). By looking at heating curve obtained from pure polyamide-6 we understand that there is a broad peak that proves presence of both α and ɣ crystals. On the other hand we observe the same peaks in nanocomposites in 0.5 vol% prepared by different processing time. However the same shoulder peaks confirm presence of both α and ɣ crystals but, there is no significant change in melting temperature and all nanocomposites especially pure polyamide-6 have rather similar melting

point. From the results of heating curves we realized, adding just 0.5 vol% graphene oxide to polyamide-6 and even increasing processing time from 4 to 15 minute does not result in any clear change in crystalline deformation in polyamide-6 and both α and ɣ-crystals are still existed.

On the other hand in cooling curves of nanocomposites we can observe apparent changes. As time extends cooling peaks show their tendency to slightly shift to higher temperatures. But from tabulated numerical results we can understand increasing processing time has an influence on enthalpies of nanocomposites and extending the time from 4 to 9 minute results in enthalpy (ΔH) increasing. The only interpretation for this phenomenon is the volume of faced exfoliation in graphene oxide sheets. It means longer processing time paves a road to exfoliate expanded graphene oxide layers within the matrix and it will result in exposing more nucleating sites for polymer chains to form its crystals and it can increase the volume of crystallinity in nanocomposite and increasing enthalpy subsequently.

Differential scanning calorimetric experiment results including heating, cooling and numerical data in function of temperature for nanocomposites prepared with different volume of graphene oxide content are reported in (figure 4.29)

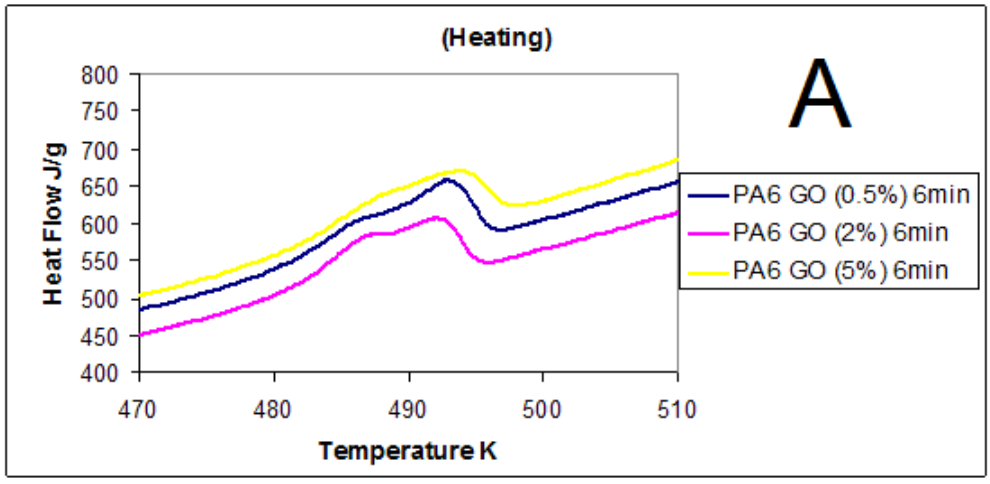

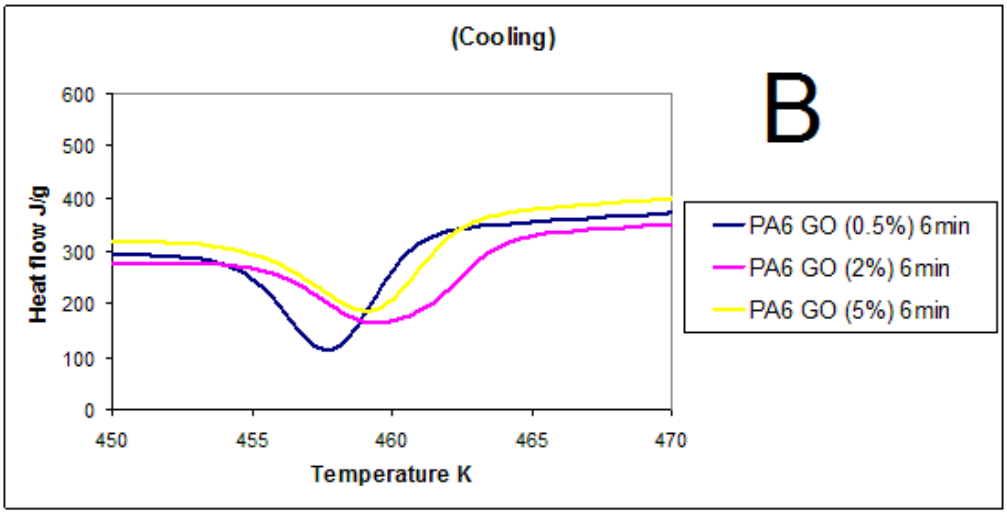

(C) Sample (cooling)	Area	Delta H (J/g)	Peak K
PA6/GO (0.5%) 6min	-493.954	-50.404	459.116
PA6/GO (2%) 6min	-492.764	-50.282	459.616
PA6/GO (5%) 6min	-502.359	-54.604	457.783

Figure 4.29) (A) DSC heating, (B) cooling curves and (C) numerical results obtained from cooling curves

By looking precisely at heating curves we can find an intensive melting peak (493K) in nanocomposite prepared with 0.5 vol% graphene oxide that belongs to α-form crystal. In other heating curves there are rather broad melting peaks that is an evidence of presence of both α and ɣ-form crystals that in 5 vol% graphene oxide becomes highly broad. We can explain this phenomenon by considering the role of graphene oxide sheets inside the polymer. Based on the other researches graphene sheets inside polyamide-6 have two different roles: they can confine the crystals and prevent them from forming α-form crystals and in the opposite by exposing nucleating sites pave a road to form ɣ-form crystals and increase the volume of crystallinity. In this case we believe increasing the volume of graphene oxide results in an enhancement in filler surface area and preventing from α-form crystal that give a chance to form ɣ-form crystals on the graphene oxide sheets. From cooling curves of nanocomposites prepared with

different volume of graphene oxide it is realized, increasing the filler results in peaks broadening and slightly shifting to higher temperature. Having longer crystallization time is evidence of longer heat releasing time and it means more crystalline phase in the material. So we can interpret it by reminding the role of graphene oxide sheets in higher volume that exposed more nucleating sites to polymer chains to form the crystals [43, 50, 51]. Numerical tabulated results of cooling curves also confirm the presumption of increasing the crystallinity by increasing graphene oxide sheets in composition with polyamide-6 when shows higher enthalpy (ΔH) values.

At the end we can conclude, higher graphene oxide sheets causes to form more ɣ- form crystals and enhancing the crystalline phase in polyamide-6. It must be noticed these results are in agreement with the previous obtained results especially in tensile test results.

Differential scanning calorimetric experiment results including heating, cooling and numerical data in function of temperature for nanocomposites prepared with different preparation methods are reported in (figure 4.30).

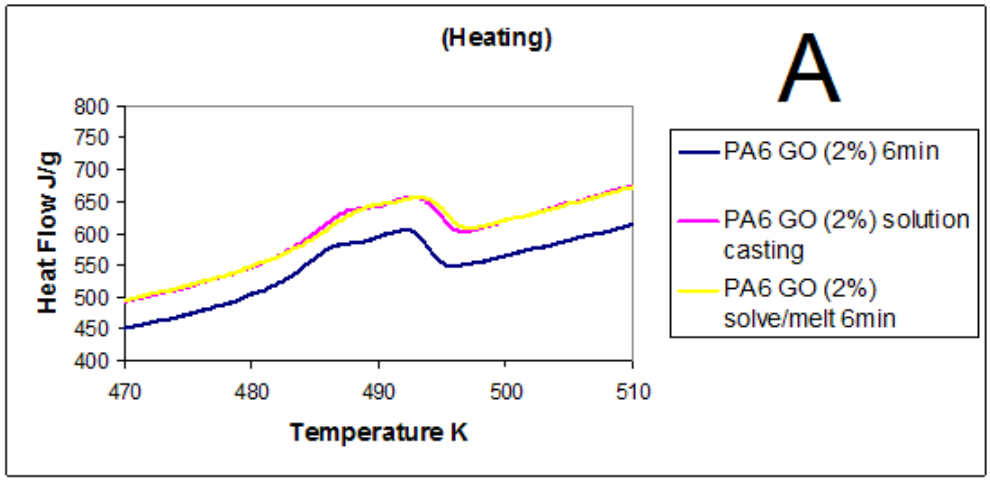

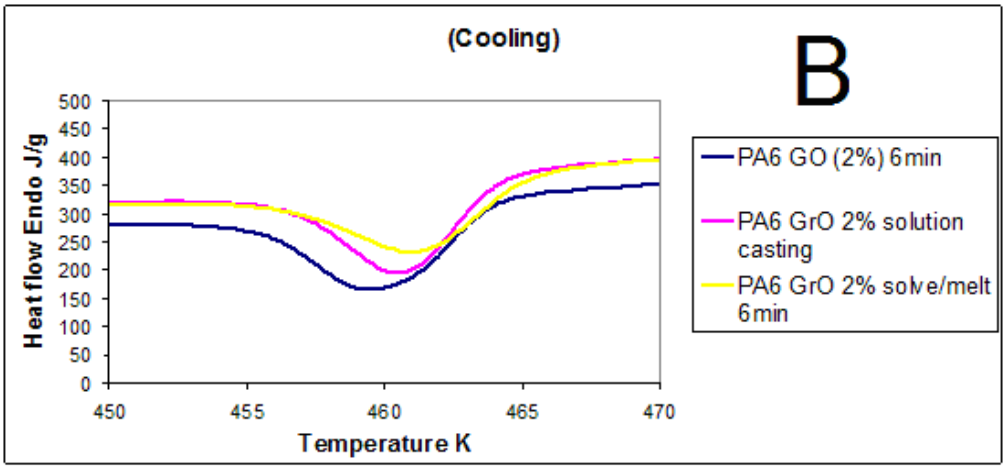

(C) Samples (cooling)	Area	Δ H (J/g)	Peak K
PA6/GO (2%) 6min	-492.764	-50.282	459.616
PA6/GO (2%) solution casting	-423.713	-48.194	460.616
PA6/GO (2%) solve/melt 6min	-406.36	-45.658	461.116

Figure 4.30) (A) DSC heating and (B) cooling curves obtained from the samples prepared with different preparation methods (C) numerical results obtained from cooling curves.

After looking at heating curves of nanocomposites prepared by different methods and with 2 vol% graphene oxide content we understand that there is no significant difference between melting point and α or ɣ crystals volume. It means melt blending, solvent casting and solvent/melt blending methods do not intervene in forming the crystals. However we still have the broad peaks which confirm presence of both α or ɣ-form crystals.

But in cooling curves there are apparent differences. The area under the curves starts to decrease as soon as melt blending is replaced with solvent casting and solvent/melt blending methods that it is exactly similar to enthalpy's trend. We can explain it by considering the effect of preparation method on the total volume of crystalline phase. We concluded before that solvent/melt blending method has more efficiency in dispersing graphene oxide sheets within the matrix and here also we believe that dispersed graphene oxide graphene sheets confine the polymer chains and prevent

them from forming freely that it decreases the total volume of crystalline phase and this is in contrast with earlier results in

Differential scanning calorimetric experiment results including heating, cooling and numerical data in function of temperature for nanocomposites prepared with different filler content are reported in (figure 4.31).

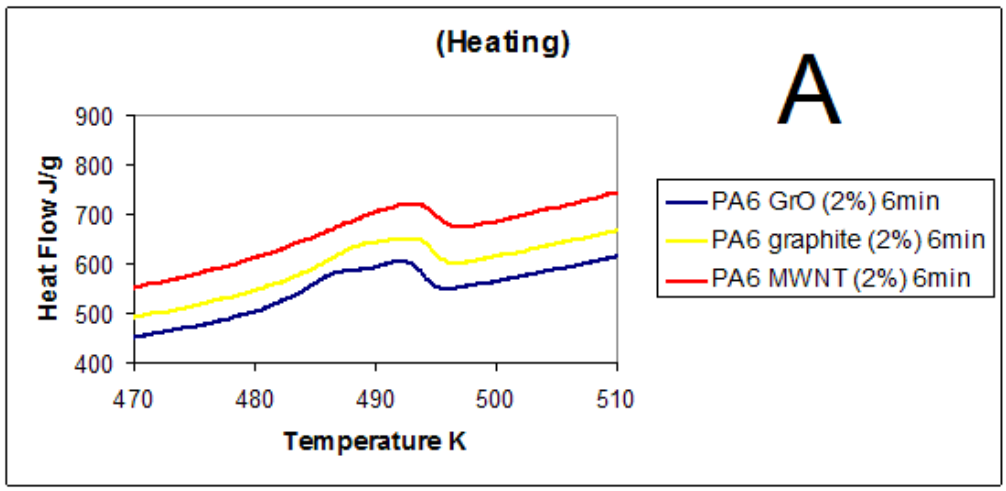

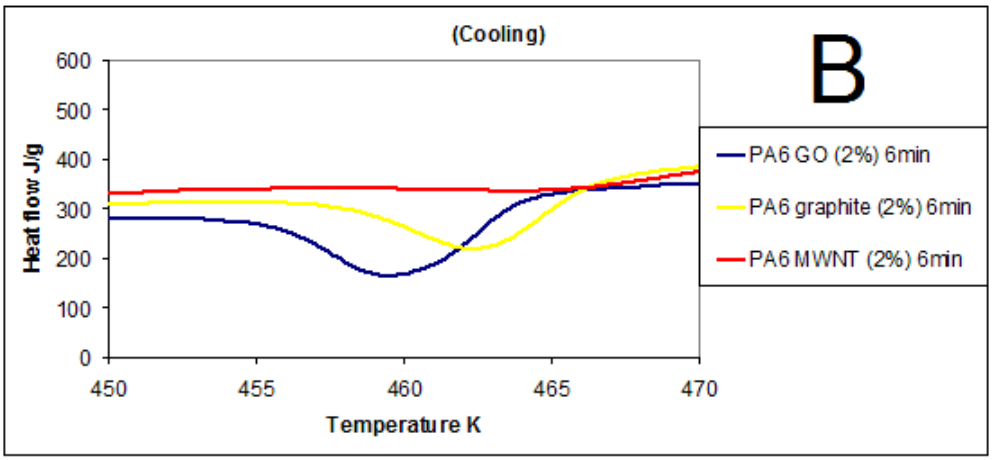

(C) Samples (cooling)	Area	Delta H (J/g)	Peak K
PA6/GO (2%) 6min	-492.764	-50.282	459.616
PA6/graphite (2%) 6min	-428.293	-46.544	462.45
PA6/MWNT (2%) 6min	-144.557	-15.885	465.273

Figure 4.31) (A) DSC heating and (B) cooling curves obtained from the samples prepared with different filler content (C) numerical results obtained from cooling curves.

As the heating curves show, adding graphene oxide and graphite in 2 vol% have a similar effect on formation of crystals in polyamide-6. In both graphene oxide and graphite flakes sheets dispersion do not distort neither α nor ɣ-form crystals and allow them to form and this is evident by observing both α and ɣ melting peaks in at 492 K and 487 K. On the other hand MWCNT curve shows lower ɣ-peak while α-peak still exists. This effect is explainable by considering the geometry of the fillers. Graphene oxide and graphite flakes are two dimensional carbon base materials which consist of stocked carbon sheets but MWCNT has one dimensional geometry that is formed of scrolled graphene sheets. Obviously in the same filler volume MWCNT endows more surface area and results in network of the tubes inside the polymer and this is the point that induces α-form crystals to form and confine ɣ-form crystals from forming and it is in accordance with other similar researches. By looking at crystallization curves and comparing with the numerical results of that we can find out that there is a small difference between nanocomposite prepared with graphene oxide and graphite. At first in graphite composite, cooling peak slightly shifts to higher temperature and in the second enthalpy decreases. These results are evidences of decreasing the total amount of crystalline phase in nanocomposite made by graphite. But in order to explain this phenomenon we have to remember that expanded graphene oxide sheets are more sensible and melt blending

process probably results in exfoliation in them that it also causes to more graphene oxide sheet separation and distribution within the matrix. Thus in the same volume, graphene oxide exposes more surface area and for sure more nucleating sites to polymer chains to form crystal phase and that is why total crystalline phase in nanocomposite made by graphene oxide is higher. In nanocomposite produced by MWCNT there is a completely broad peak that is not observable easily and shifts to higher temperature values which is the sign of increasing amorphous phase, and extremely lower enthalpy in comparison with two other composites. All these evidences confirm distortion in crystalline phase by MWCNTs. In fact in poyamide-6/MWCNT nanocomposite we have a network of intertwined fibers with much higher exposed sites to polymer chains that does not let polymer chains to form easily and distorts the crystalline phase in polyamide-6 [43, 50, 51].

This is supposed, cristallinity of the host polymer increases after filler incorporation, expecially at low loadings and in (figure 4.32) the degree of crystallinity is plotted versus filler weight fraction for all the nanocomposites investigated, according to the following equation:

$$\chi = \Delta H_m/(1-\phi_w)\Delta H^\circ_m \quad \text{equation (4.1)}$$

Where ΔH°_m is the melting enthalpy of fully crystalline PA_6: ΔH°_m=190 J g^{-1}.

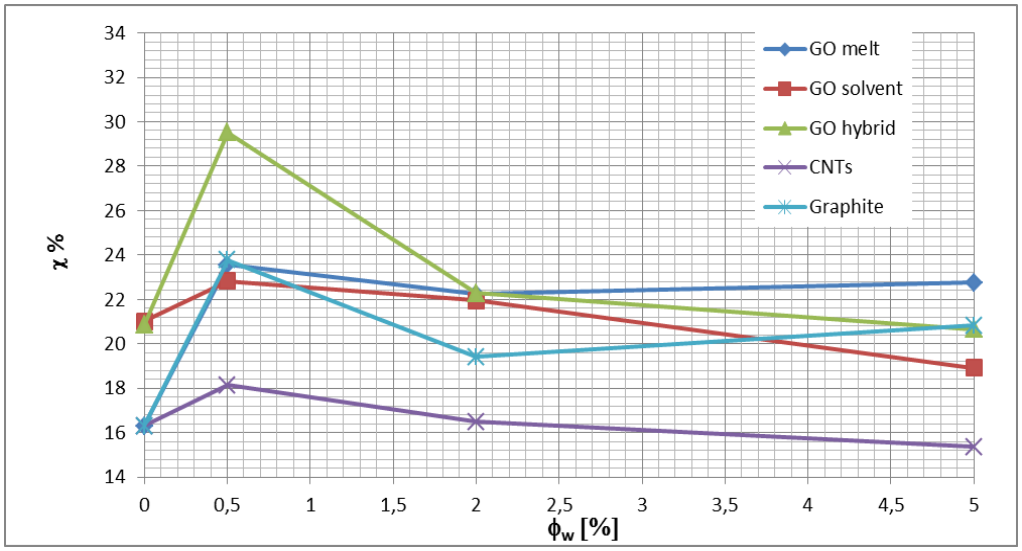

Figure 4.32) Degree of crystallinity as a function of filler weight percentage for the nanocomposites prepared

In this case we can conclude that difference in geometry and aspect ratio can strongly affect the direction of crystal forming. One dimensional fillers provoke α-form crystal formation while two dimensional fillers do not direct crystal formation in PA6. On the other hand one dimensional fillers in the same volume with two dimensional fillers have more destructive effect on crystalline phase of PA6.

4.7. Morphological analysis

SEM images of neat graphite flakes are presented in (figure 4.33).

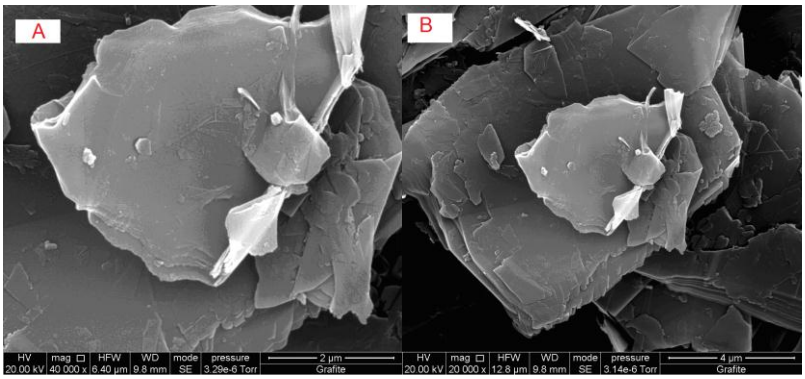

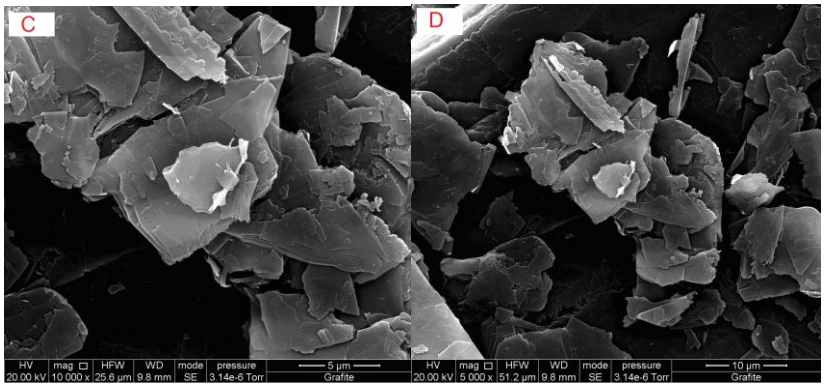

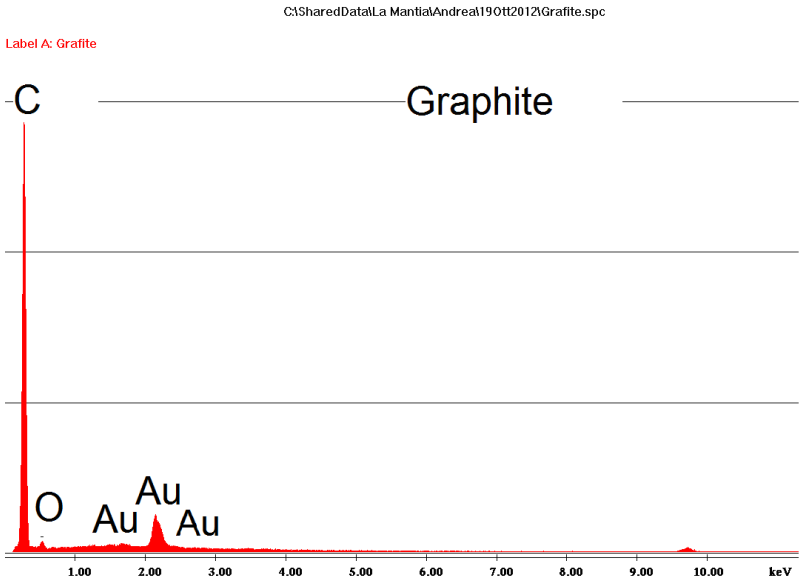

Figure 4.33) SEM images of graphite flakes with different zoom: A) 2µm B) 4µm C) 5µm D) 10µm and Energy dispersive spectroscopy (EDS) of graphite (bottom)

As it seems, NGF exhibits an extremely close flake layers, smooth and uniform surface which is constructed of compactly fastened nanosheets of graphene. It is also likely that the aspect ratio of single crystal graphite is in

the range of 100–1000. In addition EDAX examination results show an intensive and high carbon peak which naturally belongs to the main component of graphene sheets. On the other hand SEM images of graphene oxide exhibits a layered structure (figure 4.34). The graphene oxide sheets are folded onto themselves and it results in a stronger absorbance and wrinkled surface. The interlayer distance enhanced by inserting oxygen-containing functional groups among. Graphene oxide totally exhibits all specific features of intercalated graphite in comparison with other studies [52-61]. As we know carbon's peak refers to main structure of graphene oxide but presence of oxygen peak assure us about accuracy of oxidation operation. Gold's peak is because of very thin gold layer which covered surface of the samples to generate a conductive surface. But presences of Cl and Mn peaks are considered as a negative point in this case and could be due to lack of an efficient rinsing process and exhibit leftover salts of HCl and $KMnO_4$ respectively. However this method at least does not show any sulfate's peak and it verifies our procedure as a rather acceptable way to produce graphene oxide.

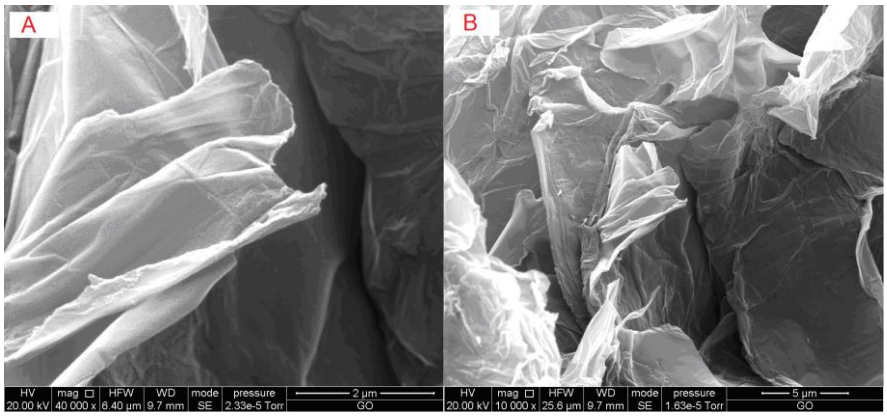

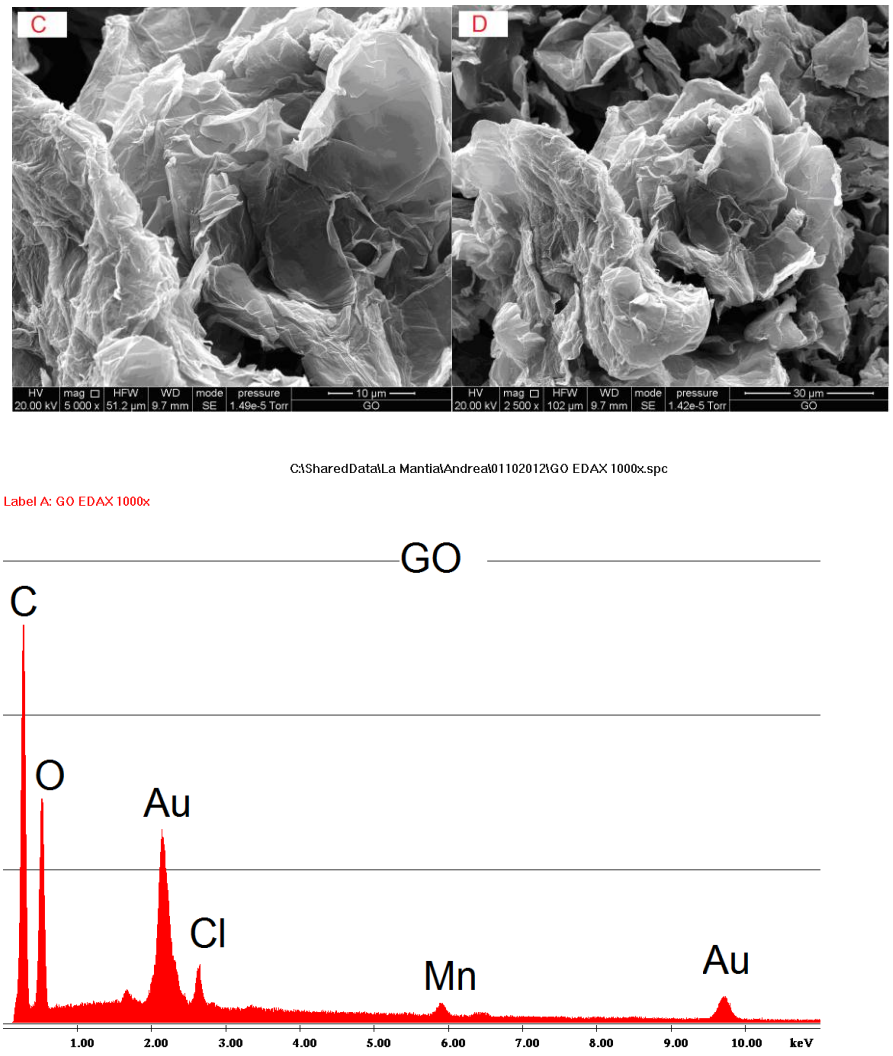

Figure 4.34) SEM images of graphene oxide with different zoom: A) 2µm B) 5µm C) 10µm D) 30µm and Energy dispersive spectroscopy (EDS) of graphene oxide (bottom)

It seems graphite because of its own hydrophobic nature do not display a homogenous texture and there are some area which performed by agglomerated graphite which confirms lower mechanical properties respect to graphene oxide nanocomposites. However this problem was not observed

in the mixtures of polyamide-6 and graphene oxide and graphene oxide well dispersed in the polymeric matrix and this is supposed that oxygen containing functional groups are presented onto the graphene layers and have the main role in giving hydrophilic nature to graphite oxide (figure 4.35).

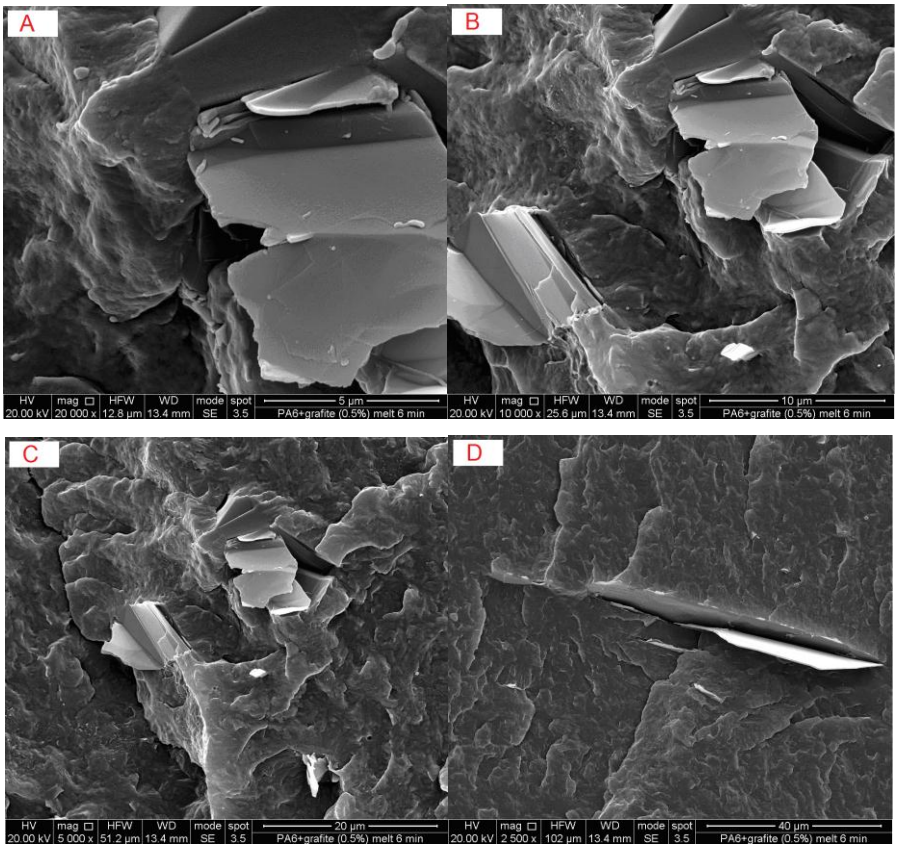

Figure 4.35) SEM images of PA6/graphite (0.5%) with different zoom: A) 5µm B) 10µm C) 20µm D) 40µm

By looking precisely at the SEM images obtained from graphene oxide nanocomposites prepared with melt blending technique we find out, graphene oxide sheets are dispersed through the matrix better than graphite flakes but, still there are some agglomerated mass of the sheets (figure 4.36). This evidence confirms our assumption about requiring a

pretreatment step to help to disperse better graphene oxide sheets through the matrix.

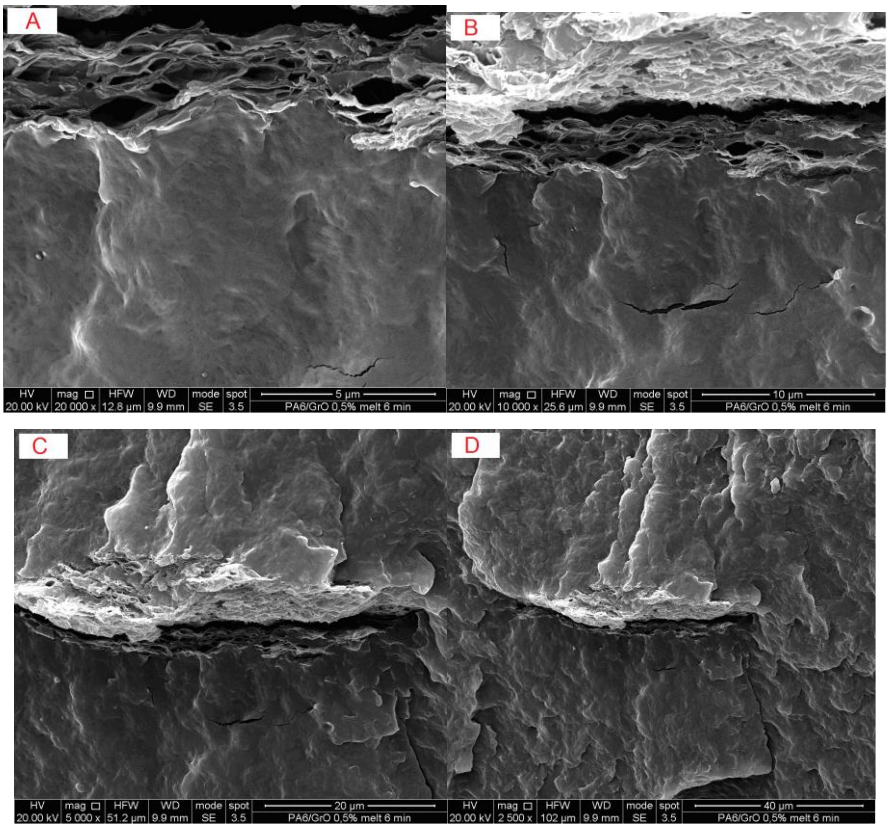

Figure 4.36) SEM images of PA6/GO (0.5%) melt 6min, with different zoom: A) 5µm B) 10µm C) 20µm D) 40µm

On the other hand SEM images obtained from graphene oxide nanocomposite prepared by solvent casting method show lower graphene oxide sheets thickness and better dispersion of through the matrix respect to melt blending method. Thus this is supposed that residual formic acid is the main reason to slighter mechanical properties of the nanocomposites prepared via this method (figure 4.37).

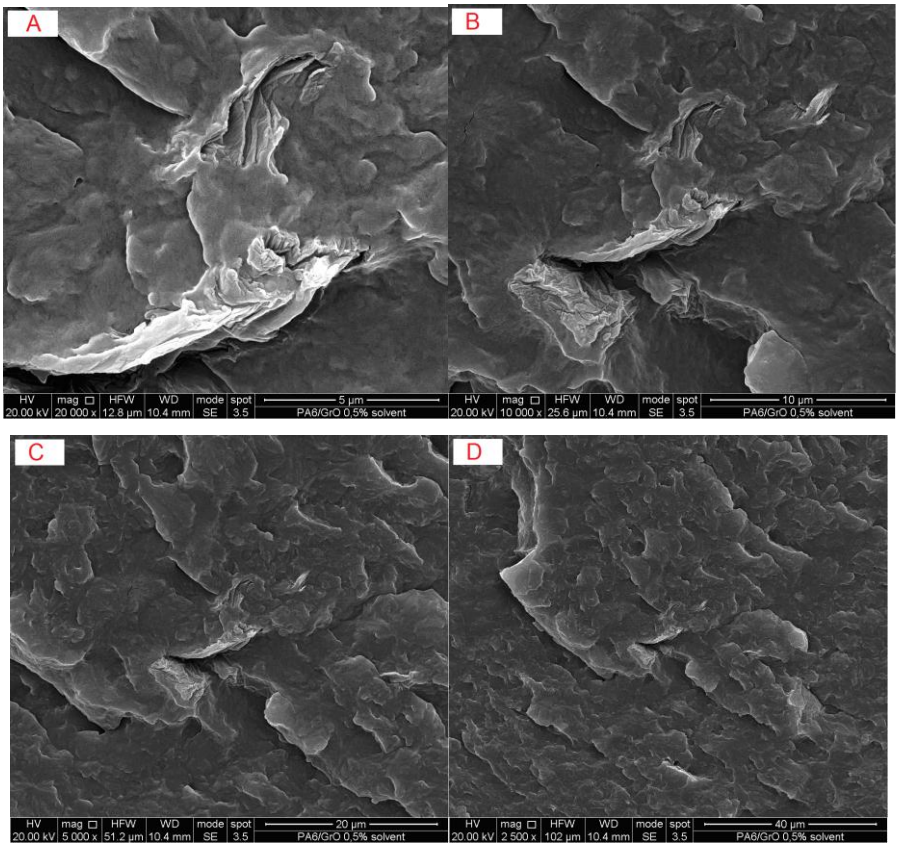

Figure 4.37) SEM images of PA6/GO (0.5%) solvent casting, with different zoom: A) 5µm B) 10µm C) 20µm D) 40µm

At the end, SEM images of graphene oxide nanocomposites prepared via complex solvent/melt blending method exhibit fine dispersion of graphene oxide sheets through the matrix and confirm this technique as the best technique in nanocomposite preparation. Graphene oxide sheets well exfoliated and covered by polymer and this is why this method exhibits the best mechanical results (figure 4.38).

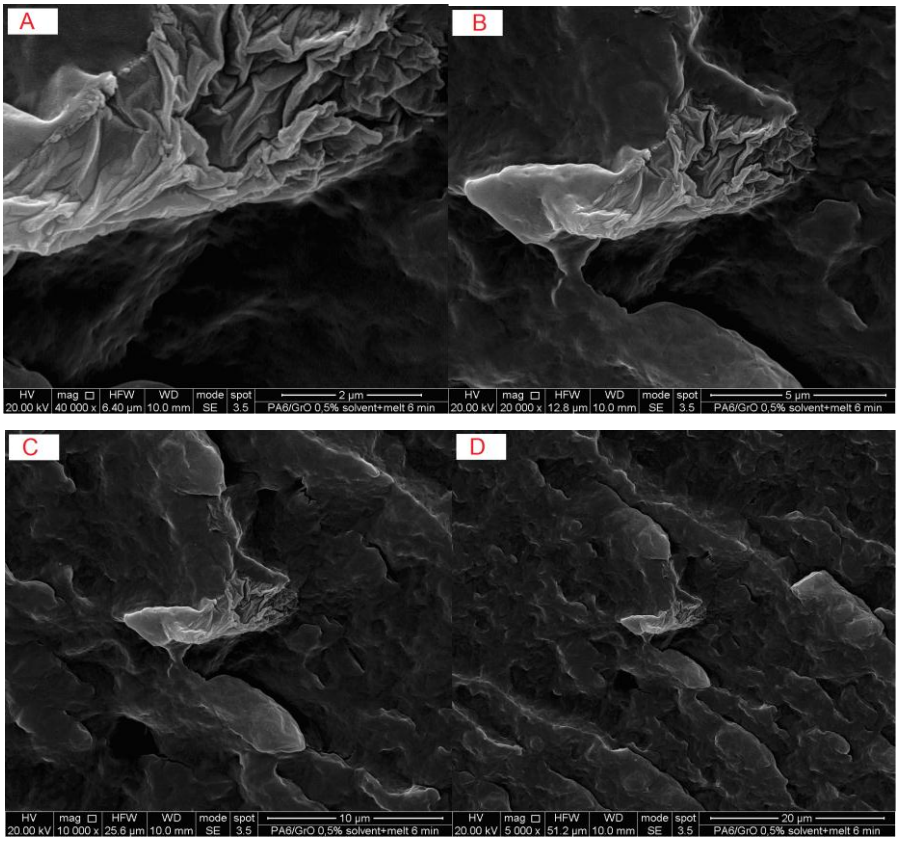

Figure 4.38) SEM images of PA6/GO (0.5%) solvent casting, with different zoom: A) 2µm B) 5µm C) 10µm D) 20µm

4.8. References

1. Tapas Kuila a, Saswata Bose a, Partha Khanra a, Nam Hoon Kim b, Kyong Yop Rhee a,b,c, Joong Hee Lee a,b,d, Characterization and properties of in situ emulsion polymerized poly(methyl methacrylate)/graphene nanocomposites, Camposites Part A: Applied Science and Manufacturing, Volume 42, Issue 11, November 2011, Pages 1856-1861.

2. Ken-Hsuan Liao, Yu-Shen Lin, , Christopher W. Macosko, , and Christy L. Haynes Cytotoxicity of Graphene Oxide and Graphene in Human Erythrocytes and Skin Fibroblasts, , ACS Applied Science and Materials Interfaces, Volume 3, Issue 7, 27 July 2011, Pages 2607-2615 .

3. Dan Chen, Xiaoyan Wang, Tianxi Liu, , Xiaodong Wang, and Jing Li , Electrically Conductive Poly(vinyl alcohol) Hybrid Films Containing Graphene and Layered Double Hydroxide Fabricated via Layer-by-Layer Self-Assembly, ACS Applied Science and Materials Interfaces, Volume 2, Issue 7, 28 July 2010, Pages 2005-2011.

4. Xin Zhao, Qinghua Zhang, and Dajun Chen, Erratum: Enhanced Mechanical Properties of Graphene-Based Poly(vinyl alcohol) Composites, Macromolecules, Volume 44, Issue 7, 12 April 2011, Page2392 .

5. Ashish Kumar Mishra, S. Ramaprabhu , Functionalized graphene sheets for arsenic removal and desalination of sea water, Desalination, Volume 282, 1 November 2011, Pages 39-45.

6. Hyunwoo Kim a, Shingo Kobayashi b, Mohd A. AbdurRahim c, Minglun J. Zhang a, Albina Khusainova a, , Marc A. Hillmyer b, Ahmed A. Abdala c, , Christopher W. Macosko, Graphene/polyethylene nanocomposites: Effect of polyethylene functionalization and blending methods, Polymer, Volume 52, Issue 8, 5 April 2011, Pages 1837-1846.

7. Takashi Kashiwagi, Richard H. Harris Jr , Xin Zhang, R.M. Briber, Bani H. Cipriano, Srinivasa R. Raghavan, Walid H. Awad, John R. Shield, Flame retardant mechanism of polyamide 6–clay nanocomposites, Polymer Volume 45, Issue 3, February 2004, Pages 881-891.

8. Xueli Wu & Jianhui Qiu & Peng Liu & Eiichi Sakai, Preparation and characterization of polyamide composites with modified graphite powders, Journal of Polymer Research October 2013, 20:284.

9. Shengtai Zhou, Lin Yu, Xin Song, Jin Chang, Huawei Zou, Mei Liang, Preparation of Highly Thermally Conducting Polyamide 6/Graphite Composites via Low-Temperature In Situ Expansion, Journal of Applied Polymer Science Volume 131, Issue 1, January 5, 2014.

10. Rajatendu Senguptaa, Mithun Bhattacharyaa, S. Bandyopadhyayb, Anil K. Bhowmicka, A review on the mechanical and electrical properties of graphite andmodified graphite reinforced polymer composites, Progress in Polymer Science 36 (2011) 638–670.

11. Kudin, K.N. Ozbas, B., Schniepp, H.C., Prud'homme, R.K., Aksay, I.A., Car, R., Raman spectra of graphite oxide and functionalized graphene sheets, Nano Letters, Volume 8, Issue 1, January 2008, Pages 36-41.

12. Adarsh Kaniyoor, Tessy Theres Baby, Thevasahayam Arockiadoss, Natarajan Rajalakshmi, and Sundara Ramaprabhu, Wrinkled Graphenes: A Study on the Effects of Synthesis Parameterson Exfoliation-Reduction of Graphite Oxide, journal of Physical Chemistry C, Volume 115, Issue 36, 15 September 2011, Pages 17660-17669 .

13. ChunHui Wua, YongZheng Zhanga, Sheng Li a, HuiJuan Zhenga, Hao Wanga, , JingBing Liua, KunWei Li b, Hui Yana, Synthesis and photocatalytic properties of the graphene–La2Ti2O7 nanocomposites, Chemical Engineering Journal, Volume 178, 15 December 2011, Pages 468-474.

14. Xin Wang a,b, Hongyu Yang a, Lei Song a, Yuan Hu a,b, , Weiyi Xing a, Hongdian Lu a,c, Morphology, mechanical and thermal properties of

graphene reinforced poly(butylene succinate) nanocomposites, Composite Science and Technalogy, Volume 72, Issue 1, 6 December 2011, Pages 1-6.

15. Jun Wanga,b,n, ZanGao a,b, ZhanshuangLi a, BinWang a, YanxiaYan a, QiLiu a, TomMann b, Milin Zhang a,b, ZhaohuaJiang c, Green synthesis of graphene nanosheets/ZnO composites and electrochemical properties, Journal of Solid State Chemistry, Volume 184, Issue 6, June 2011, Pages 1421-1427 .

16. YH Ding, P Zhang, Q Zhuo, H M Ren, Z M Yang and Y Jiang, A green approach to the synthesis of reduced graphene oxide nanosheets under UV irradiation, Nanotechnology Volume 22, Issue 21, 27 May 2011, Article number 215601.

17. Li Li Zhang, Zhigang Xiong, and X. S. Zhao, Pillaring Chemically Exfoliated Graphene Oxide with Carbon Nanotubes for Photocatalytic Degradation of Dyes under Visible Light Irradiation, ACS Nano Volume 4, Issue 11, 23 November 2010, Pages 7030-7036.

18. Omid Akhavan and Elham Ghaderi, Toxicity of Graphene and Graphene Oxide Nanowalls Against Bacteria, ACS Nano Volume 4, Issue 10, 26 October 2010, Pages 5731-5736.

19. Saswata Bose1, Tapas Kuila1, Ananta Kumar Mishra2, Nam Hoon Kim3 and Joong Hee Lee, Preparation of non-covalently functionalized graphene using 9-anthracene carboxylic acid, Nanotechnology Volume 22, Issue 40, 7 October 2011, Article number 405603.

20. Hyunwoo Kim, Ahmed A. Abdala and Christopher W. Macosko, Graphene/Polymer Nanocomposites, Macromolecules, 2010, 43 (16), pp 6515–6530.

21. Kyriaki Kalaitzidou, Hiroyuki Fukushima, Lawrence T. Drzal, A new compounding method for exfoliated graphite–polypropylene

nanocomposites with enhanced flexural properties and lower percolation threshold, Composites Science and Technology, Volume 67, Issue 10, August 2007, Pages 2045-2051.

22. Hui Quan, Bao-qing Zhang , Qiang Zhao , Richard K.K. Yuen , Robert K.Y. Li, Facile preparation and thermal degradation studies of graphite nanoplatelets (GNPs) filled thermoplastic polyurethane (TPU) nanocomposites, Composites Part A: Applied Science and Manufacturing, Volume 40, Issue 9, September 2009, Pages 1506-1513.

23. Andrews R, Jacques D, Minot M, Rantell T. Fabrication of carbon multiwall nanotube/polymer composites by shear mixing. Micromol Mater Eng 2002;287:395–403.

24. Zhang WD, Shen L, Phang IY, Liu T. Carbon nanotubes reinforced nylon-6 composite prepared by simple melt-compounding. Macromolecules 2004;37:256–9.

25. Hailin Zeng, Chao Gao, Yanping Wang, Paul C.P. Watts, Hao Kong, Xiaowen Cui, Deyue Yan, In situ polymerization approach to multiwalled carbon nanotubes-reinforced nylon 1010 composites: Mechanical properties and crystallization behavior, Polymer Volume 47, Issue 1, 3 January 2006, Pages 113-122.

26. Fangming Xianga, Jun Wua, Li Liua, Ting Huanga, Yong Wanga,b, Chen Chenc, Ya Pengd, Chongxi Jianga and Zuowan Zhoua, Largely enhanced ductility of immiscible high density polyethylene/polyamide 6 blends via nano-bridge effect of functionalized multiwalled carbon nanotubes, Polymers for Advanced Technologies Volume 22, Issue 12, December 2011, Pages 2533-2542.

27. Zhiqi Shen, Stuart Bateman, Dong Yang Wu, Patrick McMahon, Mel Dell'Olio, Januar Gotama, The effects of carbon nanotubes on mechanical

and thermal properties of woven glass fibre reinforced polyamide-6 nanocomposites, Composites Science and Technology Volume 69, Issue 2, February 2009, Pages 239-244.

28. Tran Duy Thanh, Ludmila Kapralkova, Jirˇina Hromadkova, Ivan Kelnar, Effect of graphite nanoplatelets on the structure and properties of PA6-elastomer nanocomposites, European Polymer Journal Volume 50, Issue 1, January 2014, Pages 39-45.

29. Haihui Liu, Lichen Hou, Weiwei Peng, Qiang Zhang, Xingxiang Zhang, Fabrication and characterization of polyamide 6-functionalized graphene nanocomposite fiber, Journal of Materials Science Volume 47, Issue 23, December 2012, Pages 8052-8060.

30. Pieter Gijsman , Guido Meijers, Giacomo Vitarelli, Comparison of the UV-degradation chemistry of polypropylene, polyethylene, polyamide 6 and polybutylene terephthalate, Polymer Degradation and Stability Volume 65, Issue 3, September 1999, Pages 433-441.

31. Alwar Ramani, Martin Hagen, Johan Hereid, Jianping Zhang and Michael Delichatsios, Interaction of a phosphorus-based FR, a nanoclay and PA6. Part 2 interaction of the complete PA6 polymer nanocomposites, Fire and Materials Volume 33, Issue 6, 2009, Pages 273-285.

32. Massimo Paci, Sara Filippi, Pierluigi Magagnini, Nanostructure development in nylon 6-Cloisite_ 30B composites. Effects of the preparation conditions, European Polymer Journal Volume 46, Issue 5, May 2010, Pages 838-853.

33. Carlos Arrieta, Yingying Dong, Andr_e Lan, Toan Vu-Khanh, Outdoor Weathering of Polyamide and Polyester Ropes Used in Fall Arrest Equipment, Journal of Applied Polymer Science Volume 130, Issue 5, 5 December 2013, Pages 3058-3065.

34. N.Tz. Dintcheva, G. Filippone b, F.P. La Mantia, D. Acierno, Photo-oxidation behaviour of polyethylene/polyamide 6 blends filled with organomodified clay: Improvement of the photo-resistance through morphology modification, Polymer Degradation and Stability Volume 95, Issue 4, April 2010, Pages 527-535.
35. Pierfrancesco Cerruti, Cosimo Carfagna, Thermal-oxidative degradation of polyamide 6,6 containing metal salts, Polymer Degradation and Stability Volume 95, Issue 12, December 2010, Pages 2405-2412.
36. W.S. Chowa, Z.A. Mohd Ishaka, J. Karger-Kocsisb, A.A. Apostolovc, U.S. Ishiaku, Compatibilizing effect of maleated polypropylene on the mechanical properties and morphology of injection molded polyamide 6/polypropylene/organoclay nanocomposites, Polymer Volume 44, Issue 24, 31 October 2003, Pages 7427-7440.
37. Baoli Oua, Duxin Li, Yuejun Liu, Compatibilizing effect of maleated polypropylene on the mechanical properties of injection molded polypropylene/polyamide 6/functionalized-TiO2 nanocomposites, Composites Science and Technology Volume 69, Issue 3-4, March 2009, Pages 421-426.
38. W.S. Chow, A. Abu Bakar, Z.A. Mohd Ishak, J. Karger-Kocsis, U.S. Ishiaku, Effect of maleic anhydride-grafted ethylene–propylene rubber on the mechanical, rheological and morphological properties of organoclay reinforced polyamide 6/polypropylene nanocomposites, Polymers and Polymer Composites Volume 13, Issue 8, 2005, Pages 795-805.
39. W. S. Chow, Z. A. Mohd Ishak, Mechanical, morphological and rheological properties of polyamide 6/organo-montmorillonite nanocomposites, Express Polymer Letters Volume 1, Issue 2, February 2007, Pages 77-83.
40. M. Stankowski, Anna Kropid_owska, Maria Gazda and J. T. Haponiuk, PROPERTIES OF POLYAMIDE 6 AND THERMOPLASTIC POLYURETHANE BLENDS CONTAINING MODIFIED

MONTMORILLONITES, Journal of Thermal Analysis and Calorimetry Volume 94, Issue 3, December 2008, Pages 817-823.

41. Cesar A. G. Beatrice,1 Marcia C. Branciforti, Rosa M. V. Alves, Rosario E. S. Bretas, Rheological, Mechanical, Optical, and Transport Properties of Blown Films of Polyamide 6/Residual Monomer/ Montmorillonite Nanocomposites, Journal of Applied Polymer Science,Vol. 116, 3581–3592 (2010).

42. Alireza Mojarrad, Yousef Jahani, Mehdi Barikani, Influence of Nanoclay on the Rheological Properties of Polyamide 6/Acrylonitrile Butadiene Styrene Nanocomposites, Journal of Applied Polymer Science Volume 125, Issue SUPPL. 1, 25 July 2012, Pages E571-E582.

43. Yan Liu • Zhenming Chen • Guisheng Yang, Synthesis and characterization of polyamide-6/graphite oxide nanocomposites, Materials Chemistry and Physics Volume 120, Issue 1, 15 March 2010, Pages 167-171.

44. L. As'habi & S. H. Jafari & H. A. Khonakdar & B. Baghaei, Morphological, rheological and thermal studies in melt processed compatibilized PA6/ABS/clay nanocomposites, Journal of Polymer Research Volume 18, Issue 2, March 2011, Pages 197-205.

45. R. Scaffaro, L. Botta, M.C. Mistretta, F.P. La Mantia, Preparation and characterization of polyamide 6/polyethylene blend-clay nanocomposites in the presence of compatibilisers and stabilizing system, Polymer Degradation and Stability Volume 95, Issue 12, December 2010, Pages 2547-2554.

46. R. Scaffaro, L. Botta, M. C. Mistretta, F. P. La Mantia, Processing – morphology – property relationships of polyamide 6/polyethylene blend–

clay nanocomposites, Express Polymer Letters Volume 7, Issue 10, 2013, Pages 873-884.

47. R.H. Zhang a, Y.K. Yang a,b, X.L. Xie c, Robert K.Y. Li, Dispersion and crystallization studies of hyper-branched poly(urea-urethane)sgrafted carbon nanotubes filled polyamide-6 nanocomposites, Composites Part A: Applied Science and Manufacturing Volume 41, Issue 5, May 2010, Pages 670-677.

48. Hailin Zeng , Chao Gao , Yanping Wang, Paul C.P. Watts, Hao Kong, Xiaowen Cui, Deyue Yan, In situ polymerization approach to multiwalled carbon nanotubes-reinforced nylon 1010 composites: Mechanical properties and crystallization behavior, Polymer Volume 47, Issue 1, 3 January 2006, Pages 113-122.

49. M.C. Mistretta a, M. Morreale b, F.P. La Mantia, Thermomechanical degradation of polyethylene/polyamide 6 blend-clay nanocomposites, Polymer Degradation and Stability, Volume 99, Issue 1, January 2014, Pages 61-67.

50. Yan Liua, Guisheng Yanga, Non-isothermal crystallization kinetics of polyamide-6/graphite oxide Nanocomposites, Thermochimica Acta Volume 500, Issue 1-2, 10 March 2010, Pages 13-20.

51. J. Bian, X. W. Wei, H. L. Lin, L. Wang, Z. P. Guan, Comparative Study on the Exfoliated Expanded Graphite Nanosheet-PES Composites Prepared via Different Compounding Method, Journal of Applied Polymer Science Volume 124, Issue 5, 5 June 2012, Pages 3547-3557.

52. Donghwan Cho, Sangyeob Lee, Gyeongmo Yang,1 Hiroyuki Fukushima, Lawrence T. Drzal, Dynamic Mechanical and Thermal Properties of Phenylethynyl-Terminated Polyimide Composites Reinforced

With Expanded Graphite Nanoplatelets, Molecular and Materials and Engineering, Volume 290, Issue 3, 15 March 2005 page 179-187 .

53. HAN YongQin, DING Bing & ZHANG XiaoGang, Effect of feeding ratios on the structure and electrochemical performance of graphite oxide/polypyrrole nanocomposites, Cinese Science Bulletin, Volume 56, Issue 26, September 2011, Pages 2846-2852.

54. Dan Chen, Xiaoyan Wang, Tianxi Liu, Xiaodong Wang, and Jing Li, Electrically Conductive Poly(vinyl alcohol) Hybrid Films Containing Graphene and Layered Double Hydroxide Fabricated via Layer-by-Layer Self-Assembly, ACS Applied Materials and Interfaces, Volume 2, Issue 7, 28 July 2010, Pages 2005-2011.

55. Sumin Kim a, _, LawrenceT.Drzal b, High latent heat storage and high thermal conductive phase change materials using exfoliated graphite nanoplatelets, Solar Energy Materials and Solar Cells, Volume 93, Issue 1, January 2009, Pages 136-142.

56. Jisoo Jeon,Su-GwangJeong,Jeong-HunLee,JungkiSeo,SuminKim n, High thermal performance composite PCMs loading xGnP for application to building using radiant floor heating system, Solar Energy Materials and Solar Cells, Volume 101, June 2012, Pages 51-56.

57. Kyriaki Kalaitzidou, Hiroyuki Fukushima, Lawrence T. Drzal, Mechanical properties and morphological characterization of exfoliated graphite–polypropylene nanocomposites, Composite Part A: Applied Science and Manufacturing, Volume 38, Issue 7, July 2007, Pages 1675-1682.

58. Meilu Li, Young Gyu Jeong, Poly(ethylene terephthalate)/exfoliated graphite nanocomposites with improved thermal stability, mechanical and electrical properties, Composite Part A: Applied Science and Manufacturing, Volume 42, Issue 5, May 2011, Pages 560-566.

59. Larissa Stieven Montagna, Fabiana de Carvalho Fim, Griselda Barrera Galland, Nara Regina de Souza Basso, Synthesis of Poly(propylene)/Graphite Nanocomposites by in Situ Polymerization,

Macromolecular Symposia, Volume 299-300, Issue 1, January 2011, Pages 48-562011.

60. Sumin Kim, Inhwan Do, Lawrence T. Drzal2, Thermal Stability and Dynamic Mechanical Behavior of Exfoliated Graphite Nanoplatelets-LLDPE Nanocomposites, Polymer Compoisite, Volume 31, Issue 5, May 2010, Pages 755-761 .

61. Gil Woo Jeon, Ji-Eun An, Young Gyu Jeong, High performance cellulose acetate propionate composites reinforced with exfoliated graphene, Composite Part B: Engineering.

5. Conclusions

Graphite showed its ability to be modified by the new Marcano's method and after oxidation/intercalation transform to graphene oxide. The results of XRD, Raman, XPS and SEM also confirmed this modification and faced expansion between graphene sheets which was the main goal of this modification method. In continue after mixing graphene oxide and polyamide-6 based on three solvent casting, melt blending and solvent/melt blending methods the samples were prepared. In order to have a comprehensive comparison, other samples by graphite and MWCNTs were prepared. The results of mechanical experiments confirm a meaningful enhancement in mechanical properties of PA6/GO which reassures us about the performance of Marcano's modification method to modify graphite flakes. On the other hand between three mentioned preparation methods, solvent/melt blending method showed its superiority in dispersing graphene oxide through the matrix by exhibiting the best mechanical results at 2 vol%. XRD results also showed a fine intercalation and dispersion of graphene sheets by polymer chains. The results of ATR-FTIR experiment showed the photo-oxidation shielding role of graphene oxide sheets in PA6/GO nanocomposites after 96 hour exposing to UV irradiation. DMTA experiment results indicated that graphene oxide increases the glass transition temperature of the PA6 nanocomposites and also has a positive influence on storage and loss modulus. Rheological experiment results proved the role of graphene oxide and solvent/melt blending preparation method on increasing the viscosity in PA6. DSC results confirm the influence of graphee oxide and preparation methods on crystallinity and the type of crystal formation in PA6. Morphological analysis also confirmed a fine dispersion of graphene oxide sheets within the matrix.

This is believed that Marcano's method is able to be used instead of traditional oxidation methods to modify graphite flakes. Among traditional nanocomposite preparation methods, solvent/melt blending method is able to be used widely to achieve to homogeneous nanocomposites. It seems that

6 minutes processing time is the optimum processing time and 2 vol% is the mechanical percolation threshold. At the end we can conclude that the prepared PA6/GO (2%) solvent/casting nanocomposit has so wide ability to be used in different areas and also deserve to be studied more.

List of ISI jornal publications

1. Evaluation of effect of different preparation methods and fillers on morphological, mechanical and dynamic mechanical-thermal properties of polyamide-6 nanocomposites (in processing).
2. Evaluation of rheological properties of polyamide-6 nanocomposites prepared by different preparation methods and fillers (in processing).
3. Crystallization investigation of polyamide-6 nanocomposites fabricated via different fabrication methods and fillers (in processing).
4. A. Maio, R. Fucarino, R. Khatibi, R. Scaffaro, Technologies to incorporate graphene oxide in polymer matrices (sent to Macromolecular Materials and Engineering for publication).

List of presentations in national congresses

1. A. Maio, R. Scaffaro, L. Botta, R. Fucarino, R. Khatibi, Effetto della preparativa sulle propreità di nanocompositi a base di ossido di grafene. Paper presented at XII convegno nazionale AIMAT, 2014.

List of presentations in international congresses

1. A. Maio, R. Scaffaro, R. Khatibi, S.P. Agnello, A. Piazza, L. Botta, Gianpiero Buscarino, Improved stability of graphene oxide-silica nanohybrids and related polymer-based nanocomposites (MoDeSt, agust 31st-september 4th 2014, Portorož, Slovenia).
2. A. Maio, R. Khatibi, L. Botta, R. Scaffaro, Photo-oxidation of PA6/graphene oxide films (MoDeSt, agust 31st-september 4th 2014, Portorož, Slovenia).
3. A. Maio, R. Fucarino, R. Khatibi, L. Botta, S. Rosselli, M. Bruno, R. Scaffaro, Graphene oxide-silica nanohybrids as fillers for PA6 based nanocomposites. Paper presented at 7th international conference of times of polymer (TOP) and composites, 2014.

List of courses attended

1. Principi di ingegneria chimica (Prof.Valerio Brucato) 2013.
2. Termodinamica di ingegneria chimica (Prof.Carmelo Sunseri and Prof.Salvatore Piazza) 2013.

List of seminars attended

1. process intensification for carbon capture/ Presidenza della Facoltà di Ingegneria /12-04-2012/ 10-12 o'clock.
2. Indici bibliometrcici: come valutare la propria attività scientifica/ Presidenza della Facoltà di Ingegneria/ 19-04-2012/ 15-17 o'clock.
3. La sicureza sociale diei givani ricercatori: situazione pensionistica e accesso al credito/ Presidenza della Facoltà di Ingegneria/ 3-05-2012/ 15-17 o'clock.
4. Trasferimento tecnologico e progetti di ricarca applicata/ Presidenza della Facoltà di Ingegneria/ 21-06-2012/ 9-18 o'clock.
5. Injection molding of polymers/ Iran polymer and petrochemical institute (IPPI)/ 6-7/08/2012.
6. Università e impress: come progettare la ricerca 7° programa quadro (2012-2013): casi di sucesso, buone partiche, nuovi bandi/ edificio 16/ 21-09-2012/ 9-14 0'clock.
7. Energie per la ricerca enel lab/ Presidenza della Facoltà di Ingegneria/ 22-10-2012/ 10:30-13 o'clock.
8. L'uoso dei modelli computazionali per descrivere fenomeni complessi in medicina: un nuovo approcio alla ricerca medica/ Presidenza della Facoltà di Ingegneria/ 22-10-2012/ 15:30-18:30.
9. Metodologie della didattica per giovani ricercatori dell'università di palermo/ aula lanza, orto botanico, via lincoln n. 2, palermo/ 5-7/10/2012.
10. Shaping stem cell micro-environment through biomimetic materials and microfluidic platform/ Presidenza della Facoltà di Ingegneria/ 23-11-2012.

11. Modifiche superficiali dei materiali metallici mediante tecnologie plasma" (Prof.ssa E. Angelini) 10:00 Aula B020 (Edif.6), viale delle Scienze, Università di Palermo 22 marzo 2013.

12. "Stress-related instabilities during anodic oxide growth" (Prof. J. Proost),Aula conferenze DICAM, viale delle Scienze, Università di Palermo 6 Giugno 2013.

13. "Development of polymer as vector for gene therapy Molecularly imprinted polymers: a powerful technic for selective sequestration of molecule target" (Prof.ssa L. Mespouille) Presidenza della Facoltà di Ingegneria , Aule satelliti, viale delle Scienze, Università di Palermo 27 giugno 2013.

14. "Specializzazione cellulare tramite stimoli meccanici" (Prof. Paolo Netti), Presidenza della Facoltà di Ingegneria, viale delle Scienze Università di Palermo. 11 luglio 2013.

15. "Il prototipo REAPOWER di UNIPA. Produzione di energia elettrica da gradienti salini: primo impianto pilota in Italia, Aula Capitò, Presidenza della Facoltà di Ingegneria, viale delle Scienze Università di Palermo. 13 marzo 2014.

16. "New aspects for economical evaluations in the 21th century. Application to food, nutraceutical and pharmacy market" (Prof. Ignacio Gracia Fernández), Aula Gainazzi Ed.6, viale delle Scienze Università di Palermo. 1-2 luglio 2014.

List of summer schools attended

1. Advances in materials sciences and technologies/ hotel continental terme, Ischia porto (NA)/ 11-15/07/2012.

2. GRICU PhD national school (16-20/09/2013):

- Biochemtex event (16/09/2013) 8:30-16:00.

- Free radical polymerization: kinetics, statistical thermodynamics and engineering aspects (17/09/2013) 8:45-20:00.

- Free radical polymerization: kinetics, statistical thermodynamics and engineering aspects.

Advanced topics in sustainable chemical engineering (18/092013) 8:45-20:00.

Advanced topics in sustainable chemical engineering (19/09/2013) 8:30-18:45.

- Nanotechnologies (20/09/2013) 8:45-20:00.

Acknowledgment

Special thanks to my supervisor professor Roberto Scaffaro for all the supports he gave me during my three-year research, to my colleagues Dr.Andrea Maio, Dr.Luigi Botta and all who helped me in "dipartimento di ingegneria chimica, gestionale, informatica, e meccanica" at university of Palermo, to Dr.Simone Agnello and physics department at university of Palermo, to Dr.Antonella Glisenti at university of Padova.

Hereby I dedicate this thesis to my parents for all the support that gave me in all the years of my life.